Aerodynamic Nuances on Wings Subjected to Ground Effect

By

Jose Vanir Valenzuela

A Thesis Presented in Partial Fulfillment
of the Requirements for the Degree
Master of Science

Approved February 2024 by the
Graduate Supervisory Committee:

Timothy Takahashi, Chair
Werner Dahm
Huei-Ping Huang

ARIZONA STATE UNIVERSITY

May 2024

ABSTRACT

This thesis aims to determine how finite wing aerodynamic loads change in proximity to the ground. In this study, the primary design tool is an inviscid panel method code, VORLAX. The validation tool is a commercial volume grid CFD package, ANSYS FLUENT. I use VORLAX to simulate wings with different incidences and aspect ratios to look at how ground effect impacts spanwise loading and incipient flow separation. Then the results were compared to widely published equations such as McCormick, Torenbeek, and Hoerner & Borst. Because I found that these "famous" equations function best only for specific conditions, I propose a new empirical equation to estimate ground effect lift as a function of aspect ratio and incidence. Using Stratford's method to predict signs of flow separation in the inviscid solutions, I found that variations in the height above the ground were not significant enough to change the stall angle of low aspect ratio wings. I did find early signs of flow separation with increasing aspect ratio. I observe significant changes in spanwise loading when in ground effect; as I narrow the gap, the transverse loading builds higher near the center of the wing. These effects were more apparent in wings with smaller aspect ratio; higher aspect ratio wings experience a higher loading gradient near the tips in proximity to the ground. I found that high aspect ratio wings have a smaller stall angle compared to that of lower aspect ratio wings; these trends are consistent between the potential flow solution and the volume grid CFD viscous solution.

DEDICATION

This thesis is dedicated to my loving parents, Rosy Archuleta de Valenzuela and Jose Luis Valenzuela, and my brother beloved Luis Roschel Valenzuela, for all the sacrifices they have made to support my educational goals and self-improvement. None of this would have been possible without them. I will always thank you and cherish all your love and care.

ACKNOWLEDGMENTS

I would like to express my deepest gratitude and a special thanks to Professor Dr. Takahashi for his unwavering support and guidance throughout the entire process of completing this thesis and undergraduate education. None of this work would have been possible without his invaluable mentorship, input, and encouragement. His expertise, patience, and dedication have been instrumental in shaping the outcome of this research. I am truly fortunate to have had such an inspiring mentor and friend by my side. I am deeply honored to have had the opportunity to work alongside Professor Dr. Takahashi.

TABLE OF CONTENTS

Page

CHAPTER Page

APPENDIX

LIST OF TABLES

Table Page

LIST OF FIGURES

Figure Page

Figure Page

Figure Page

Figure Page

Figure Page

Chapter 1: Introduction

Aircraft pilots feel the “ground effect” when they fly in close proximity to the earth’s surface. They note changes in lift, pitching moment and drag. While conventional aircraft experience ground effect only during takeoff and landing maneuvers, specialized vehicles may be designed to exploit ground effect. Among flying machines, Russian engineers developed a series of Ekranoplan’s, from the Russian экранопла́н, to rapidly fly over the Caspian sea. These sea planes exploit the increase in usable lift-coefficient and reduction in lift-induced drag found in ground effect to have a “cruise” altitude measured in dozens not thousands of feet; see Figure 1.

Figure 1. A-90 Orlyonok Ekranoplan [1]

Among ground machines, race car designers exploit the ground effect to produce high downforce generating wings to improve steering and braking traction, such as the aerodynamic surfaces found in race cars found in Formula 1 racing, see Figure 2.

Figure 2. Red Bull Racing – 2023 Sergio Perez, RB16B Formula One car with high downforce front wing [2]

Some experts claim generally that the stalling angle of attack is less in ground effect, by approximately 2–4-°, than in free air. [3] Of course, if the flow over a wing separates lift will decline and drag will increase. Some aircraft can rotate so nose high on the ground that they can stall their main wings before tail strike. Under such an over-rotation event, an aircraft might never leave the ground. For example, the early De Havilland Comet jetliner had a recommended takeoff attitude of a=6° incidence; its wing would stall if it were pitched to α = 9°. Under those conditions, the aircraft could easily overrun the runway. [4]

Alternatively, with higher thrust an aircraft might well leave the ground with a partially stalled wing. During certification testing of the Gulfstream G650, the test pilots over-rotated on the ground pitching the nose up passed the predicted “In-Ground-Effect” stall point. The G650, with tall landing gear, had a tail strike angle-of-attack far past its stall angle-of-attack. When the aircraft became airborne with one wing stalled, the resulting uncommanded roll led to a fatal crash. [5] See Figure 3.

Figure 3. Remains of the flight-test Gulfstream G650 after pilots continued takeoff with an in-ground-effect stalled wing [5]

Given this background, I set out to obtain a better understanding of the underlying mechanics of ground effect. In this thesis, I investigate the influences of different wing characteristics in proximity to the ground. I document the effects of incidence, aspect ratio with varying heights above the ground and compare the results with known equations used for ground-effect aerodynamics. In addition to changes in total lift, and total drag, I also studied how the height above the ground impacts the nuanced pressure distribution of the wing and affects flow separation. Among the many research goals, I sought out whether stall onset generally occurs at higher or lower angles of attack in ground effect.

Chapter 2: Potential Flow Modelling Strategies

2.1 Introduction to VORLAX

This thesis uses the legacy inviscid panel method code VORLAX to simulate wings under different conditions. VORLAX is a generalized vortex lattice method that creates an approximation of the surface vorticity of a wing by solving a discrete vortex lattice. VORLAX was initially created by Luis Miranda, Robert D. Elliott, and William M. Baker, while at Lockheed under a NASA contract.[6]. VORLAX was later refined and enhanced by TJ Souders along with co-author Takahashi.[7]

Panel method codes are a type of numerical method used for CFD simulations that discretize the boundary of an object into a series of panels. These panels are then used to approximate the behavior of fluid flow around the object, allowing for the calculation of various properties such as pressure and velocity. VORLAX only requires a discretization of the object's surface, rather than the entire fluid domain, resulting in a more efficient set-up process.

2.2 Using VORLAX to Predict Ground Effect

Another capability of VORLAX is that it can also simulate flows in ground effect. VORLAX, while limited as an inviscid code, has unique capabilities for this type of research. Since VORLAX can model both double-impermeable (thin) lifting surfaces as well as single-impermeable (sandwich panel, or "thick") lifting surfaces, it can help determine what effects are attributed solely to the incidence and camber of a finite lifting surface in proximity to the ground, and what other effects stem from thickness. For the purposes of this thesis, VORLAX's compressibility corrections and supersonic capabilities are not used. In this thesis I use both the VORLAX "thin lifting surface" and sandwich panel" features to solve for the pressure distribution over the surface of the wings; see Figure 4.

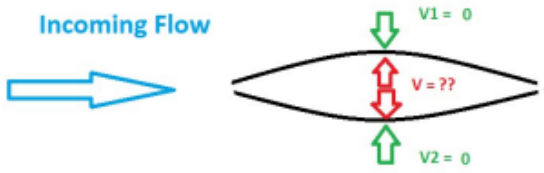

Figure 4. VORLAX Sandwich Panel Formulation

VORLAX "in ground effect model" is a critical element used in this thesis. VORLAX models "ground effect" by generating a fictitious "image plane" through the automatic generation of "reflected" companion panels. The *HAG* ("height above the ground") flag controls the distance separating the real model from the "reflected" companion model; the code input governs the distance separating the moment-reference-center of the primary model from the moment-reference-center of the "reflected" companion; see Figure 5. It is possible for the user to generate nonsensical geometry if the primary model is placed in close proximity to the "image plane" and then modeled at high angles of attack. Physically this would represent a solution where part of the real wing would cross the ground plane.

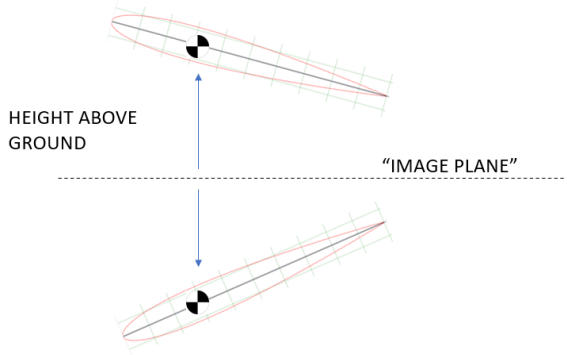

Figure 5. VORLAX "In Ground Effect" Model

2.3 Predicting Flow separation with an Inviscid Panel Method

The generalized vortex lattice method is a potential flow model; hence it lacks any ability to model shock waves or flow separation. Lacking a viscous model, VORLAX cannot directly estimate skin friction drag. With the relatively coarse sandwich panel meshes employed here, I also note that VORLAX pressure drag computations will not be very accurate, as leading-edge-suction effects are poorly resolved. For thin panels, VORLAX uses Lan's method to analytically estimate leading-edge suction.

I understand that the trust range of VORLAX includes almost any geometry so long as the predicted pressures do not exceed the shockwave producing critical pressure coefficient for a swept, finite wing and do not imply separated flow conditions.

This thesis looks at the small and moderate angle-of-attack response of finite wings in ground effect. For the purposes of this research, I consider the primary application to be for downforce generation on a race car. I address stall onset though viscous volume grid CFD results as a well as through the use of the Stratford Criteria used to interrogate the inviscid pressure predictions made by VORLAX. [8][9]. I later discuss more about Stratford's criteria for flow separation in the procedure section.

Chapter 3: Introduction on Ground Effect and Experimental Setup

3.1 General Observations on Spanwise Flow

The generally accepted understanding of finite wings is that the chordwise flow on the wing creates a difference in pressure; when it generates lift, there are lower pressures over the top surface than the bottom surface. This difference in pressure is what creates a net force upwards which creates lift. This difference in pressure extends across the span to the wing tips. As a result, the slight difference in directions in the flow creates vortices extending downward and behind the wing. This is referred to as the vortex wake. Thus, the resultant angle of attack known as the geometric angle of attack is the sum of the "effective" angle of attack and the induced angle of attack. Consequently, the direction of the lift component is effectively changed creating a horizontal body force component known as induced drag also known as drag due to lift. This was first noticed by Wieselsberger where he defined the change in angle of attack as a reduction in C_l required to achieve a given coefficient of lift.[10][11]

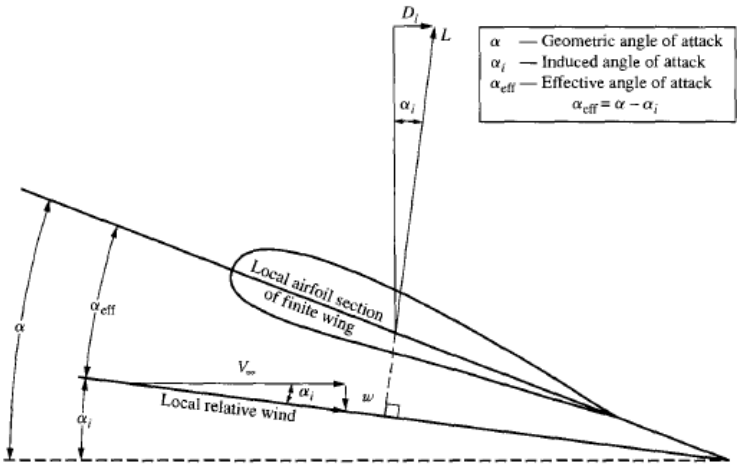

Figure 6. Changes in angle of attack creating induced drag due to local flow in the wing [20]

Figure 7. Picture of a commercial aircraft where wing tip vortices are visible [23]

3.2 Modeling Ground Effect procedures and the Method of Images

Wings that are in proximity to the ground can experience a reduction in induced drag, and other changes in their aerodynamic loads. VORLAX uses the method of images to calculate the ground effect for wings in proximity to the ground. The influences of "ground-effect" in a wing are normally studied by comparing the coefficient of induced drag in free air with the coefficient of induced drag close to the ground hence in ground effect. According to McCormick, downwash velocities decrease when the airplane is operating close to the ground [12]. Since the ground is a solid boundary to which the normal component of velocity must vanish, its presence alters the streamline pattern that exists around the airplane out-of-ground effect. McCormick (as does Miranda) places a companion vortex system opposite to the wing at distance equal to twice the height of the airplane above the ground; refer to Figure 5. [12][6] Thus, midway between the two systems, their induced velocities in the vertical direction will cancel, satisfying the boundary condition along the ground. Similarly, Torenbeek created a two-dimensional analysis of the flow field resulting from the airfoil in free-air

and the induced velocity distribution created by the vortices formed by the image vortices below the ground.[13]

Using the legacy inviscid panel method code, VORLAX, I can now look more closely into changes in the spanwise lift distribution (bound vorticity) and chordwise pressure profiles (leading edge suction) developed by finite wings in ground effect. From these solutions, I can better understand how and why aggregate aerodynamic properties change. I also documented how chordwise pressure profile changes impact stall-onset and help understand how detail design features may aid or hinder both the maximum lift coefficient (Cl_{max}) and the maximum angle-of-attack before stall (α_{max}). Finally, I use ANSYS FLUENT to verify the inviscid observations.

I started my investigation of the ground effect characteristics of race-car wings by using a flat plate model in VORLAX with a rectangular wing with approximately the surface area of the 2020 F1 regulation wing as a starting reference point [14]. In addition, the results were modeled at Mach 0.21, which is approximately 150 mph at sea level, this is a representative of an average cruising speed in the straights. However, the results from this research can also be applied towards any type of wing at low subsonic speeds in which aircraft normally approach runways during takeoff- and landing.

Figure 8. Picture of an F1 car where wing tip vortices are visible [24]

The Reynolds Number used in the viscous CFD calculations is based on this reference speed at sea level.

To make this study more general yet, I investigated the effects that aspect ratio has on ground effect as applied to wing dimensions beyond those of a racecar. As a result, different simulations were performed where *AR* was doubled with each iteration with various distances above the ground as a function of the chord length, and by varying the *HAG* to span ratio. The distance above ground at the moment reference center is input in VORLAX using the "HAG" variable to denote the height above the ground and thus enabling ground-effect.

Chapter 4: Spanwise Efficiency and Induced Drag

Equation (1) shows how the coefficient for induced drag is computed. Where the maximum Oswald efficiency is defined as that of a wing with elliptical load distribution on free air as shown in equation (2). Using equation (1) and equation (2) is possible to find the measured efficiency of the wing as the ratio of the measured induced drag with the ideal induced drag as shown in equation (3).

$$CD_i = \frac{CL^2}{\pi ARe} \tag{1}$$

$$CD_{ideal} = \frac{CL^2}{CD_i \pi} \tag{2}$$

$$e = CD_i / CD_{ideal} \tag{3}$$

Where the aspect ratio of the wing is:

$$AR = \frac{b^2}{S_{ref}} \tag{4}$$

The aspect ratio can also be represented as:

$$AR = \frac{b}{c} \tag{5}$$

The lift influence in ground effect was found using equation (6) as the ratio of the coefficient of lift at some *HAG* over the coefficient of lift on free air. The induced drag influences were measured using the ratio of the induced drag coefficient over the square of the coefficient of lift in proximity to the ground over the same ratio in free air, as shown in equation (7). The overall ground effect influence is measured using equation (8).

$$Lift\ Ground\ Effect\ Influcence = \frac{[C_L(\alpha)]_h}{[C_L(\alpha)]_\infty} \tag{6}$$

$$Induced\ drag\ ground\ effect\ influence\ = \frac{\left(\frac{C_{Di}}{C_L^2}\right)_h}{\left(\frac{C_{Di}}{C_L^2}\right)_\infty} \tag{7}$$

$$Ground\ effect\ influence\ = \frac{\left(\frac{Cl}{C_L^2}\right)_h}{\left(\frac{C_{Di}}{C_{Di}^2}\right)_\infty} \tag{8}$$

I will compare the computational results with published equations such as McCormick's equation (9), Hoerner & Borst equation (10), Torenbeek (11) and the updated Torenbeek equation (12). The estimate the induced drag on wings as shown on [16].

McCormick:

$$\frac{(C_{Di}/C_L^2)_h}{(C_{Di}/C_L^2)_\infty} = \frac{(33h/\pi\ \mathrm{b})^{1.5}}{1 + (33h/\pi\ b)^{1.5}} \tag{9}$$

Hoerner & Borst:

$$\frac{(C_{Di}/C_L^2)_h}{(C_{Di}/C_L^2)_\infty} = \frac{(16h/\mathrm{b})^2}{1 + (16h/b)^2} \tag{10}$$

Torenbeek:

$$\frac{(C_{Di}/C_L^2)_h}{(C_{Di}/C_L^2)_\infty} = 1 - \exp\left[-2.48\left(\frac{2\mathrm{h}}{\mathrm{b}}\right)^{0.768}\right] \tag{11}$$

Torenbeek later updated his equation to account for changes in aspect ratio. Equation (11) shows Torenbeek' s updated version to calculate the influences of induced drag as a function of *AR* and the coefficient of lift [13].

$$\frac{(C_{Di}/C_L^2)_h}{(C_{Di}/C_L^2)_\infty} = \frac{1 - \exp\left[-2.48\left(\frac{2\text{h}}{\text{b}}\right)^{0.768}\right]}{1 - \beta C_L/(\frac{4\pi ARh}{b})} \tag{12}$$

$$\text{Where: } \beta = \sqrt{1 + \left(\frac{2h}{b}\right)^2} - \frac{2h}{b}$$

Later Valenzuela & Takahashi created equation (13) to fit the results. [26] started with a similar form as Torenbeek's equation but with updated coefficients, and a power β that is terms of both the aspect ratio and the angle of attack to better fit the results found with VORLAX.

Valenzuela & Takahashi propose:

$$\frac{(C_{Di}/C_L^2)_h}{(C_{Di}/C_L^2)_\infty} = 1 - \exp\left[-2.6\left(\frac{2\text{h}}{\text{b}}\right)^{\beta}\right] \tag{13}$$

$$\text{Where: } \beta = -0.09\ln(\text{AR})\sec(-5.5\alpha(\text{rad})) + 0.84$$

Chapter 5: Predicting Incipient Flow Separation Through Stratford's Method

In this chapter, I modelled pressure distributions using a "Sandwich" panel in VORLAX where two thin sheets are used to define the top and lower surface of an airfoil. For this study I model a symmetrical NACA 0012 airfoil with zero camber. While VORLAX is a useful tool for design due to ease of setup and quick execution, being an inviscid code, it cannot directly predict flow separation. That is why I incorporated Stratford's method to predict signs of early flow separation.

According to Prandtl, flow separation occurs by excessive momentum loss near the wall in a boundary layer trying to move downstream against an adverse pressure gradient. Thus, due to this rapid deceleration of the flow usually at the top surface for a conventional lifting airfoil and aft of the airfoil the flow detaches from the wing creating vorticity and an area of low pressure. This drastically reduces the performance of the wing, which is why it is important to obtain a deep understanding of conditions when flow separation starts to occur.

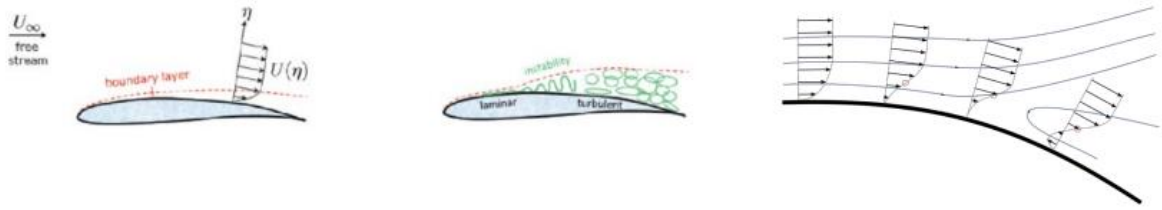

Figure 9. Diagram of Boundary Layer with Flow Separation Onset [25]

There are multiple methods for predicting flow separation with different approaches such as by creating a boundary layer analysis such as in Thwaites Method, doing a boundary layer stability analysis, using flow visualization techniques, doing wall shear stress separation method, or using fundamental principles of fluid mechanics such as with the Kutta-Joukowski Criterion. Each of these methods comes with its own set of advantages and disadvantages. For this investigation I used Stratford's method since it is considered to provide an accurate prediction of flow separation regions based on local skin friction coefficients, it can be applied on flat plate geometries, and it has relatively low computational cost compared to other more demanding methods. Additionally, it doesn't

require a detailed knowledge of the boundary layer. Stratford's method is a means to predict when and where flow will start to separate based on the nuance of an inviscid pressure distributions. [28] and [29]. Stratford's Equation to predict flow separation is shown below in equation (14) as shown in [8] and [17]. Where "*x*" is the distance from the leading edge to the trailing edge of the airfoil, and $\overline{C_p}$ is the coefficient of pressure in canonical form as shown in equation (15) and equation (16). Then, the derivative of the coefficient of pressure distribution was estimated using forward difference. Lastly, the Reynolds Number was calculated using standard atmospheric conditions at sea level and a Mach number of 0.21.

$$S = \frac{\overline{C_p}\left[x\left(\frac{d\overline{C_p}}{dx}\right)\right]^{\frac{1}{2}}}{(10^{-6}Re)^{\frac{1}{10}}} \tag{14}$$

$$\overline{C_p} = \left(\frac{u_\infty}{u_0}\right)^2 \left(C_p - 1\right) + 1 \tag{15}$$

$$\overline{C_p} = \frac{C_p - C_{p_{min}}}{1 - C_{p_{min}}} \tag{16}$$

Canonical pressure distributions can be useful for separation analysis. To change the pressure distribution to canonical form I used equation (16); the "canonical pressure distribution" is equal to zero at the point of peak suction in standard form. In addition, the stagnation point of the airfoil is clearly shown in canonical form where the coefficient of canonical pressure is equal to 1. "The canonical plot is the one that is meaningful in separation analysis. With magnitude effects scaled out, much more can be told by a simple inspection than by a conventional plot. We dwell on the canonical pressure distribution at some length because most working aerodynamics do not realize its value" [8]. Therefore, using equation (16) and equation (14) is possible to obtain the value for *S* from Stratford's equation. According to Stratford, when the *S* parameter exceeds 0.39, the flow cannot

remain attached. Using this metric, is possible to estimate the percentage of the chord length where flow first separates.

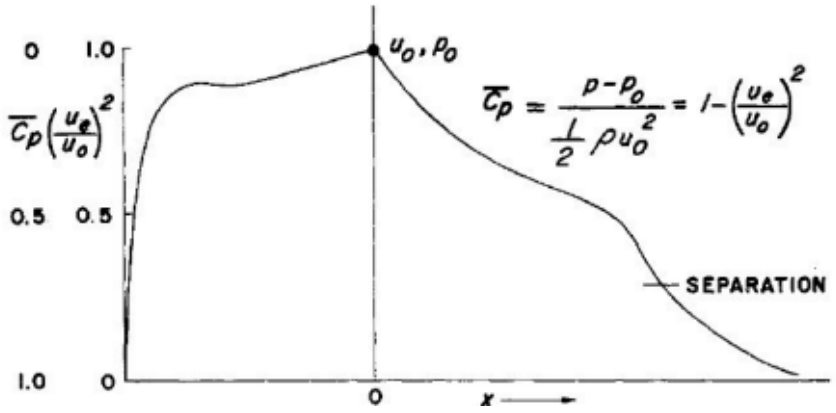

Figure 10. Example Pressure Distribution in Canonical Form [8]

Chapter 6: Predicting Lift, Drag and Incipient Flow Separation through Volume Grid Viscous CFD

Next, I compared the results from VORLAX with CFD based results obtained with ANSYS FLUENT. A NACA 0012 wing was subjected to a virtual wing tunnel in ANSYS FLUENT in which I was able to change the wing and tunnel characteristics, such as, the wing aspect ratio, chord length, incidence, and the height above the ground. I simulated a flow of approximately 156 mph (70-m/s), which could be considered the average speed of racecars. Trade studies were computed using a wing with an aspect ratio of 1.98, 3.96, and 7. 92, and multiple variations of the height above the ground. The flow was initialized at the inlet and in the *x*-direction (chordwise direction) of the wing tunnel.

I modeled the wing tunnel as a rectangular volume enclosing the airfoil, with the length of the sidewalls as 55% longer than the span of the airfoil. I consider this distance to be far enough to minimize wall interference in the airfoil while still capturing important characteristics of some of the flow's wake for analysis. The top wall was modeled as being far from the airfoil to minimize interference. The bottom wall height was varied to measure the ground effect influences. Next, I varied the wing's aspect ratio, incidence and the height above the ground and conducted multiple trade studies. To change the height above the ground I changed the positioning of the wing with respect to the wing tunnel. The reference height above the ground was measured with respect to the leading edge of the airfoil while keeping track of the distance from the aerodynamic center of the airfoil.

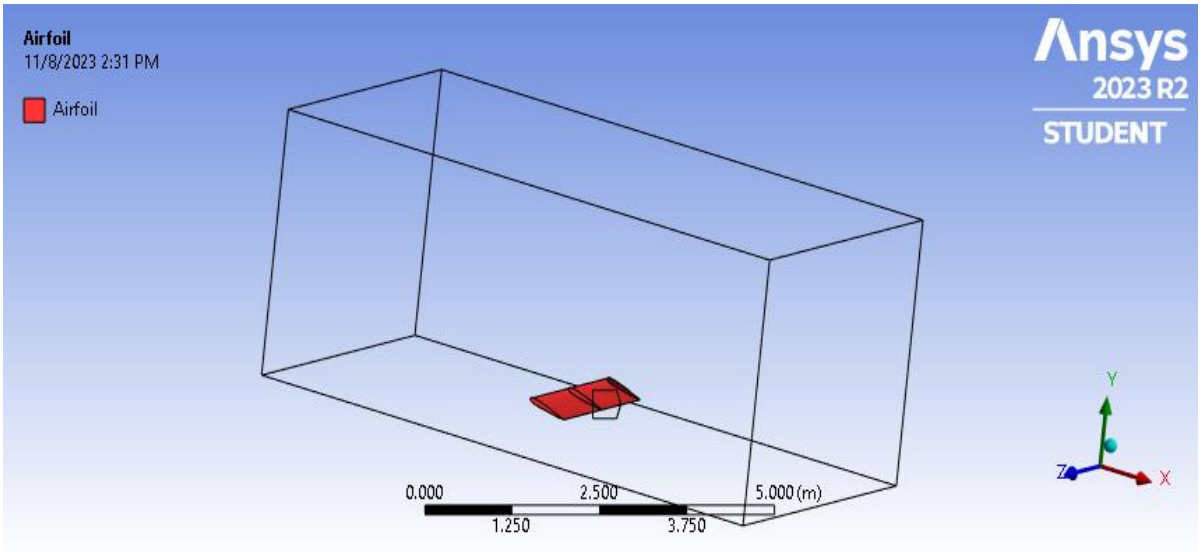

Figure 11. ANSYS Fluent Wing Model

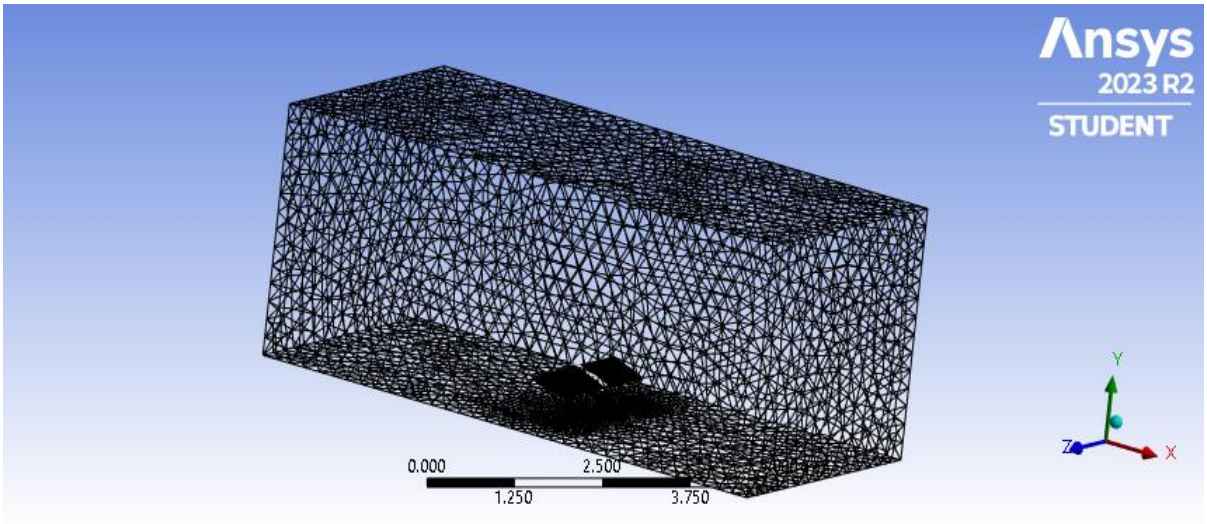

Figure 12. ANSYS Fluent Mesh

I modeled the flow in ANSYS Fluent using a pressure based $k-\omega$, SST model, with the "no turbulent viscosity" setting. The term "no turbulent viscosity" in ANSYS Fluent does not imply that there is no turbulence in the flow; rather, it refers to a particular way ANSYS Fluent solves eddy viscosity in the turbulent model. I chose the $k-\omega$, SST model since it is believed to perform slightly

better than the standard $k-\epsilon$ in near-wall flows of boundary layers and adverse pressure gradients but may lead to worse results in turbulent flows that are far away from the walls.

The $k-\omega$ model derives from the standard $k-\epsilon$ model, a very common turbulence model. The standard $k-\epsilon$ where k stands for the turbulent kinetic energy and ϵ refers to the turbulent dissipation rate in the eddy viscosity expression $v_T = C_\mu \frac{k^2}{\epsilon}$. It is known as a "two-equation" model since it consist of a linear equilibrium closure for the Reynolds stresses $\overline{u_i' u_j'}$ along with modeled transport equations for k and ϵ resulting in mean flow continuity and momentum equations, the gradient transport hypothesis and two additional transport equations for k and ϵ to obtain the eddy viscosity v_T. [27] While the $k-\epsilon$ is currently one of the most widely used models in CFD, depending on the software, there may be some variations in the five constants used for closure in the set of equations in the model. Certain models may use a different set of such constants to optimize the results depending on the application. The $k-\omega$ model, Shear Stress Transport (SST) is an extension of the $k-\epsilon$ that instead of working in terms of ϵ introduces the adverse turbulent time scale term $\omega \sim \frac{\epsilon}{k}$ thus the resulting eddy viscosity is given by $v_T = \frac{k}{\omega}$. The SST model employs the $k-\omega$ formulation in the inner region of the boundary layer where the flow is predominantly viscous-dominated and then switches to the $k-\epsilon$ model in the outer region where the flow becomes inertial dominated.

With this hybrid approach, I believe that these settings improve the performance of the model, especially in applications in the vicinity of walls. Considering that in this thesis the ground effect is being investigated which consists of near the wall flows I consider that the $k-\omega$, SST model is the most optimal option for this research.

The boundary conditions were modeled as having the inlet as the absolute reference point and moving walls having the same velocity as the flow. I computed the model with fifty iterations for each trade study. The chord length was used as the reference length, and the product of the chord and span as the reference area as shown in equation 20. I chose an edge sizing of 120 divisions with a default growth rate of 1.2 and a local minimum size of $2.8 * 10^{-3}$ m. In addition, I added an inflation

mesh around the body. The boundary conditions were set up with an automatic time step, a conservative length scale method and a verbosity of 0. The inlet and outlet were selected with an absolute reference frame, with a specification method of "Intensity and Viscosity Ratio" with a turbulent intensity percentage of 1 percent and a turbulent viscosity ratio of 10. The boundary conditions at the airfoil were set up as a stationary wall with a "No slip" shear condition with a standard roughness. Finally, the boundary conditions at the walls were set up as a moving wall, with absolute motion with a translational velocity in the x-direction with the same velocity magnitude as in the inlet.

$$a = \sqrt{\gamma RT} \tag{17}$$

$$M = \frac{\mu_\infty}{a} \tag{18}$$

$$Re = \frac{\rho v L}{\mu} \tag{19}$$

$$S_{ref} = b\, c \tag{20}$$

To compare the results using VORLAX I calculated the approximate Mach number for the wing by using equations (17) and (18), with the designated flow speed 155-mph (70-m/s) with a speed of sound of ~760-mph (340.17-m/s) found using standard atmospheric conditions at sea level; this reflects operation at M~0.21, which was used in VORLAX. The Reynolds Number was calculated using equation (19) with the wing operating at Re~$2.97x10^6$.

Chapter 7: Results

In this chapter, I show the results obtained with VORLAX using a flat plate. Multiple trade studies were performed by varying the incidence angle of the airfoil, the aspect ratio, and the height above the ground.

7.1 Predicting Ground Effect through Flat Plate Panel Method Models (VORLAX)

Torenbeek postulated an equation that functions best for many types of wings that corrects for changes in incidence and aspect ratio by using a correction factor β. The induced upwash produced by the vortices from the image is usually expressed as a reduction of the angle of attack required to achieve a given C_L. [13]. That is precisely what it was observed since the slope of C_L vs α changed when the wing was in close proximity to the ground with a more significant variation found on small aspect ratios. The value for the slope was significantly smaller than two p per radian as predicted by thin airfoil theory at small aspect ratios with decreasing difference as the aspect ratio increased. This can be observed in Figure 13, 14, and 15.

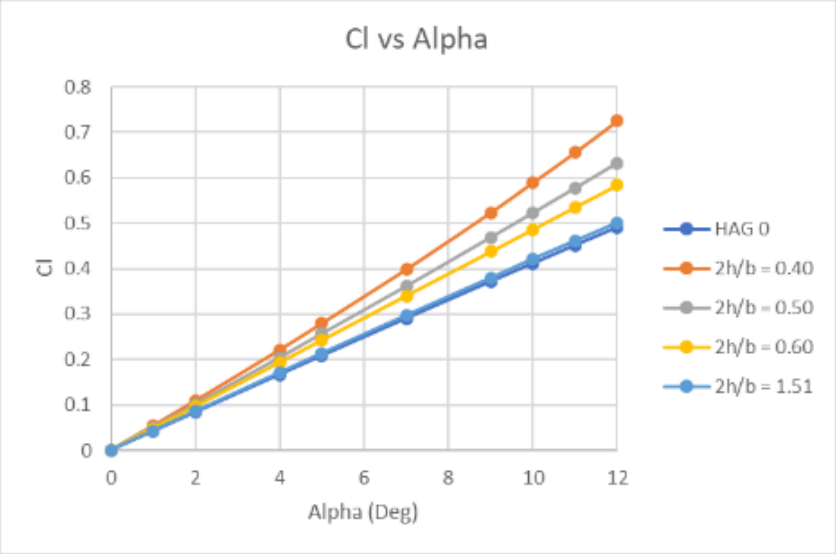

Figure 13. $Cl\ vs\ \alpha$ for varying height above the ground. AR = 1.98

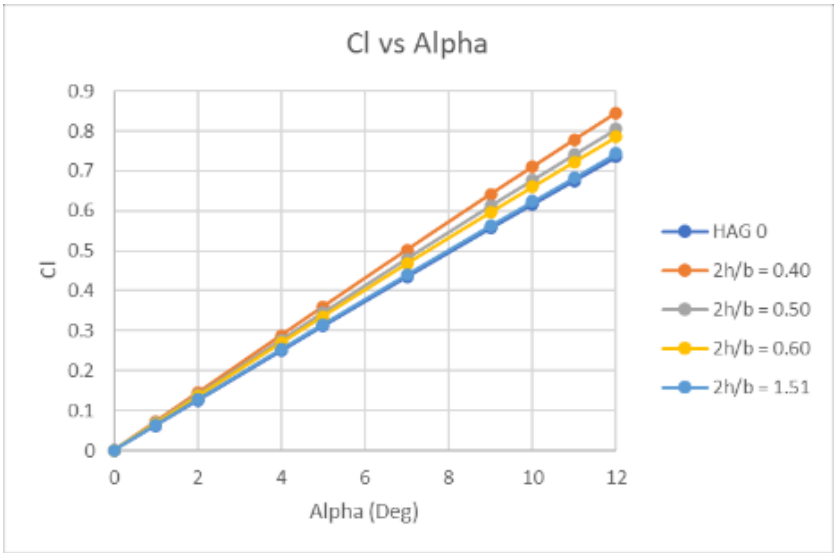

Figure 14. C_l vs α for varying height above the ground. AR = 3.96

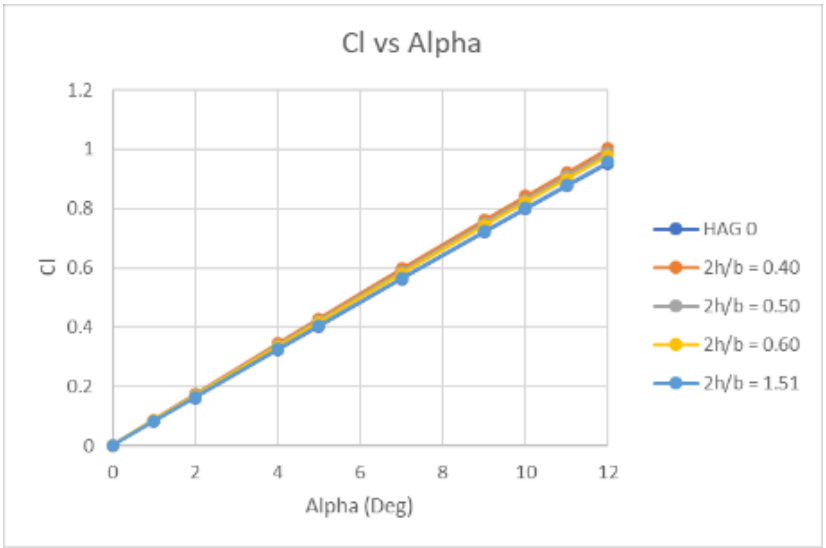

Figure 15. C_l vs α for varying height above the ground. AR = 7.92

Just as in the previous results shown, similarly I can observe a stronger variation on wings with a smaller aspect ratio in the coefficient of drag versus angle of attack as shown in Figure 16, and Figure 17.

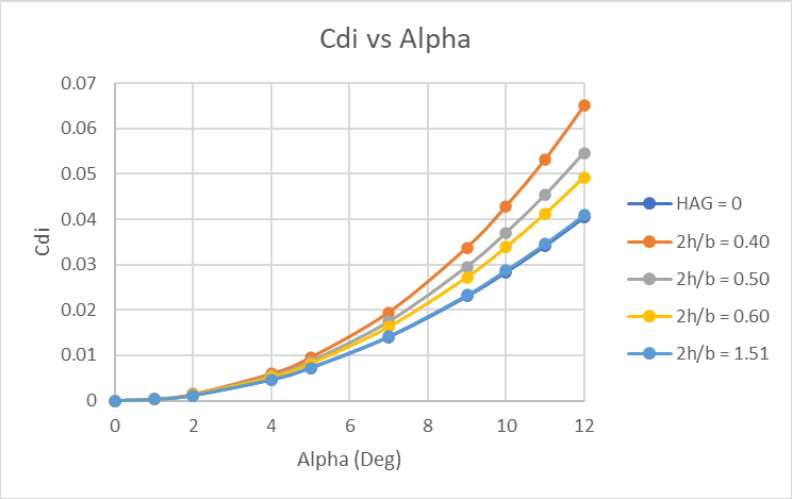

Figure 16. Oswald Efficiency vs α for varying height above the ground. AR = 1.98

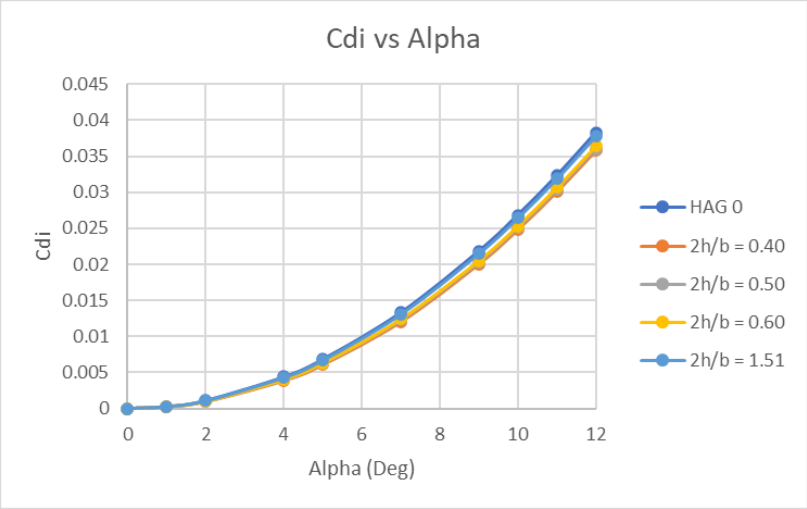

Figure 17. CD vs α for varying height above the ground. *AR = 7.92*

While the theoretical maximum Oswald efficiency is 1 for a wing with an elliptical loading, I can observe that for a wing experiencing ground effect the efficiency is higher than 1 which can be attributed to the increase in the coefficient of lift and the decrease in the coefficient of drag. This can be clearly seen in Figure 18, and Figure 19.

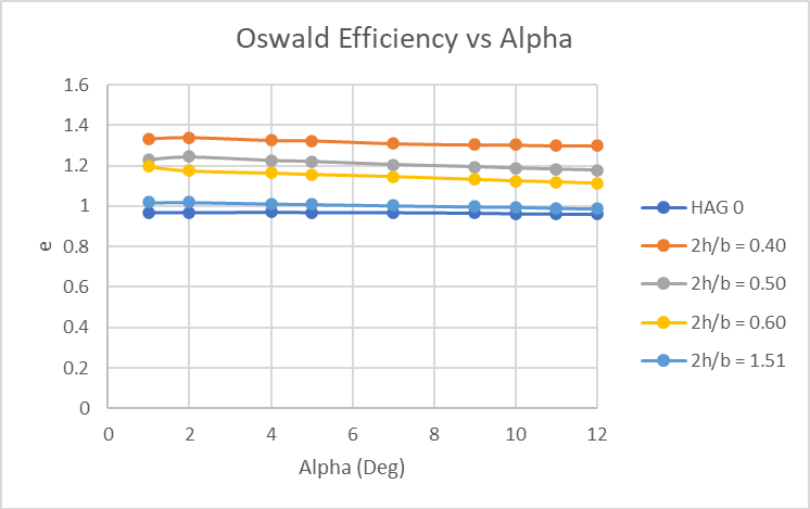

Figure 18. Oswald Efficiency vs α for varying height above the ground. AR = 1.98

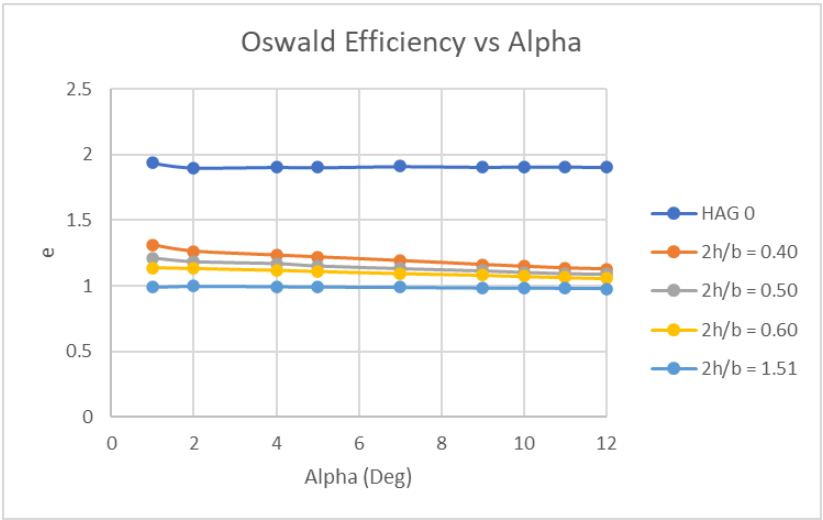

Figure 19. Oswald Efficiency vs α for varying height above the ground. AR = 7.92

Next, I looked at the ground effect influences on the coefficient of lift in free air over the coefficient of lift in ground effect ratio against the height above the ground. Similarly, I observe the ground effect influences on the coefficient of drag. This is shown in Figures 20 through Figure 25.

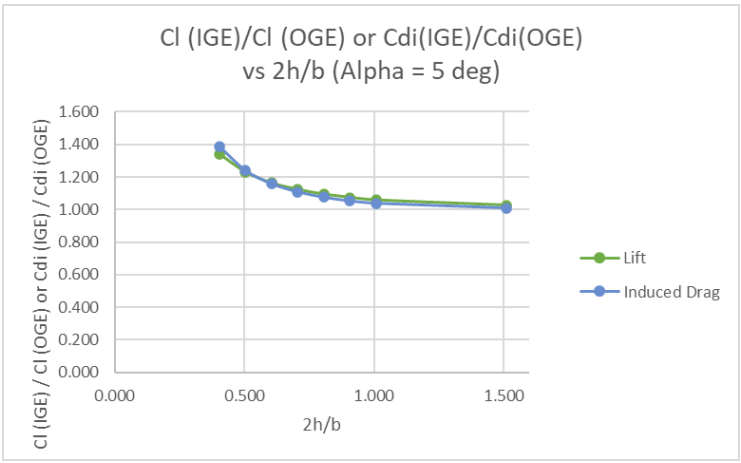

Figure 20. Ground Effect Influence vs height above the ground. AR = 1.98. α=5°

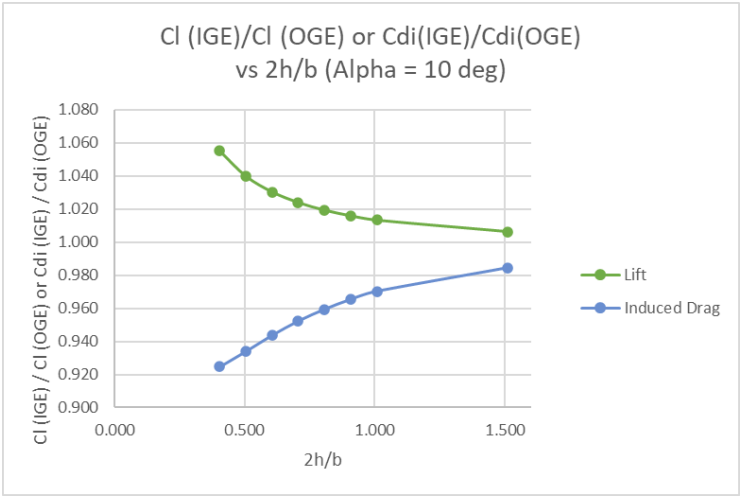

Figure 21. Ground Effect Influence vs height above the ground. AR = 1.98. α=10°

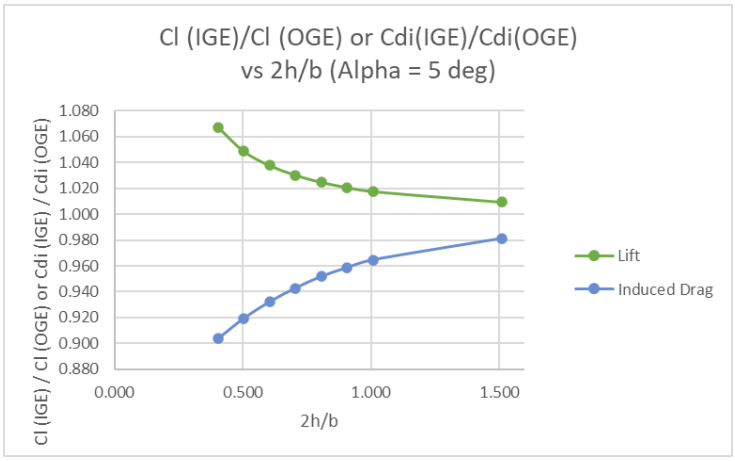

Figure 22. Ground Effect Influence vs height above the ground. AR = 3.96. α=5°

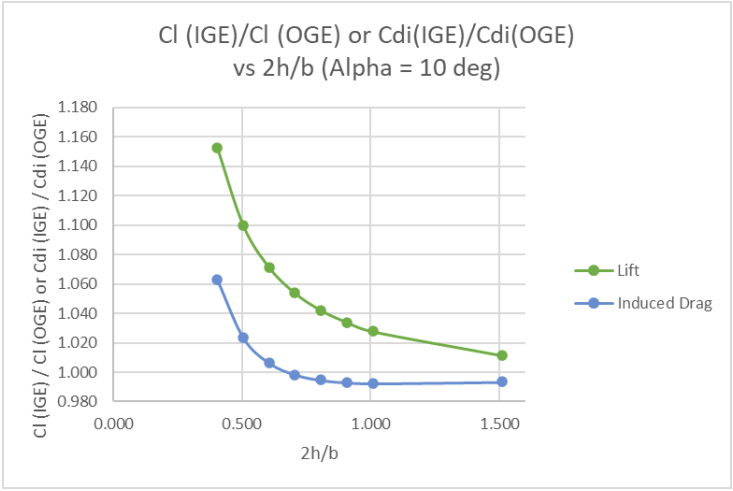

Figure 23. Ground Effect Influence vs height above the ground. AR = 3.96. α=10°

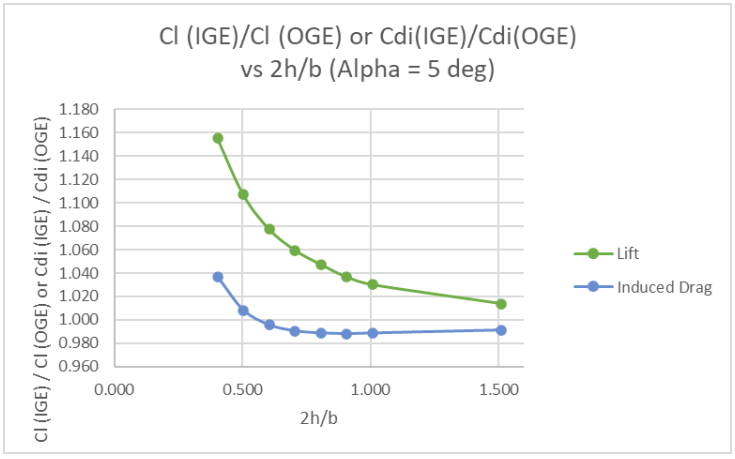

Figure 24. Ground Effect Influence vs height above the ground. AR = 7.92. α=5°

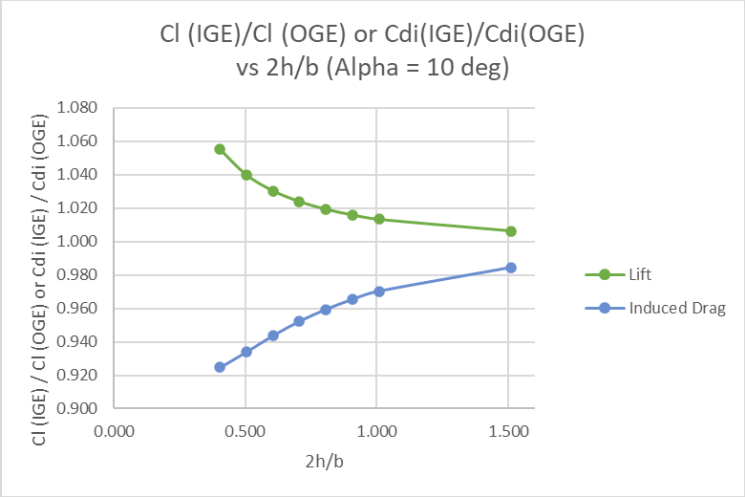

Figure 25. Ground Effect Influence vs height above the ground. AR = 7.92. α=10°

Furthermore, I can observe the changes in C_l and C_{Di} as a function of the height above the ground and span ratio on Figure 26, Figure 27, and Figure 28. Again, I observe a similar pattern with a stronger variation on wings with a smaller aspect ratio. Additionally, it was interesting to see that a smaller aspect ratio wing in ground effect at a higher angle of attack has almost the same lift and induced drag influence as that of a higher aspect ratio wing at a lower angle of attack. This can be observed in Figure 26. This agrees with the results shown in Figure 28 for the Oswald efficient versus the height against the ground. I can see how for wings close to the ground there is an increase in Oswald efficiency.

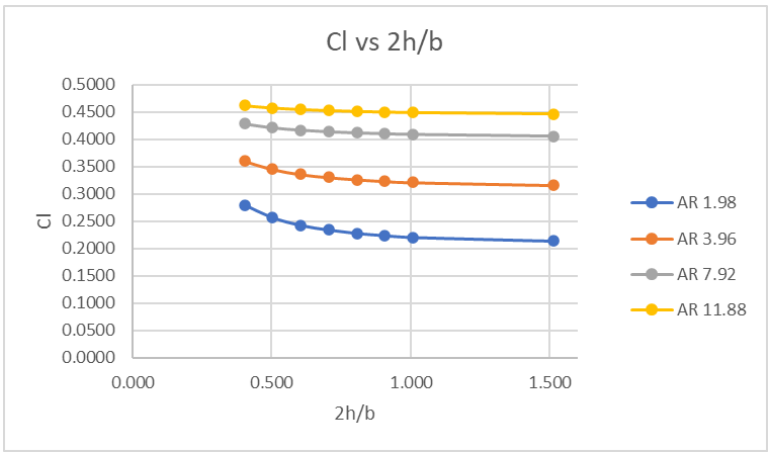

Figure 26. Ground Effect Influence on Cl vs height above the ground for multiple aspect ratio

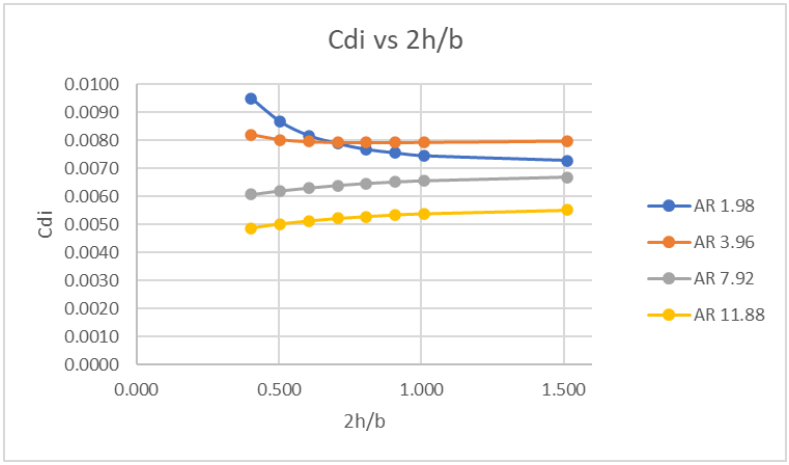

Figure 27. Ground Effect Influence on Cl vs height above the ground for multiple aspect ratio

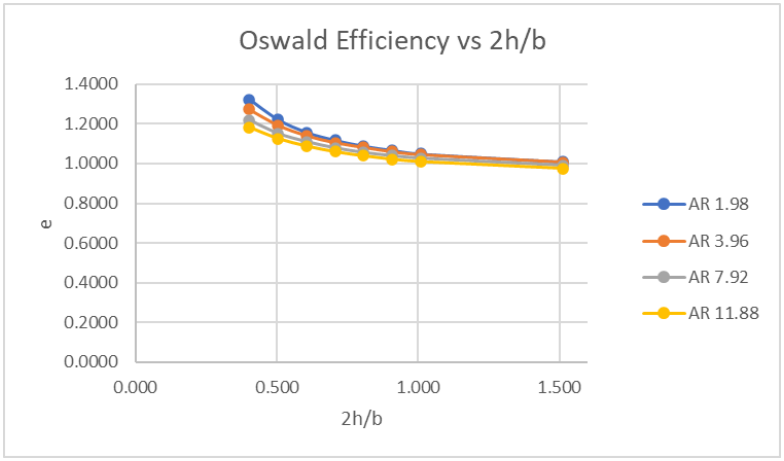

Figure 28. Oswald Efficiency, versus height above the ground for varying AR. α=5°

7.2 Comparison of Flat Plate VORLAX to Empirical Methods

Next, I compared the ground effect influence using equation (8) with the known equations, Equations (9), (10) and (12) for multiple incident angles and aspect ratios. The results are shown in Figure 29, through Figure 39. I can see that significant variations occur on the induced drag influence with increasing incidence and aspect ratios. While the ground effect influence increases with increasing aspect ratio, it appears that changes in aspect ratio are not as significant as they are with changes of incidence. Additionally, I can also see that changes in the ground effect influence are minimum for low aspect ratios. Next, Figure 29 through Figure 39 shows that at high angles of attack and high aspect ratios, the ground effect influence closely follows McCormick's equation. While Hoerner and Borst equation overpredicts the effect in all cases.

Torenbeek's equation seems accurate only when α<5- °. I also compared the results using the updated Torenbeek equation (12) with the correction factor equation (12) and in terms of CL and the AR. VORLAX results for high aspect ratios are better matched with Torenbeek's correction factor. Nevertheless, the updated Torenbeek equation overpredicts the simulated values at low aspect ratios.

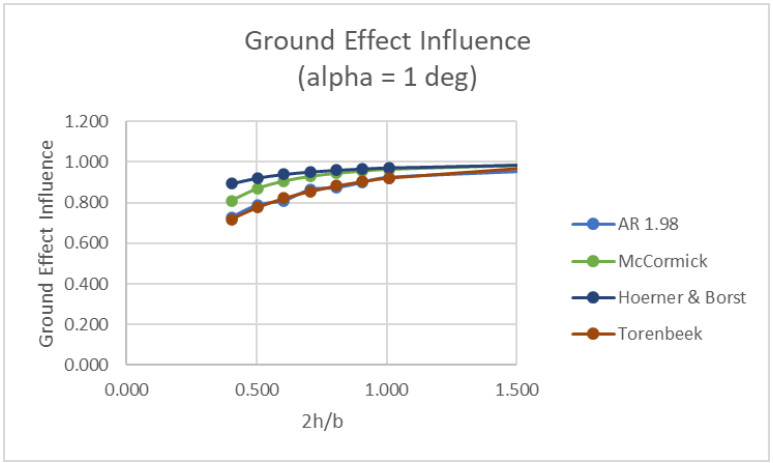

Figure 29. Induced drag influence versus height above the ground. AR = 1.98. α=1°

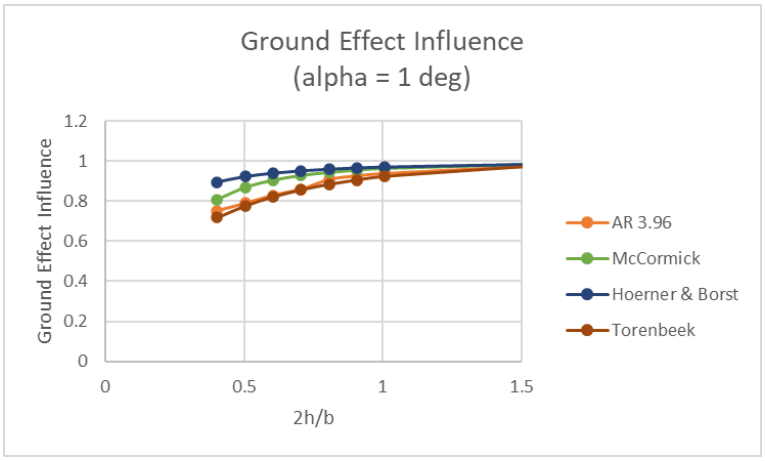

Figure 30. Induced drag influence versus height above the ground. AR = 3.96. α=1°

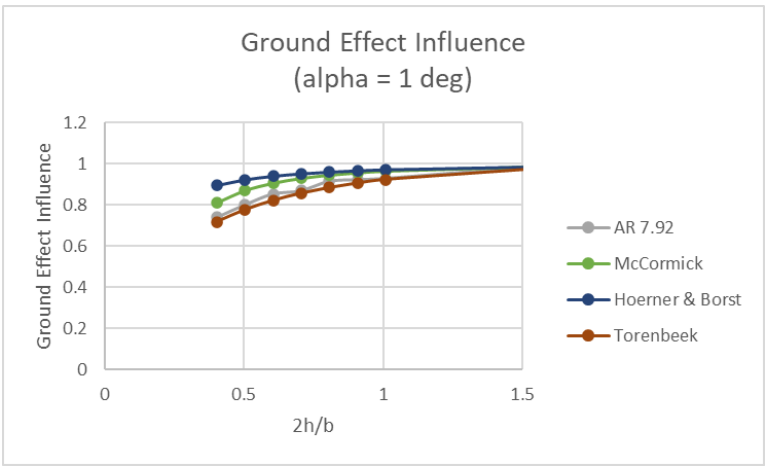

Figure 31. Induced drag influence versus height above the ground. AR = 7.92. α=1°

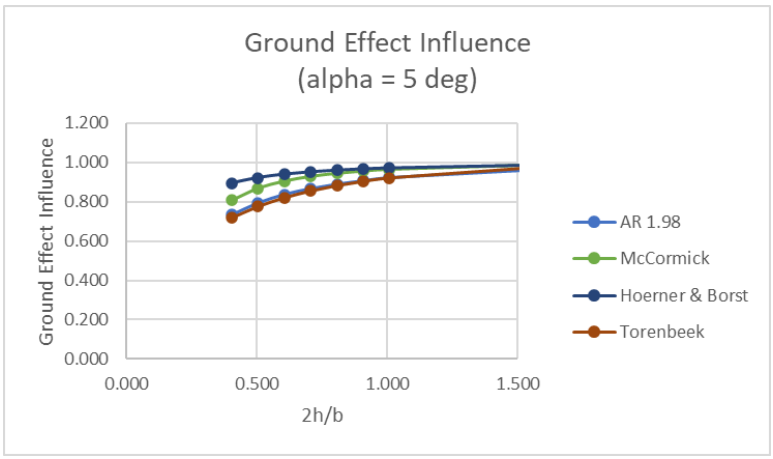

Figure 32. Induced drag influence versus height above the ground. AR = 1.98. α=5°

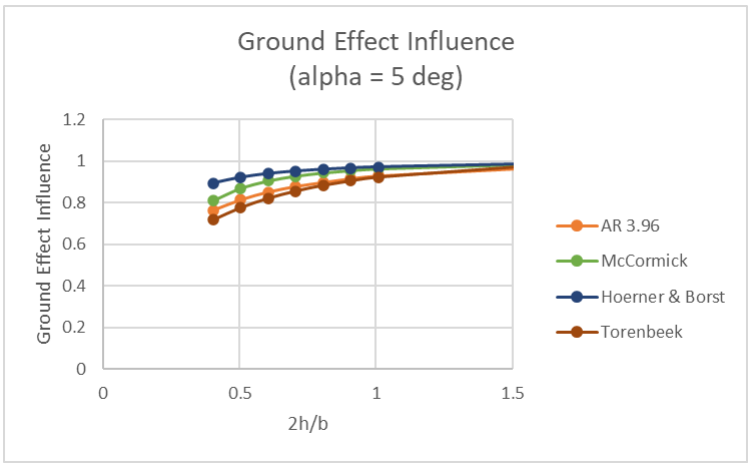

Figure 33. Induced drag influence versus height above the ground. AR = 3.96. α=5°

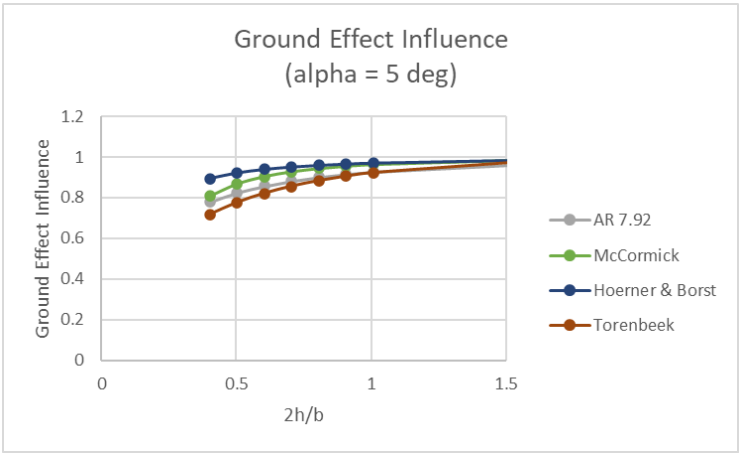

Figure 34. Induced drag influence versus height above the ground. AR = 7.92. α=5°

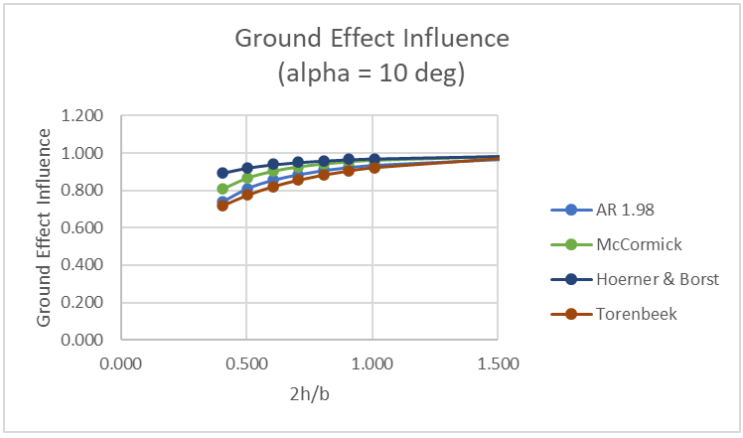

Figure 35. Induced drag influence versus height above the ground. AR = 1.98. α=10°

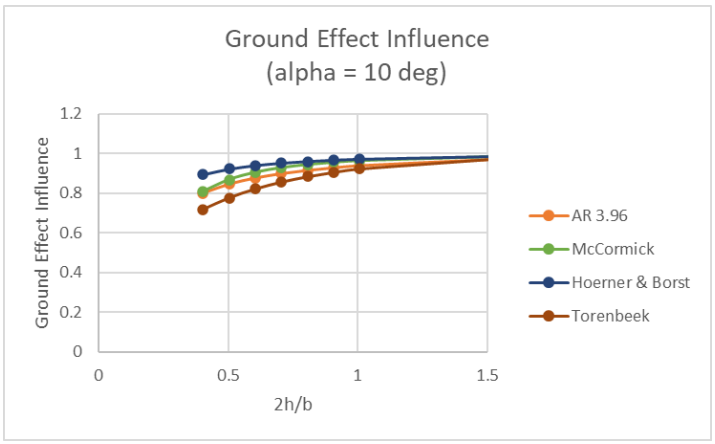

Figure 36. Induced drag influence versus height above the ground. AR = 3.96. α=10°

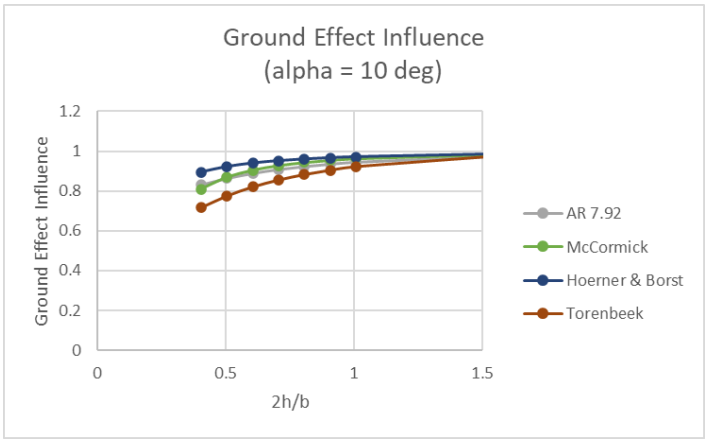

Figure 37. Induced drag influence versus height above the ground. AR = 7.92. α=10°

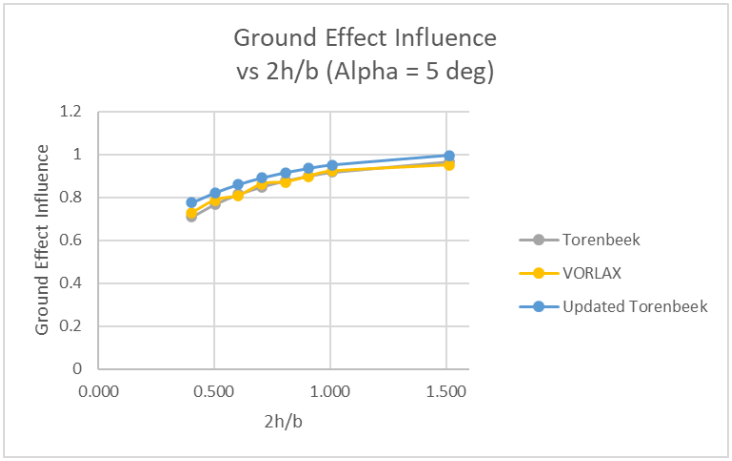

Figure 38. Comparison of Torenbeek's equation and Updated equation with correction factor $\boldsymbol{\beta}$. AR = 1.98

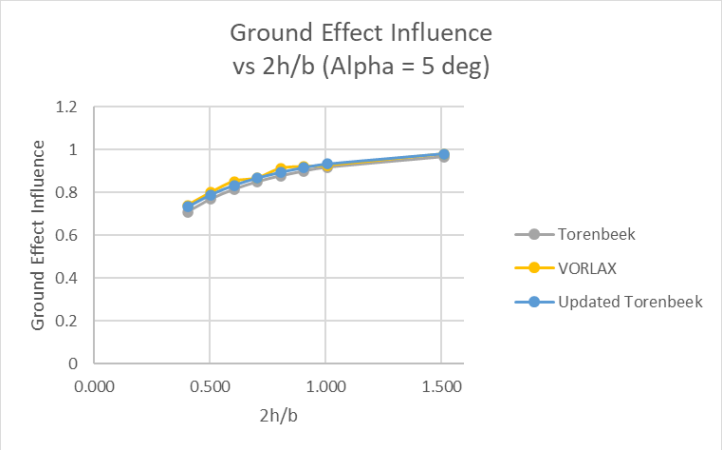

Figure 39. Comparison of Torenbeek's equation and Updated equation with correction factor $\boldsymbol{\beta}$. AR 15.84

Furthermore, VORLAX results seem to predict higher ground effect influence when the height above the ground to span ratio is small. While McCormick's equation has a sharper change for small h/b ratios it seems to slighly underpredict the data for small aspect ratios and then overpredict the data as the aspect ratio increases.

Additionally, from Figure 39 is possible to see that the ground effect influence on induced drag is small for small aspect ratios and incidence. This seems to suggest that a stronger ground effect influence is created on wings with higher aspect ratio due to influences in spanwise flow. This is as expected since circulation patterns are significantly different on wings with high aspect ratios compared to smaller aspect ratio wings. "As the wing chord is made longer and longer, it reaches into the space of the "fully" developed vortex system, thus interfering with its pattern: and the vortex field in turn affects the flow past the foil section" [10]. As a result lift production in wings on small aspect ratios comes mainly from the leading edge and thus changing the lift-curve slope with a smaller curvature than that predicted by lifting-line theory. Therefore, the flow on small aspect ratio wings differs from that predicted by 2-D flow thereby significantly changing the values for aerodynamic loading and hence induced drag and consequently ground effect influences. While the flow in high aspect ratio wings tend to have a more pronounce spanwise flow with smaller wing tip vortices.

Finally, from these previously shown figures is possible to see that as the aspect ratio increases changes in the ground effect influcence on lift and drag are less pronounce agreeing withprevious observations.

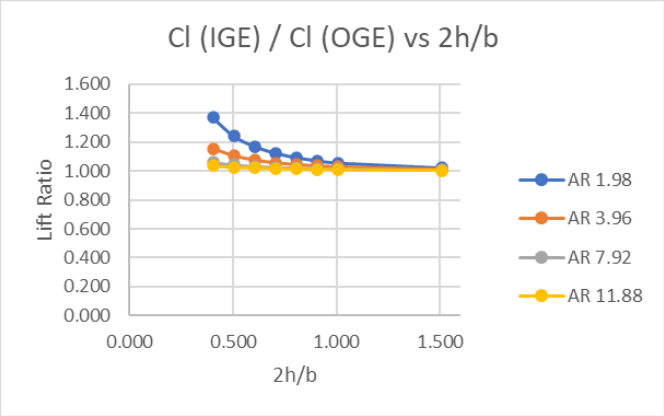

Figure 40. Lift and Induced Drag Influence vs 2h/b for multiple Aspect Ratios. AR = 1.98

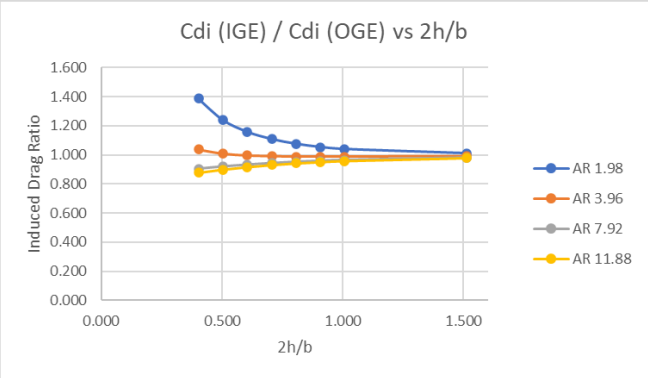

Figure 41. Lift and Induced Drag Influence vs 2h/b for multiple Aspect Ratios. AR = 7.92

Next, I also plotted the results as a 3-D surface to show the ground effect influence in terms of various angles of attack as shown on Figure 42 and through Figure 45. I can see how closely results from VORLAX match Torenbeek's data for small aspect ratios and heights close to the ground. However, as the aspect ratio increases VORLAX results seem to go towards McCormick's equation at higher height above the ground-over-span ratios.

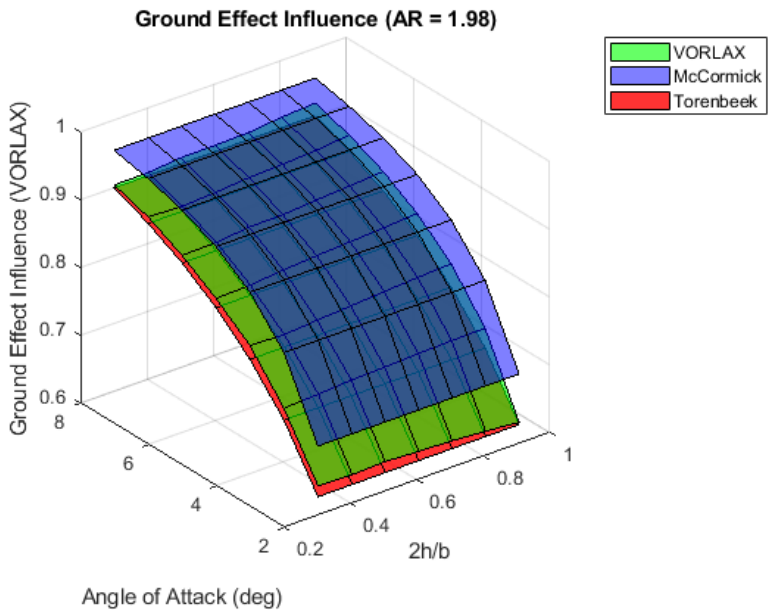

Figure 42. Surface plot for ground effect influence versus height above the ground. AR = 1.98

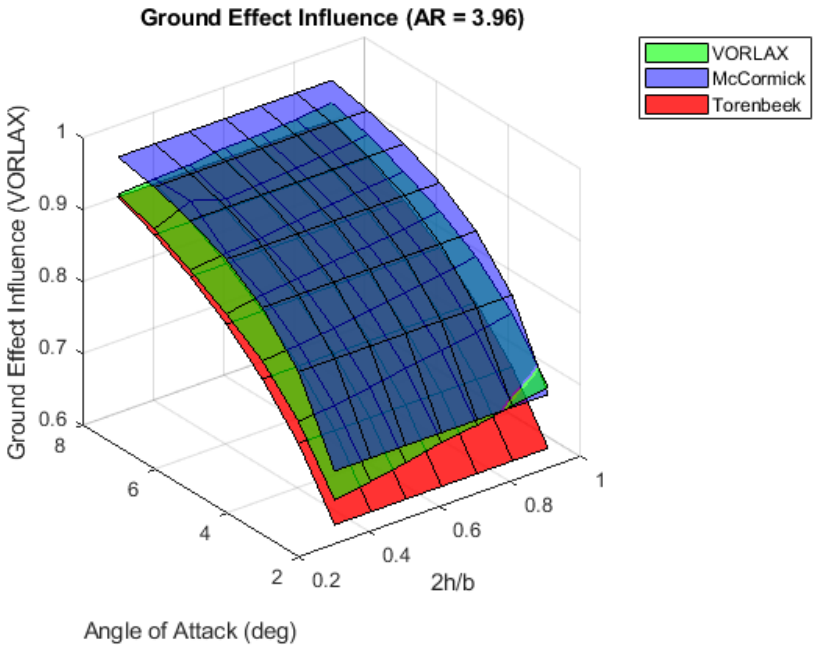

Figure 43. Surface plot for ground effect influence versus height above the ground. AR = 3.96

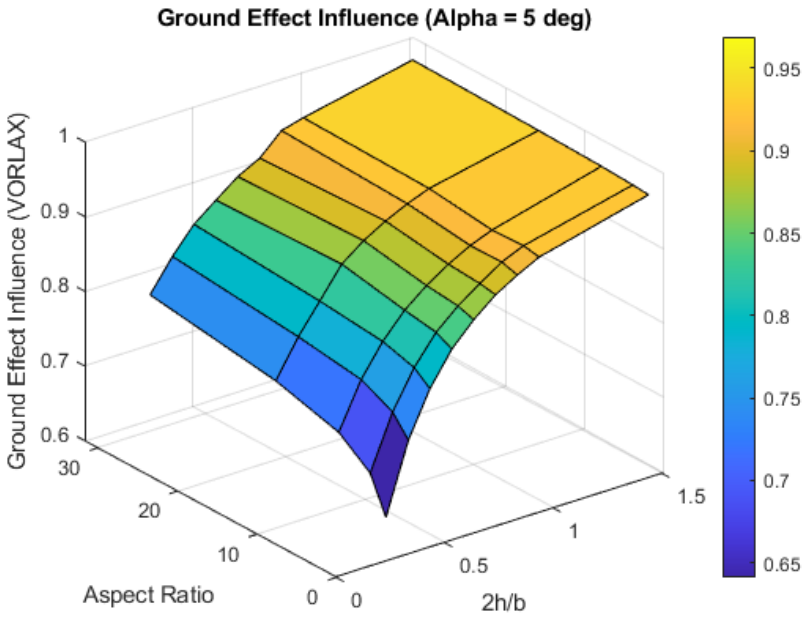

Figure 44. Surface plot for induced drag influence versus height above the ground and span ratio

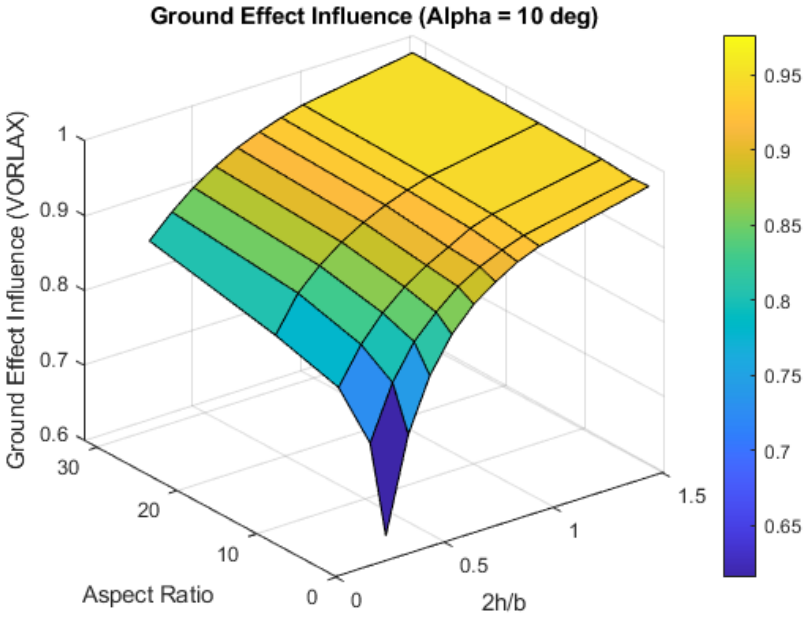

Figure 45. Surface plot for induced drag influence versus height above the ground and span ratio

Figure 46 through Figure 49 shows similar plots as in Figure 42 and Figure 43 however, on this occasion I fitted the results predicted by Valenzuela & Takahashi equation (13) [26] along with

VORLAX results, McCormick and updated Torenbeek. I can see from Figure 46 that Valenzuela & Takahashi equation (13) closely fit VORLAX results with the next equation closely following is that of Torenbeek with the β correcting factor.

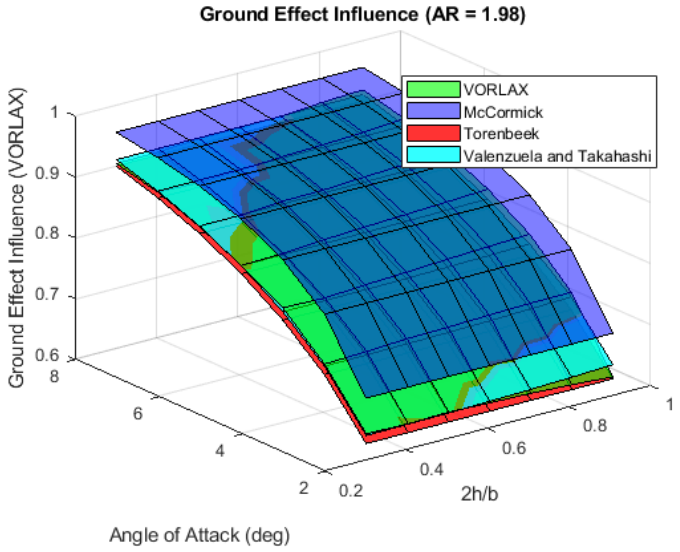

Figure 46. Surface plot for induced drag influence versus height above the ground. AR = 1.98

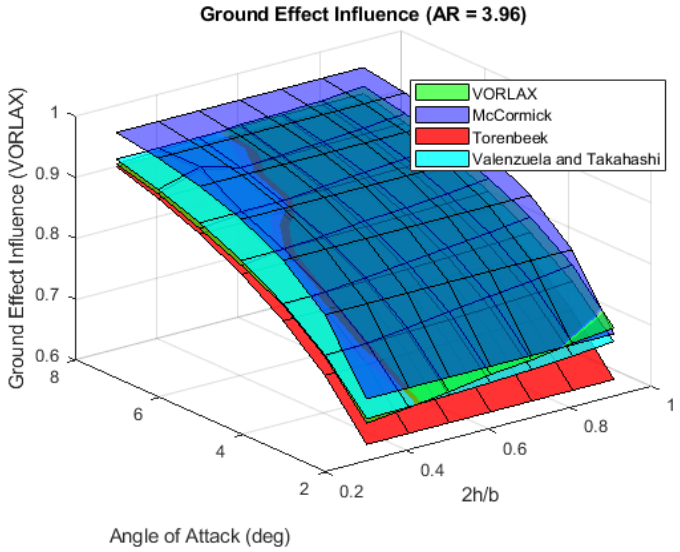

Figure 47. Surface plot for induced drag influence versus height above the ground. AR = 3.96

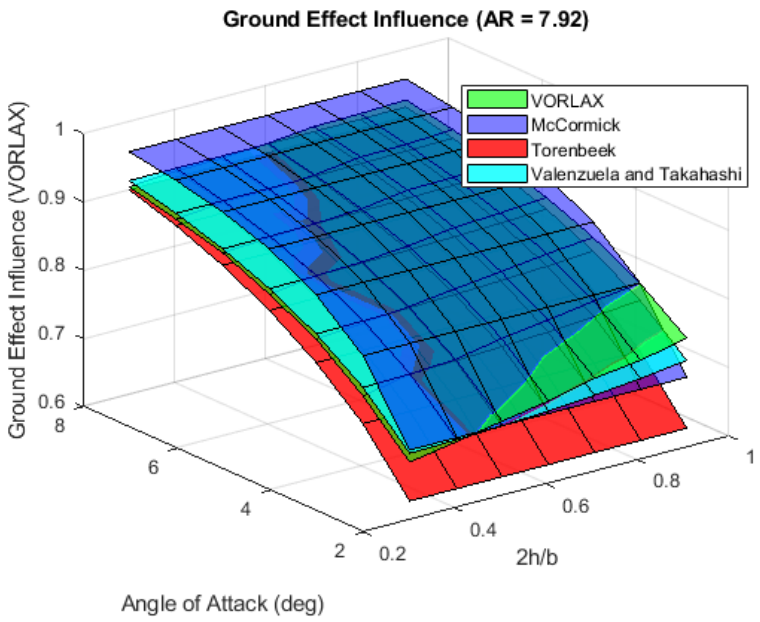

Figure 48. Surface plot for induced drag influence versus height above the ground. AR = 7.92

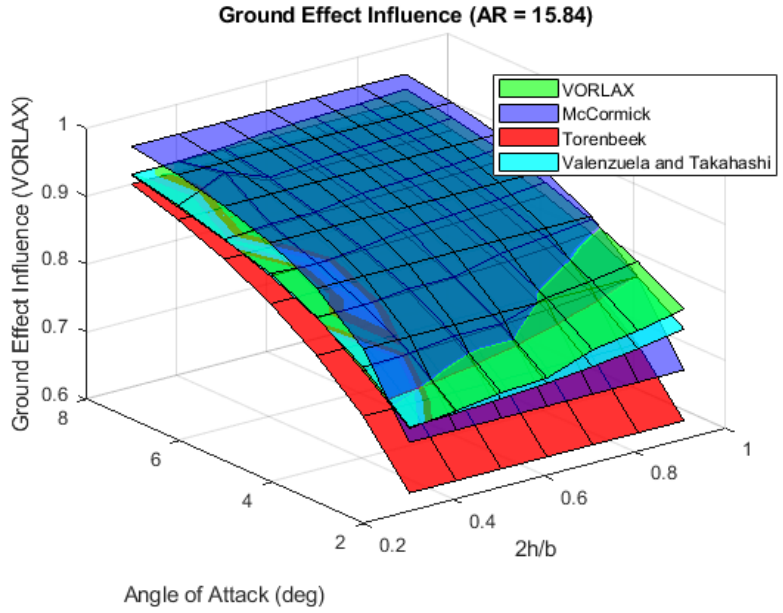

Figure 49. Surface plot for induced drag influence versus height above the ground. AR = 15.84

7.3 Comparison of Sandwich Panel VORLAX Surface Pressures to Volume Grid CFD Span Loads.

Next, I looked at the spanwise load distribution of the airfoils using VORLAX. Torenbeek also acknowledges that a change occurs in the spanwise loads for wings on ground effect causing early flow separation. “The induced adverse pressure gradient at the leading edge may result in early separation, while blocking or even reversal of the flow” [13].

Figure 50, Figure 51, and Figure 52 show the results for the sectional load, which is the coefficient of lift multiplied by the local chord of the airfoil across the span length to show the spanwise distribution of the lift. Results show that for an airfoil in proximity to the ground the spanwise load distribution increases with increasing angle of attack as expected where the load distribution became more elliptical with increasing incidence. However, it was observed that for a wing in ground effect the load distribution increased more rapidly near the center of the airfoil compared to the tips of the airfoil. As a result, it is expected that an airfoil in ground effect would achieve a non-elliptical spanwise distribution that is flatter near the center of the airfoil with a higher gradient near the tips. This effect is aggravated as the airfoil becomes closer to the ground, or with increasing aspect ratio. Hence, an airfoil with a low aspect ratio shows a spanwise load distribution that is flatter across the span with a small gradient near the tips. This agrees with previous results, since I observed that the Oswald efficiency of an airfoil increased as the airfoil was found closer to the ground. Thus, a wing found in ground effect would experience a greater load gradient near the tips. Therefore, to maintain an ideal elliptical lift distribution in a wing in ground effect I would need to increase the twist at the wing tips if the objective is to minimize ground effect influences.

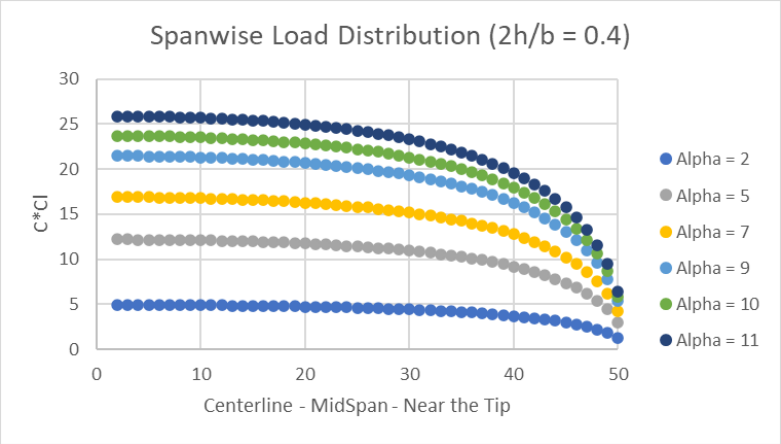

Figure 50. Spanwise Load Distribution with changing height above the ground and incidence

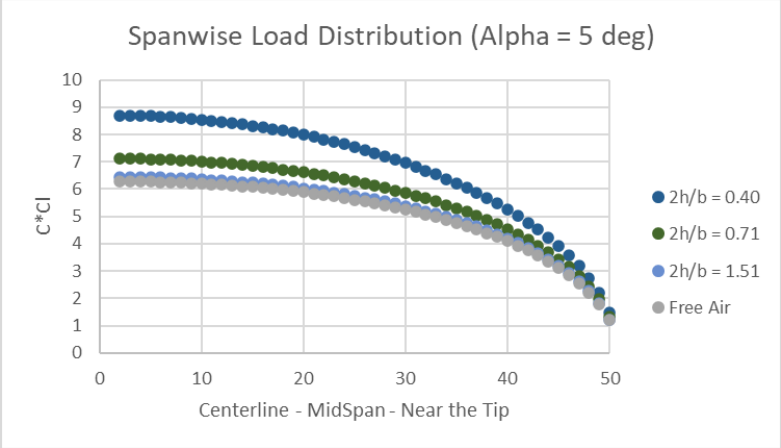

Figure 51. Spanwise Load Distribution with changing height above the ground and incidence

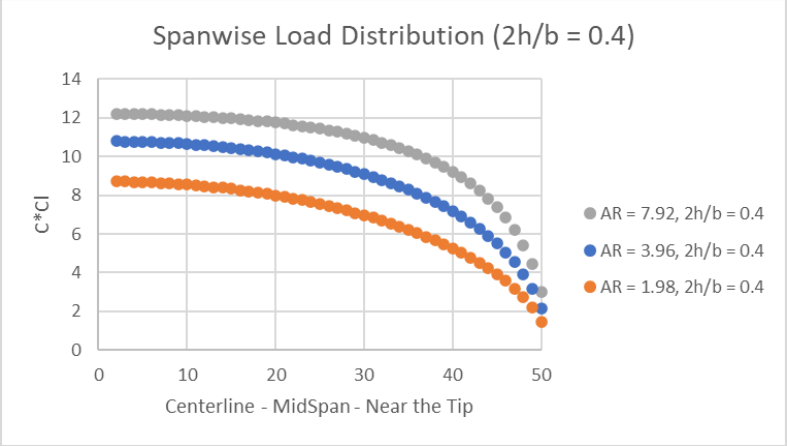

Figure 52. Spanwise Load Distribution with changing height above the ground and incidence

7.4 Flow Separation Analysis Using Sandwich Panel VORLAX Surface Pressures

Figure 53 through Figure 58 show the changes in pressure in canonical form for wings with varying *HAG* (Height above the ground). The results show a slight change in the pressure distribution on wings in proximity to the ground compared to wings in free air far from the ground. As a result, I can see that wings that are on ground effect have a slightly higher velocity gradient near the trailing edge than those compared to off-ground effect. Using Stratford's method, I can estimate at what percentage of the chord length the flow starts to separate starting from the trailing edge of the airfoil. Thus, this can imply an early flow separation. However, I was not able to detect significant changes in flow separation within the pressure curves using Stratford's method. Nonetheless, there were some variations, especially near the trailing edge of the airfoil. As expected, flow started to separate earlier as the angle of attack increased but the changes in pressure distribution with wings in ground effect were not very significant with changes of the height above the ground. Thus, it seems to indicate that the stall angle of an airfoil may not be a strong function of the height above the ground but rather just a function of incidence and aspect ratio and other quantities not studied in this investigation such as camber, twist or swept. I can see that there are no significant changes in the canonical pressure distribution with changing *HAG*. Nevertheless, I see that these changes become slightly more apparent at a higher angle of incidence and increase aspect ratio.

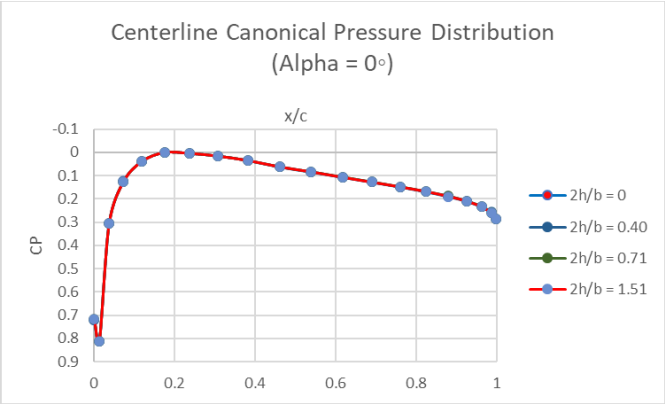

Figure 53. Canonical Pressure Distribution. AR = 1.98. α=0°

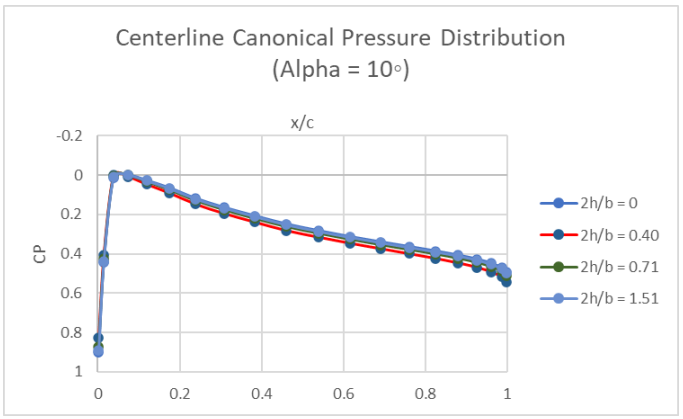

Figure 54. Canonical Pressure Distribution. AR = 1.98. α=10°

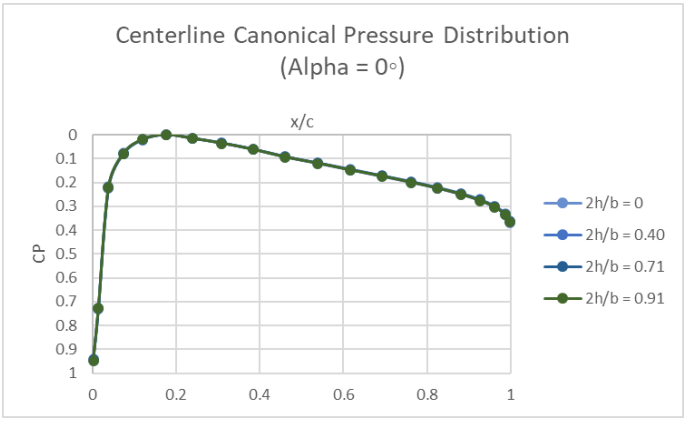

Figure 55. Canonical Pressure Distribution. AR = 3.96. α=0°

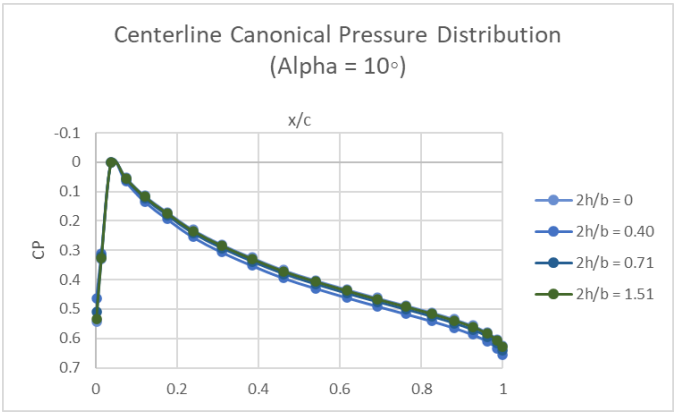

Figure 56. Canonical Pressure Distribution. AR = 3.96. α=10°

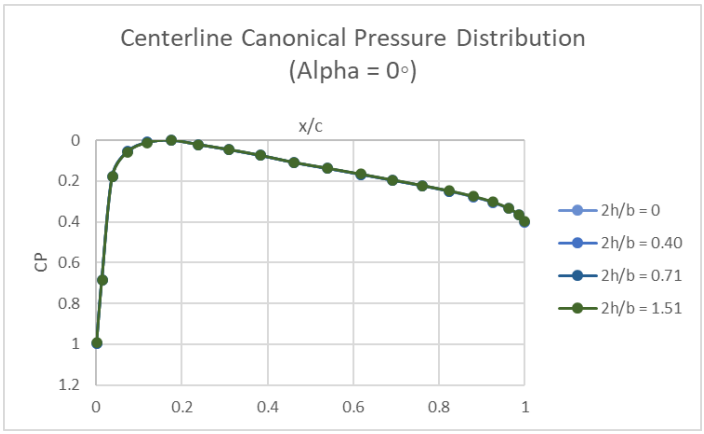

Figure 57. Canonical Pressure Distribution. AR = 7.92. α=0°

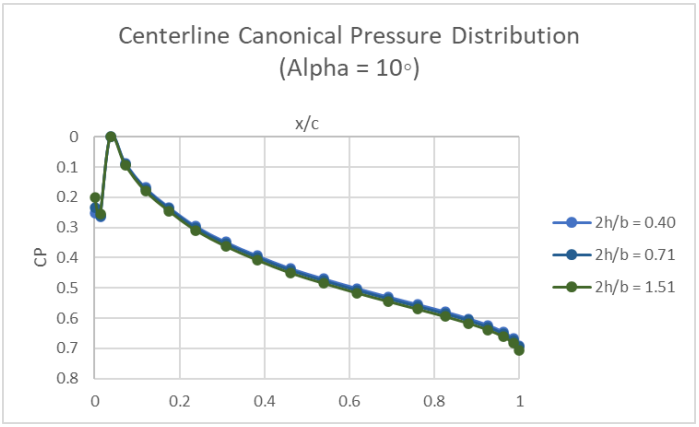

Figure 58. Canonical Pressure Distribution. AR = 7.92. α=10°

Figure 59 through Figure 66 shows the pressure distribution in Canonical form for an airfoil in ground effect. The plots on the left show the results for an airfoil with *2h/b* = 0.40 and *AR*=1.98, and the plots of the right have an airfoil with an aspect ratio of 7.92 also with *2h/b* = 0.40. The values shown in red on the plots indicate where the flow would have separated in the airfoil. I can see that the flow separation initiates at the trailing edge of the airfoil. As expected, I can see that flow separation is greater at higher incidence angles. In addition, I can see that there is a higher percentage of detached flow in the higher aspect ratio with *AR*=7.92 when compared to the wing under the same conditions with a smaller aspect ratio of *AR*=.98. For instance, at *2h/b* = 0.40, the wing with an aspect ratio of 7.92 has about 8% of the chord percentage of detached flow at an

incidence angle of 5-° , while the wing with an aspect ratio of 1.98 at the same conditions has only 4% detached flow. Thus, it appears that flow separation is more significant with changes of incidence and aspect ratio, but much less noticeable with changes of height above the ground. Results with detailed percentage of separated flow are shown on Table 2, in the appendix section.

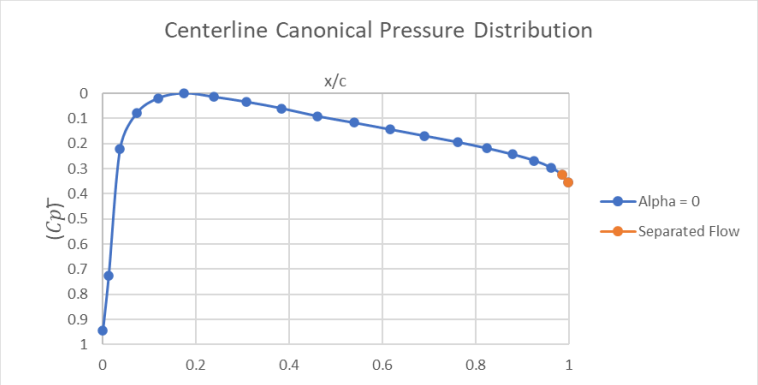

Figure 59. Canonical Pressure Distribution for 2h/b = 0.40. AR = 1.98, α=0°

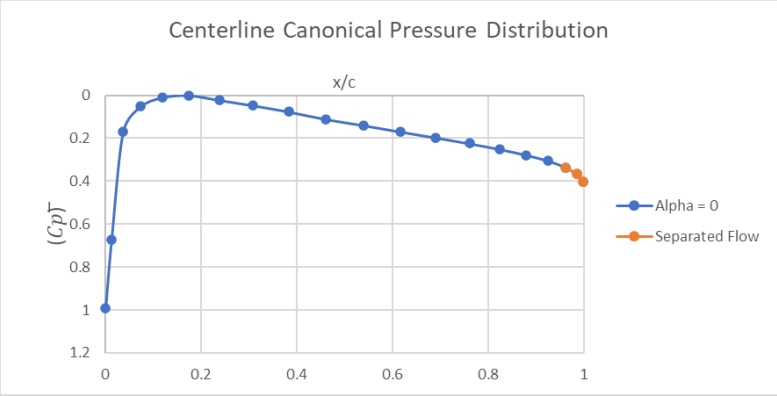

Figure 60. Canonical Pressure Distribution for 2h/b = 0.40. AR = 7.92. α=0°

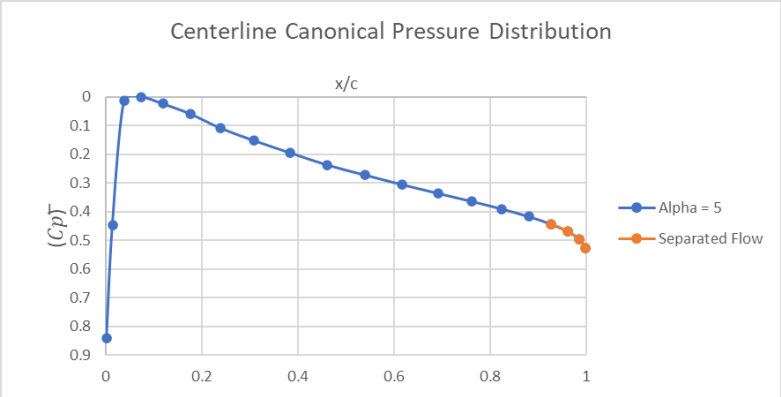

Figure 61. Canonical Pressure Distribution for 2h/b = 0.40. AR = 1.98. α=5°

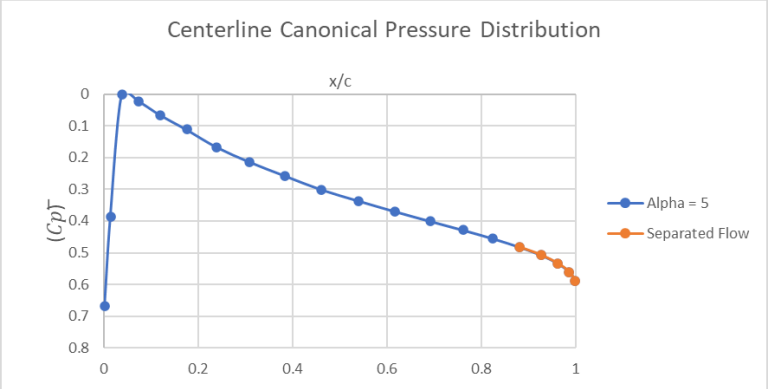

Figure 62. Canonical Pressure Distribution for 2h/b = 0.40. AR = 7.92. α=5°

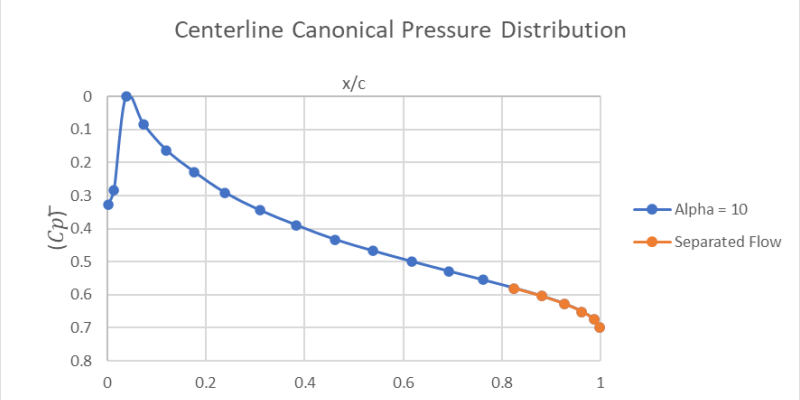

Figure 63. Canonical Pressure Distribution for 2h/b = 0.40. AR = 1.98. α=10°

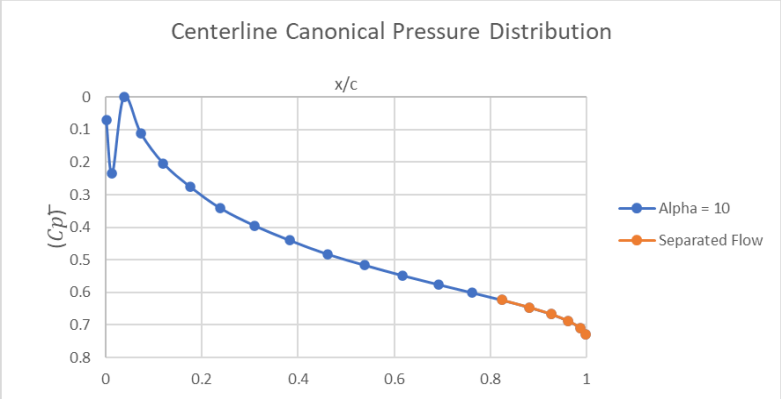

Figure 64. Canonical Pressure Distribution for 2h/b = 0.40. AR = 7.92. α=10°

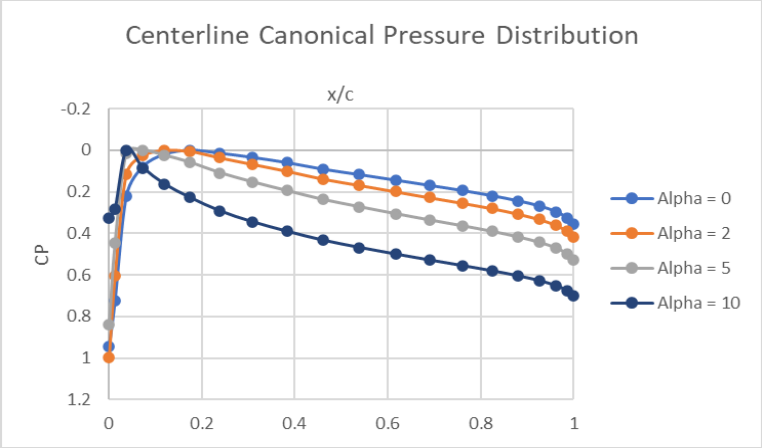

Figure 65. Canonical Pressure Distribution for 2h/b = 0.40. AR = 1.98

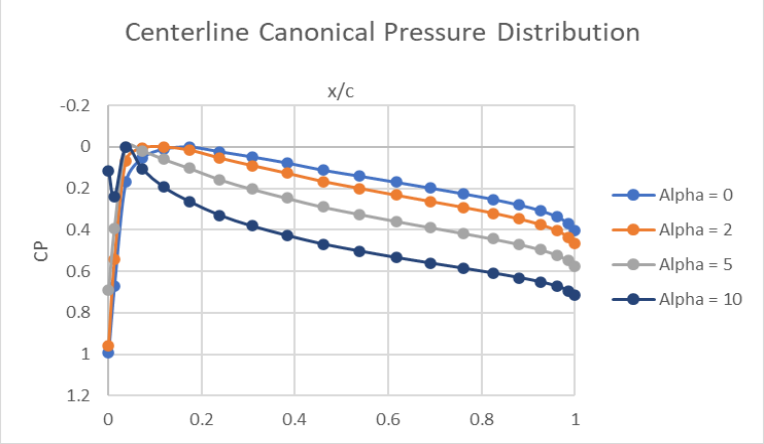

Figure 66. Canonical Pressure Distribution for 2h/b = 0.40. AR = 7.92

7.5 Comparison of Flat Plate VORLAX to Volume Grid CFD for Overall Lift, Drag and Stall Onset

Next, I present the results obtained using CFD with ANSYS FLUENT compared with the vortex lattice method of VORLAX for varying incidence and aspect ratio.

Figure 67 through Figure 75, show the comparison results for the coefficient of drag and the plotted against the incidence of the wing for a NACA 0012 wing with an aspect ratio of 1.98, 3.96, and 7.92, respectively. The top plot shows coefficient of drag versus the angle of attack for varying *HAG* and the bottom plot shows the coefficient of lift for varying *HAG*. Just as in the previous parts multiple simulations were computed using factors of two times the height over the span to observe the effects of the ground effect. The results shown in blue are the results found using ANSYS FLUENT and the simulated wing tunnel analysis while the results in red are the results found using VORLAX. The results shown on the plots show the values found just before the wing started to stall. Near the stall results in ANSYS FLUENT did not converge. The plots for the coefficient of drag had to be slightly adjusted by shifting them based on the coefficient of zero drag found.

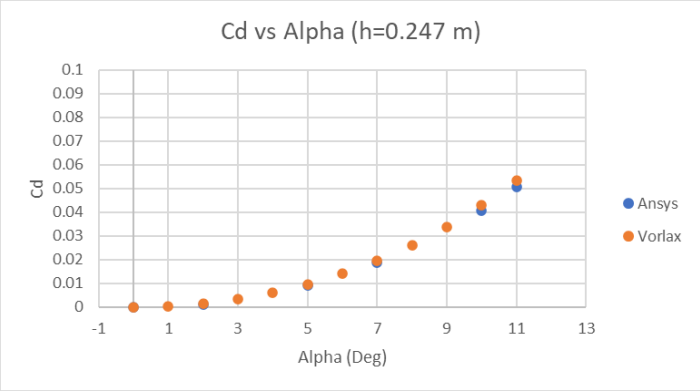

Figure 67. CD vs α for NACA 0012 with AR = 1.98, and 2h/b = 0.40

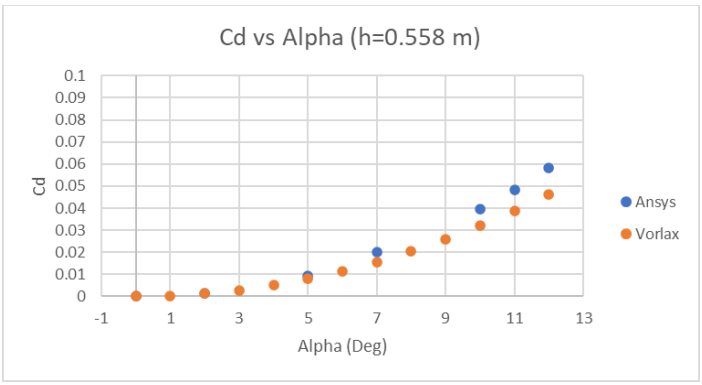

Figure 68. CD vs α for NACA 0012 with AR = 1.98, and 2h/b = 0.91

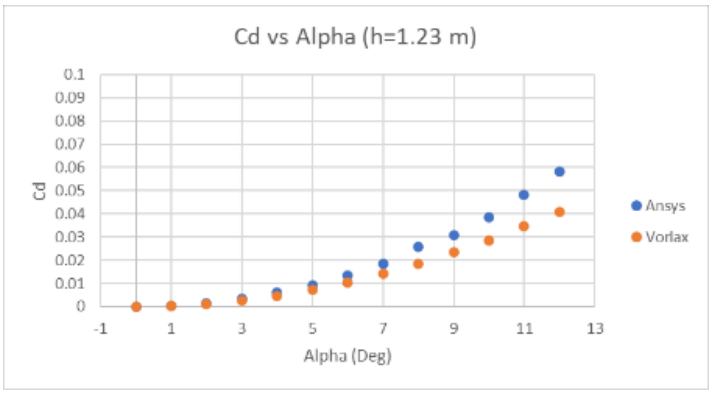

Figure 69. CD vs α for NACA 0012 with AR = 1.98, and 2h/b = 1

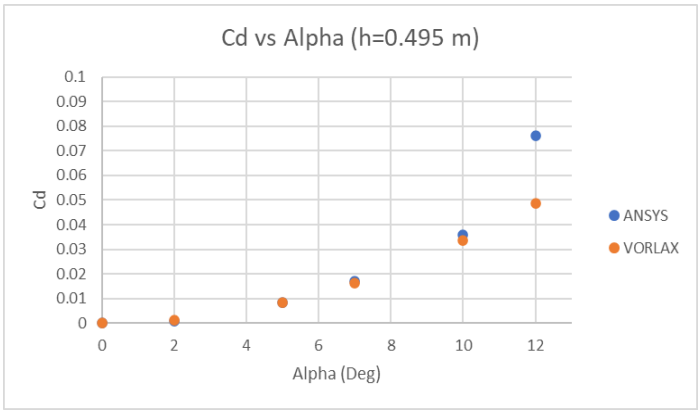

Figure 70. CD vs α for NACA 0012 with AR = 3.96, and 2h/b = 0.40

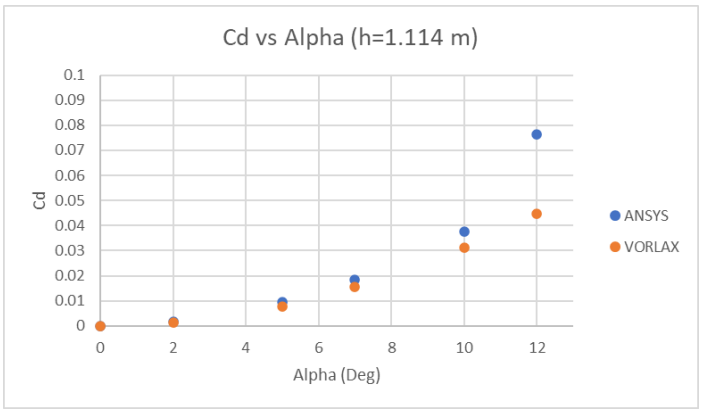

Figure 71. CD vs α for NACA 0012 with AR = 3.96, and 2h/b = 0.91

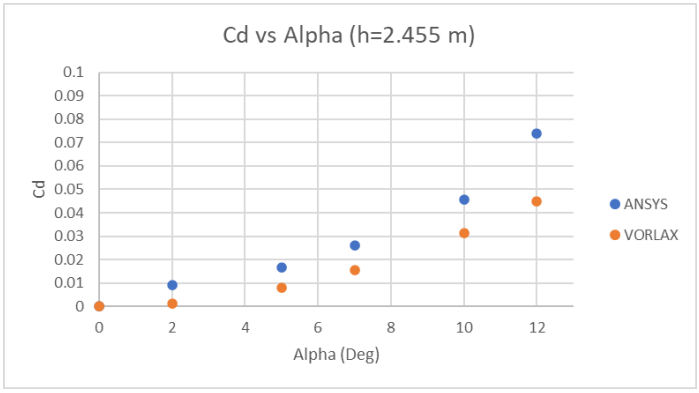

Figure 72. CD vs α for NACA 0012 with AR = 3.96, and 2h/b = 1

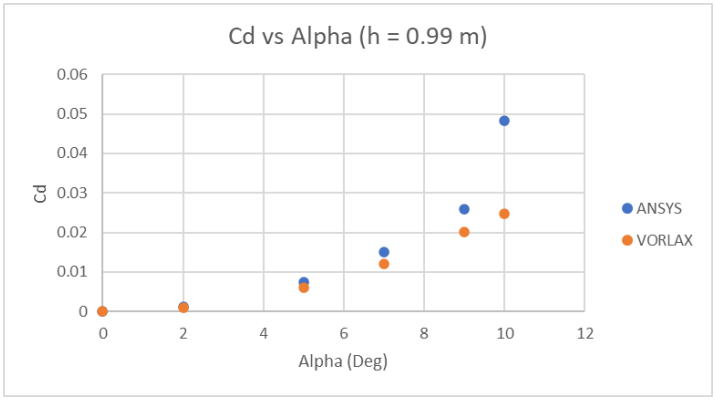

Figure 73. CD vs α for NACA 0012 with AR = 7.92, and 2h/b = 0.40

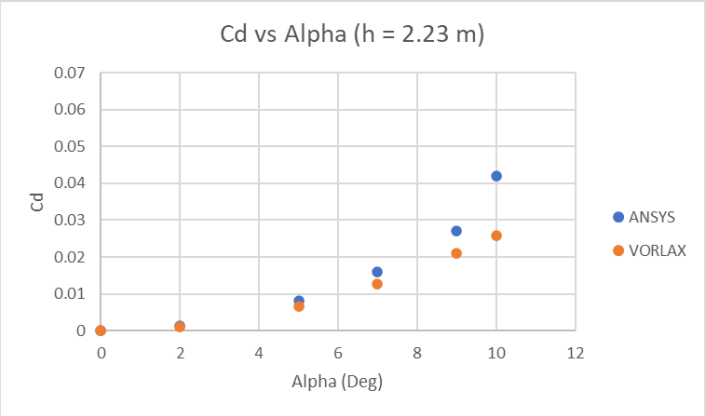

Figure 74. CD vs α for NACA 0012 with AR = 7.92, and 2h/b = 0.91

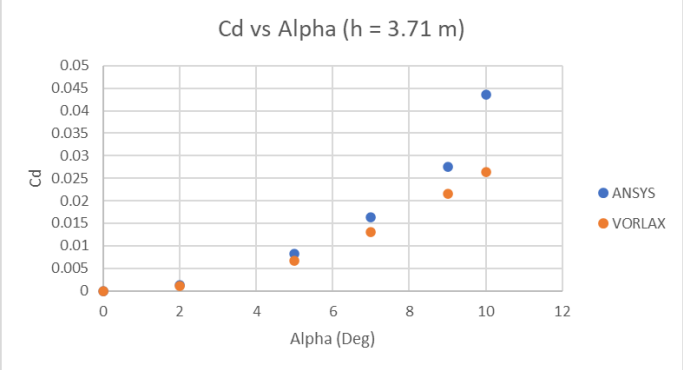

Figure 75. CD vs α for NACA 0012 with AR = 7.92, and 2h/b = 1

Similarly, Figure 76 through Figure 84 show the coefficient of lift versus angle of attack for varying heights above the ground. Just as in the previous figures shown for the coefficient of drag, results for the coefficient of lift show a NACA 0012 with an aspect ratio of 1.98, 3.96 and 7.92 with varying $2h/b$ =0.40, 0.91, and $2h/b$ = 1.

Since VORLAX is an inviscid code, it fails to predict the stall of the airfoil which was very clearly shown on the ANSYS FLUENT results. Nevertheless, VORLAX can be a great resource under some specific circumstances and in conjunction with other methods to estimate flow separation. VORLAX results were computed much more quickly in comparison with CFD results that required dozens of hours to compute as opposed to minutes with VORLAX.

While it is broadly known that the stall angle of attack is normally less than that of a wing in free air, it is not certain whether the stall angle of attack is a function of the height above the ground for wings

in ground effect. An interesting observation from the results as shown on the results for the medium to high aspect ratio wing with *AR* of 3.96, and 7.92, was that the stall angle seems to be mostly unaffected with variations of heights for the NACA 0012 wing. The stall angle for the selected wing with medium *AR*=3.96 and large aspect ratio *AR*=7.92 always occurred just past 10-°. Hence, the results indicate that there is not a strong correlation of the height above the ground with the stall angle for wings of medium to large aspect ratios.

However, when testing the airfoil with a small aspect ratio of 1.98 as wings found in racecars results from ANSYS FLUENT differed from VORLAX results as shown in Figure 67, Figure 68, and Figure 69. I can see that as the *HAG* increases the wing with an aspect ratio of 1.98 can sustain higher angles of attack before the flow on the wing starts to separate and become turbulent and stall as compared to the medium and large aspect ratio wings. This was apparent when observing the values for *CL* given by ANSYS FLUENT for each iteration. Results for low angles of attack quickly converge to a value, while results near the stall region started to diverge with no apparent convergence as the angle of attack increases. This is to be expected with viscous flow simulation. However, using these stall indications I could study the stall onset as a function of the height above the ground. Thus, results from ANSYS FLUENT seemed to indicate that the wing has an early stall for low distances above the ground. The stall for the small aspect ratio wing occurred at 12-° for a height less than 50% of the height-to-span ratio and a stall of 13-° for higher heights above the ground. A noticeable difference compared to the 10-° stall found with the medium and large aspect ratio. Similar results were found when looking at the coefficient of drag versus the incidence of the wing as shown in FIGURES 20.

Moreover, from Figure 67, Figure 68, and Figure 69, I can see the results from ANSYS FLUENT start to deviate from those obtained using VORLAX as the height above the ground. This is especially noticeable in the small aspect ratio wing with an *AR* of 1.98. Yet, VORLAX and ANSYS FLUENT results from the medium and large aspect ratio with *AR* 3.96 and *AR* 7.92 are more closely match with smalls deviations as the height above the ground increases, with a significant less difference with the large aspect ratio wing. Hence, there is strong evidence that as the aspect ratio increases results from

VORLAX approximate more closely to CFD results found using ANSYS FLUENT for wings in the presence of ground effect. Lastly, since the height above the ground in the ANSYS FLUENT calculations was varied as a reference to the aerodynamic center, since the results for the coefficient of lift appeared to accurately match those from VORLAX, I can assume that VORLAX uses the aerodynamic center as reference point as well.

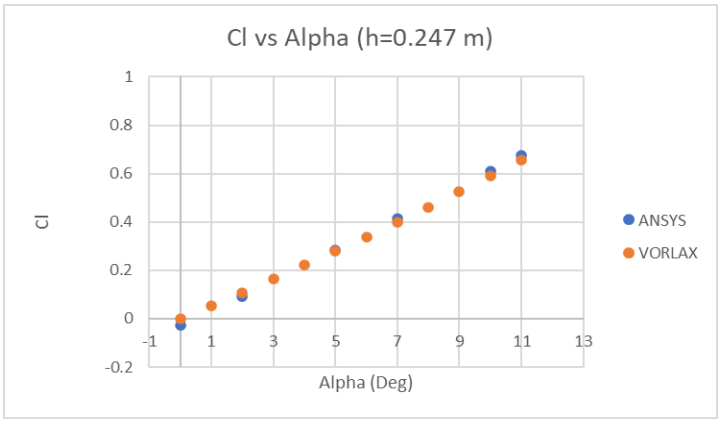

Figure 76. Cl vs α for NACA 0012 with AR = 1.98, and 2h/b = 0.40

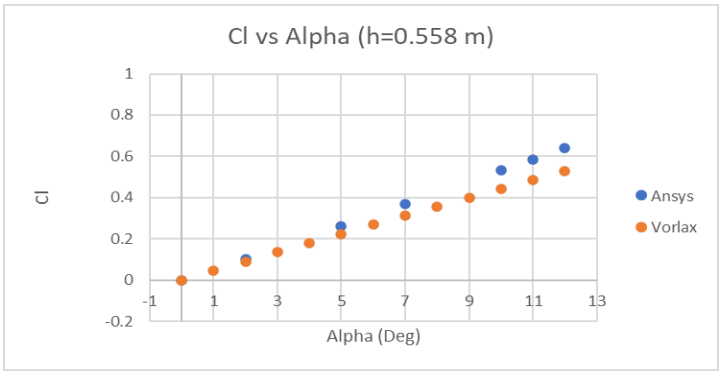

Figure 77. Cl vs α for NACA 0012 with AR = 1.98, and 2h/b = 0.91

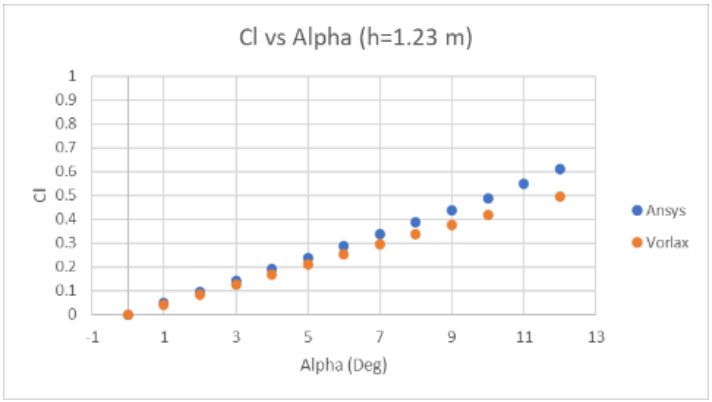

Figure 78. Cl vs α for NACA 0012 with AR = 1.98, and 2h/b = 1

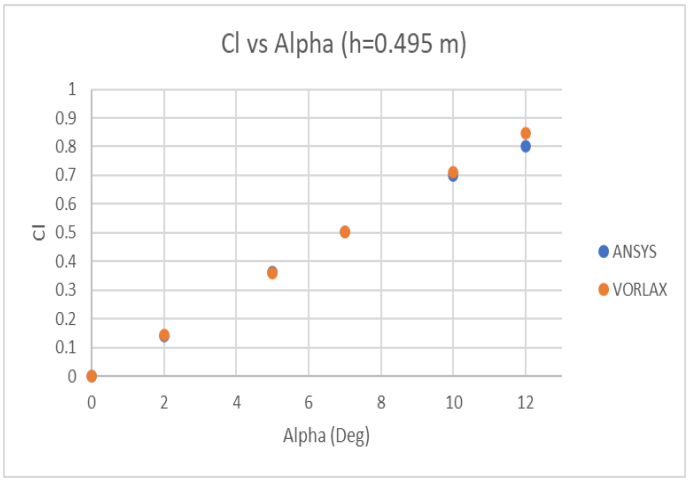

Figure 79. Cl vs α for NACA 0012 with AR = 3.96, and 2h/b = 0.40

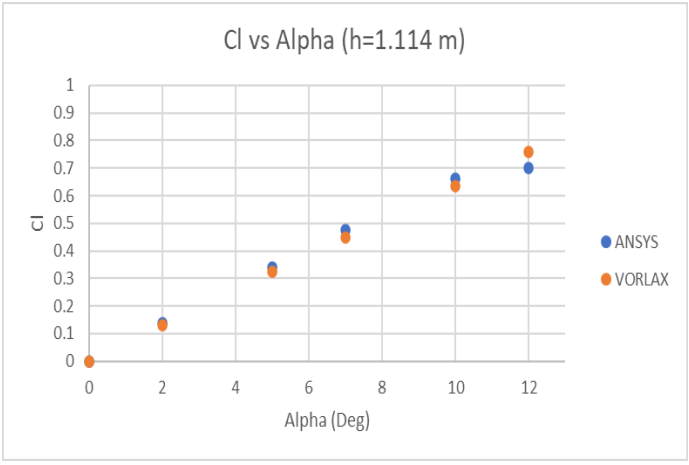

Figure 80. Cl vs α for NACA 0012 with AR = 3.96, and 2h/b = 0.91

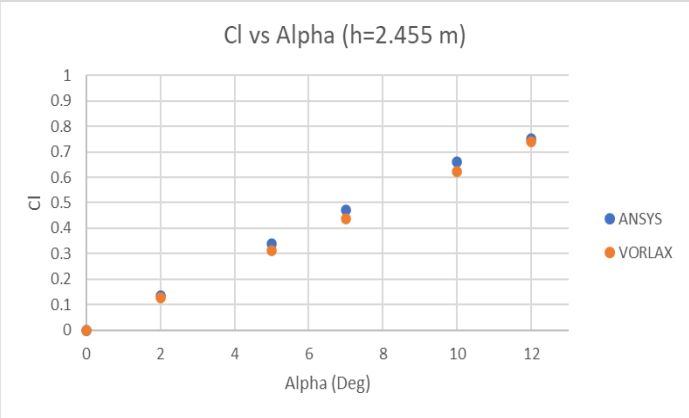

Figure 81. Cl vs α for NACA 0012 with AR = 3.96, and 2h/b = 1

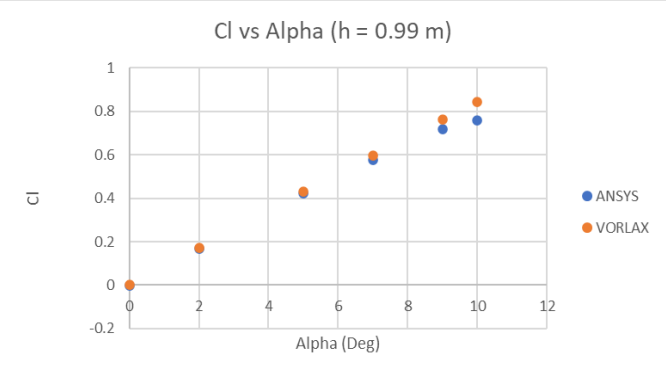

Figure 82. Cl vs α for NACA 0012 with AR = 7.92, and 2h/b = 0.40

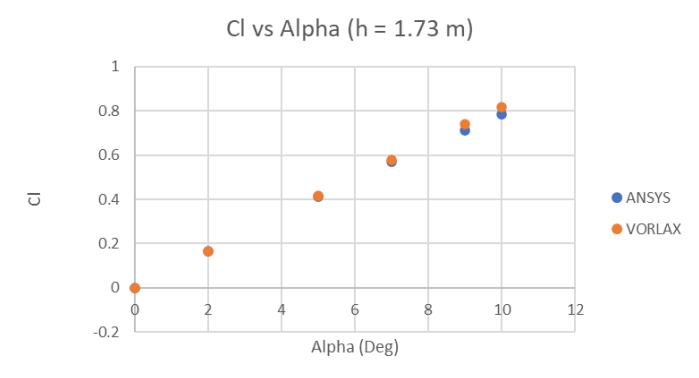

Figure 83. Cl vs α for NACA 0012 with AR = 7.92, and 2h/b = 0.91

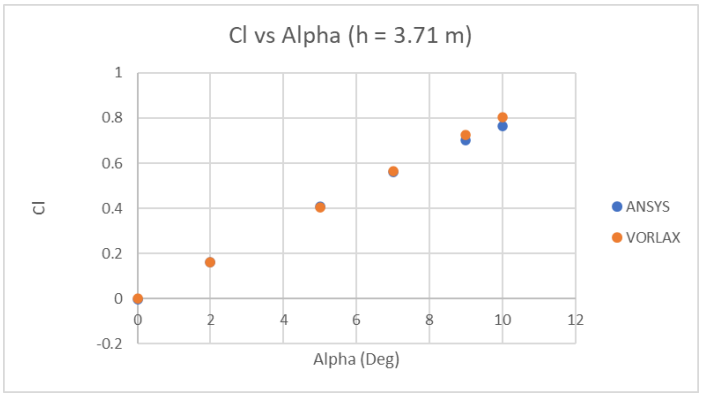

Figure 84. Cl vs α for NACA 0012 with AR = 7.92, and 2h/b = 1

Next, Figure 85, Figure 86, and Figure 87 show the coefficient of lift versus the incidence angle as the height above the ground varied. In VORLAX parlance, *HAG=0* represents the airfoil in "free air" denoting a height far from the ground. In these figures I can easily see the variations of the coefficient of lift and angle of attack slope Cl_{α}. As expected for wings operating in ground effect there is an increase in lift for any given angle attack due to the changes in their pressure distribution, decrease of induced drag and other changes in the flow patterns around the wing. As a result, this affects the lift angle of the attack slope, increasing the slope as the wing comes closer to the ground. This was evident in the results found using VORLAX as previously shown.

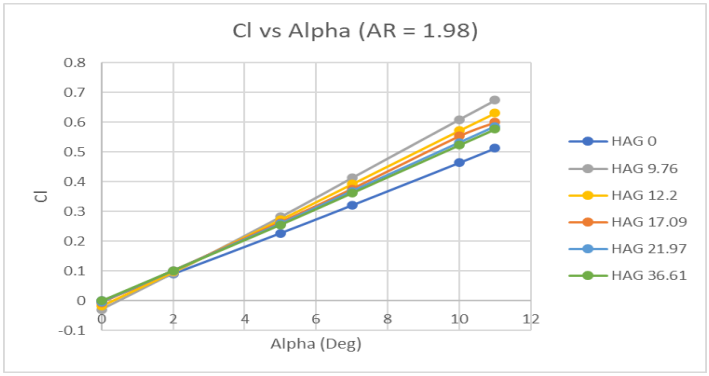

Figure 85. CL versus α for variation of height above the ground. AR = 1.98

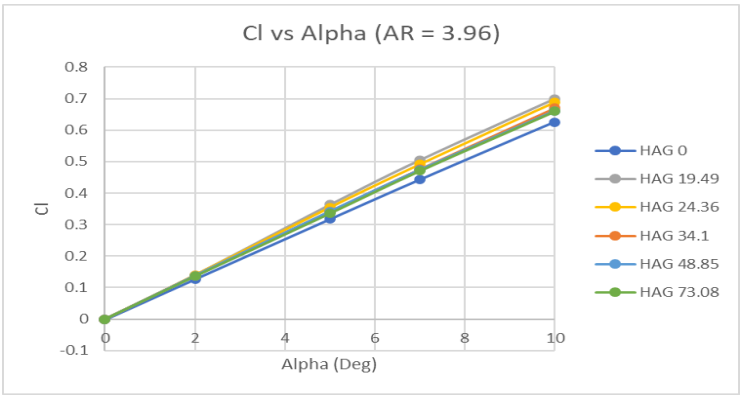

Figure 86. CL versus α for variation of height above the ground. AR = 3.96

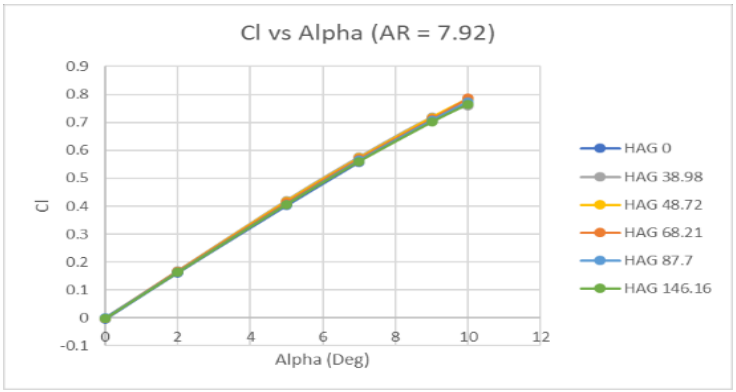

Figure 87. CL versus α for variation of height above the ground. AR = 7.92

Additionally, just as in the results found with VORLAX, viscous CFD results show this increase in lift due to ground effect is much more apparent in small aspect ratio wings with decreasing ground effect influence as the aspect ratio becomes larger. This is to be expected considering that the induced drag of a wing is aspect ratio dependent as shown in equation (1), or more precisely a function of their span as Max Munk postulated [22]. Hence, the faster increase in lift compare to its induced drag thereby an increase in efficiency become less apparent on wings with larger aspect ratios. This explains the results shown in the previous figures with minimal change in the curve slope of the coefficient of lift with the high aspect ratio wing.

Next, I see in Figure 88 through Figure 114, comparing the ANSYS FLUENT results to the VORLAX results. In Figures 88 through Figure 96 show the ground effect influence on the coefficient of lift using equation (6) for multiple aspect ratios and angles of attack.

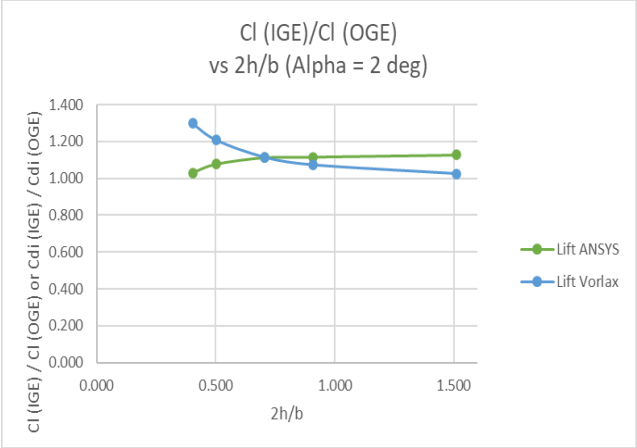

Figure 88. Ground Effect Influences on Cl, AR = 1.98, α=2°

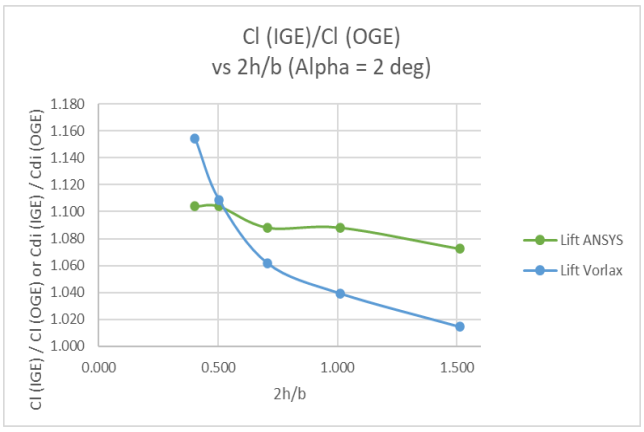

Figure 89. Ground Effect Influences on Cl, AR = 3.96, α=2°

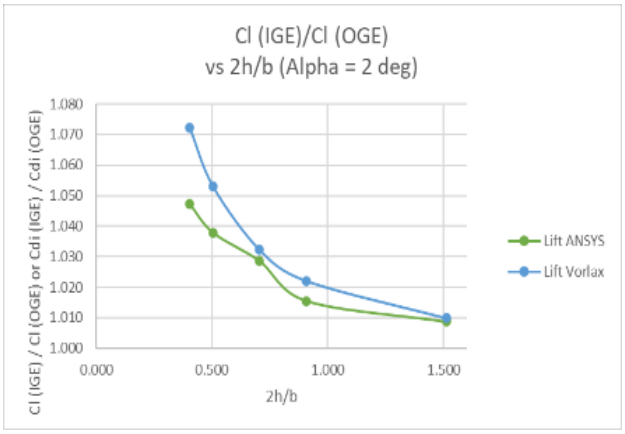

Figure 90. Ground Effect Influences on Cl, AR = 7.92, α=2°

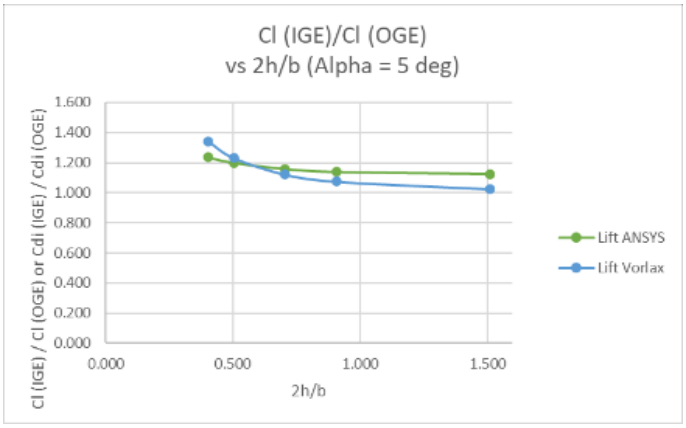

Figure 91. Ground Effect Influences on Cl, AR = 1.98, α=5°

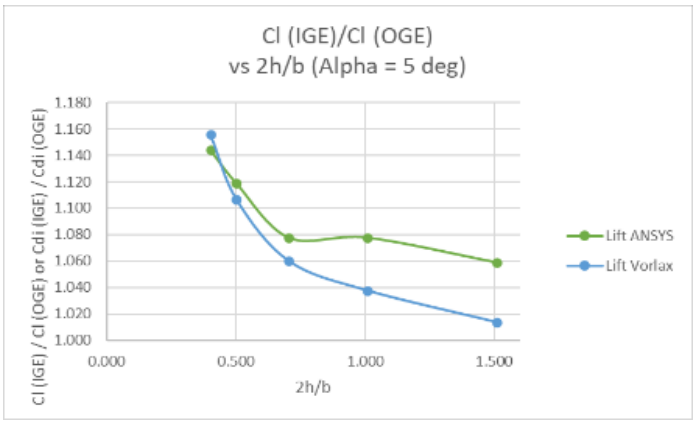

Figure 92. Ground Effect Influences on Cl, AR = 3.96, α=5°

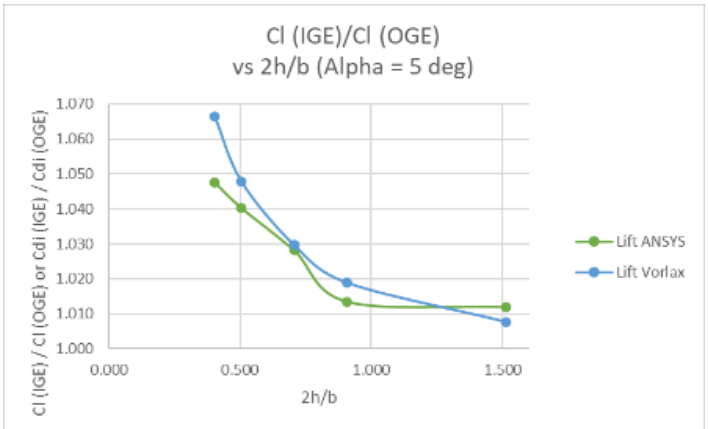

Figure 93. Ground Effect Influences on Cl, AR = 7.92, α=5°

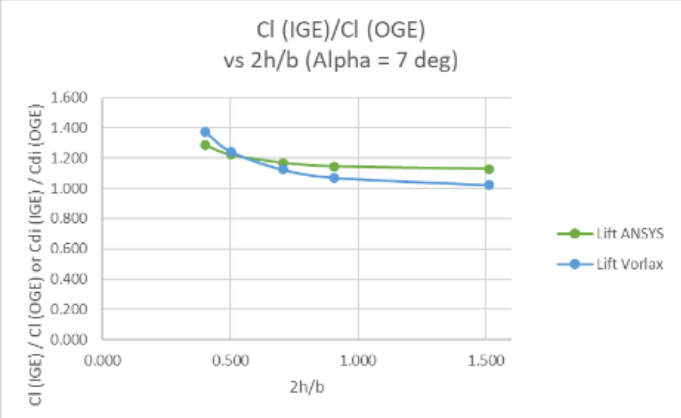

Figure 94. Ground Effect Influences on Cl, AR = 1.98, α=7°

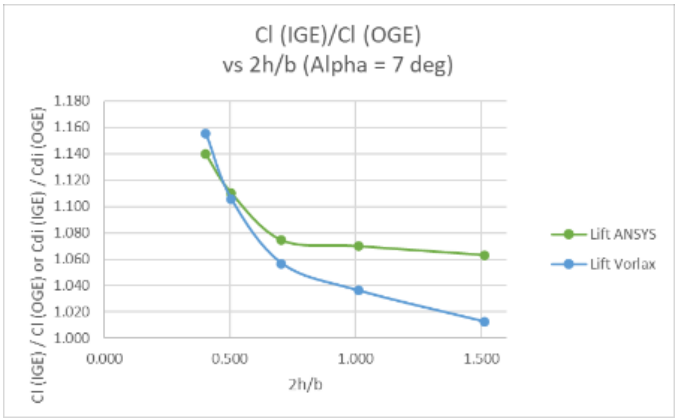

Figure 95. Ground Effect Influences on Cl, AR = 3.96, α=7°

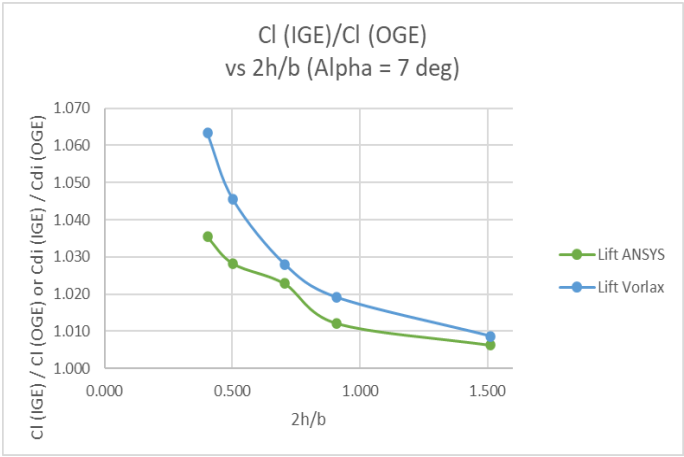

Figure 96. Ground Effect Influences on Cl, AR = 7.92, α=7°

Similarly, Figures 97 through Figures 104 show the ground effect influences in the coefficient of drag using equation (7), and finally Figures 105 through Figure 114 show the overall ground effect influence using equation (8). I investigate the influence found on the wing with changing height above the ground, incidence, and aspect ratio. It was observed that the viscous CFD results were much more congruent with VORLAX and the updated Torenbeek equation. when comparing the ground effect influence, while Barnes and McCormick, and Horner & Borst were providing, and overestimate just as previously observed. Therefore, in the next three figures I only show the comparison between the updated Torenbeek equation, VORLAX, and the viscous CFD results, as shown on the right-hand side of the plots.

I can see from the results of the medium aspect ratio wing of $AR = 3.96$, that as the angle of attack increases the results for the coefficient of lift ratio closely match those from VORLAX with the viscous CFD results. However, the results start to deviate as the HAG becomes smaller and for small angle of attack, as the general trend of lift influences was observed to reverse with increasing ground effect influence with increasing height under these conditions. However, as the aspect ratio increases CFD and VORLAX results for the ground effect influence for the lift ratio start to closely match. A similar trend occurs for the ratio of the coefficient of drag in ground effect over the coefficient of drag off ground effect. However, in this case I can observe a larger disparity which is suspected to be the result of precision and rounding errors since values for the coefficient of induced drag deals with much smaller quantities very close to zero. This could also explain some of the discrepancies shown in the ground effect influence found using CDF when compared to VORLAX and known equations as shown in the plots on the right on the following figures. Notwithstanding, results for the ground effect influence are also found in agreement for the large aspect ratio wing. However, to increase the precision of the ANSYS FLUENT results would require creating a finer mesh and expanding the “wing tunnel” size which would substantially increase the computational time required for each test study.

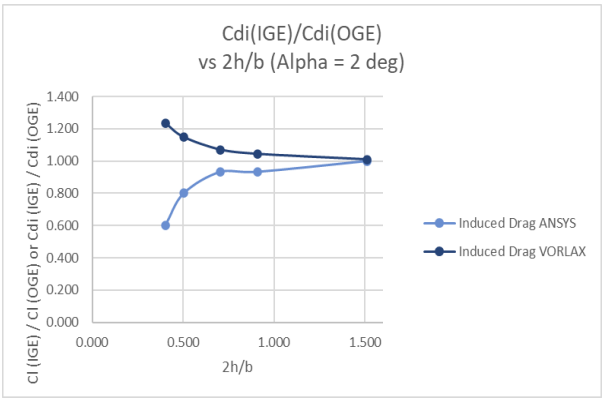

Figure 97. Ground Effect Influences on Cdi, AR = 1.98, α=2°

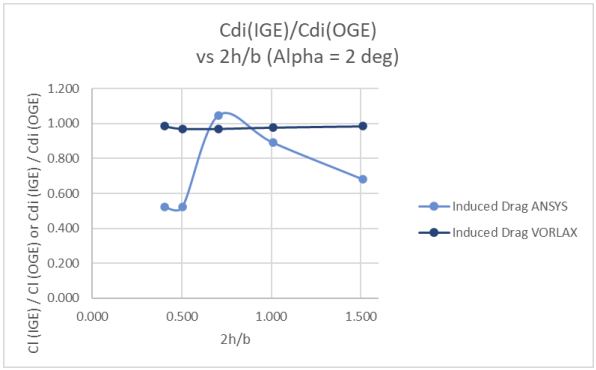

Figure 98. Ground Effect Influences on Cdi, AR = 3.96, α=2°

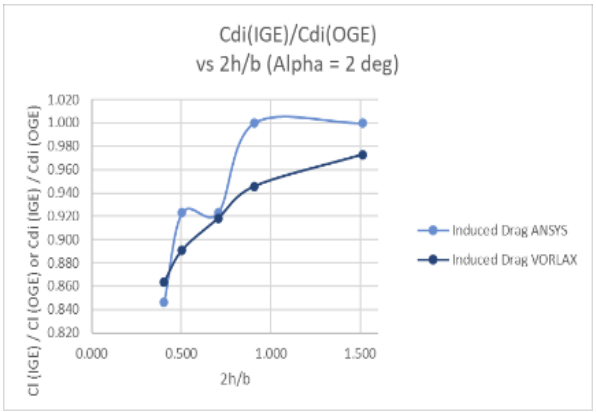

Figure 99. Ground Effect Influences on Cdi, AR = 7.92, α=2°

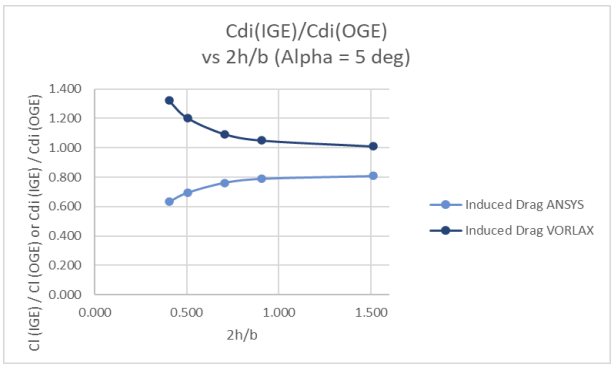

Figure 100. Ground Effect Influences on Cdi, AR = 1.98, α=5°

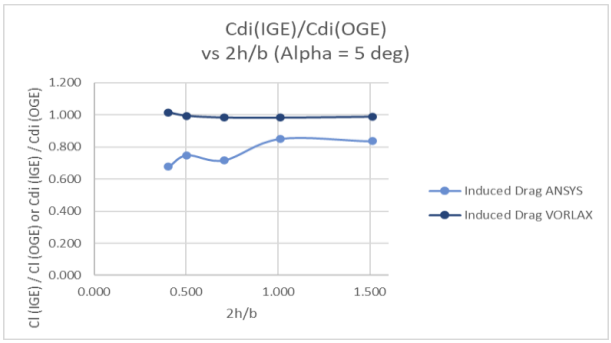

Figure 101. Ground Effect Influences on Cdi, AR = 3.96, α=5°

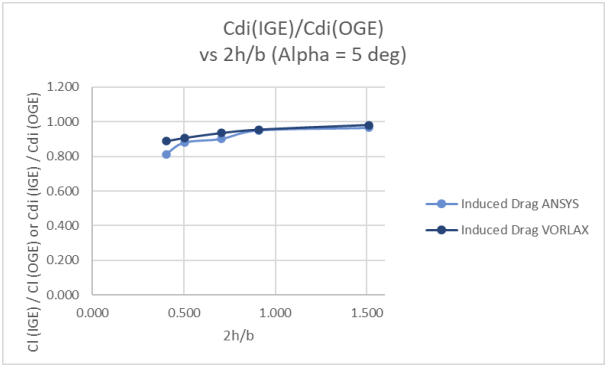

Figure 102. Ground Effect Influences on Cdi, AR = 7.92, α=5°

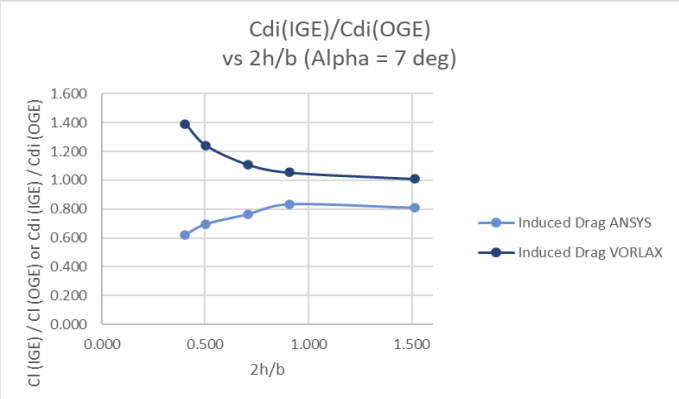

Figure 103. Ground Effect Influences on Cdi, AR = 1.98, α=7°

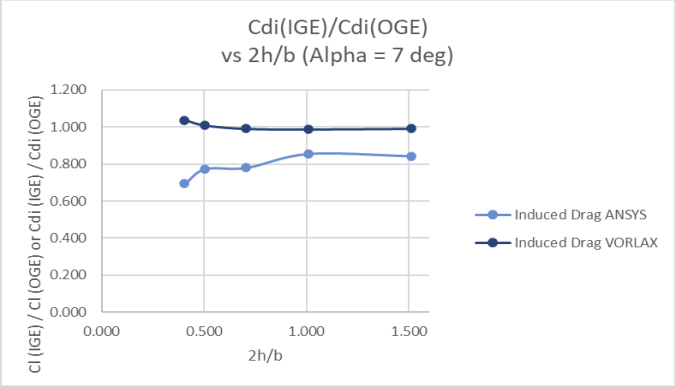

Figure 104. Ground Effect Influences on Cdi, AR = 3.96, α=7°

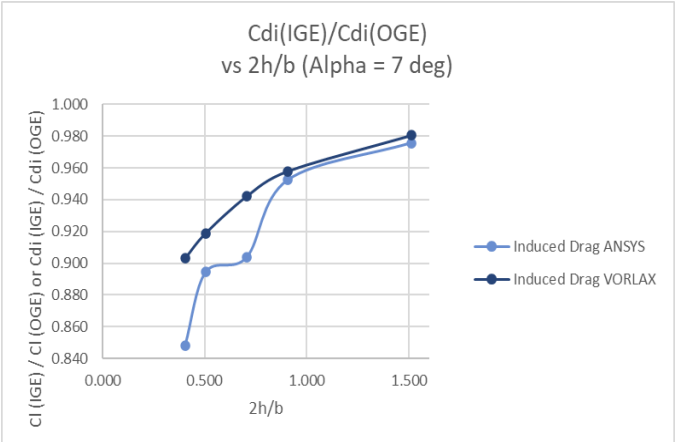

Figure 105. Ground Effect Influences on Cdi, AR = 7.92, α=7°

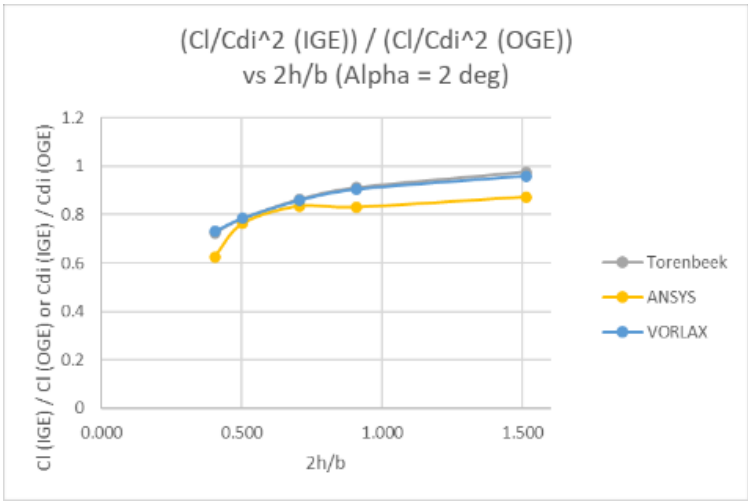

Figure 106. Ground Effect Influence, AR = 1.98, α=2°

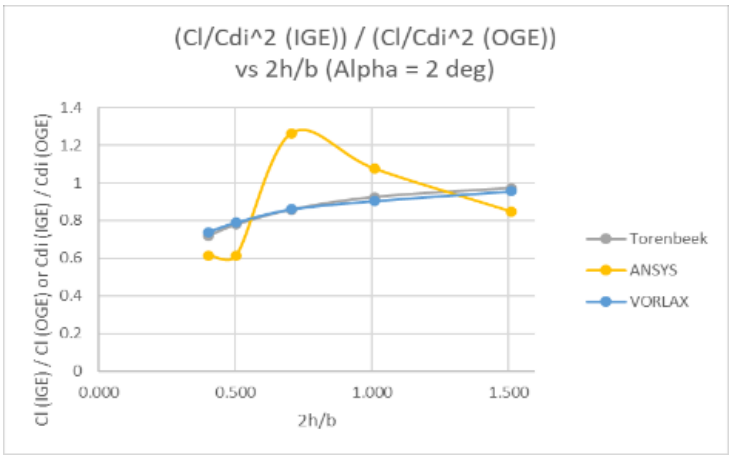

Figure 107. Ground Effect Influence, AR = 3.96, α=2°

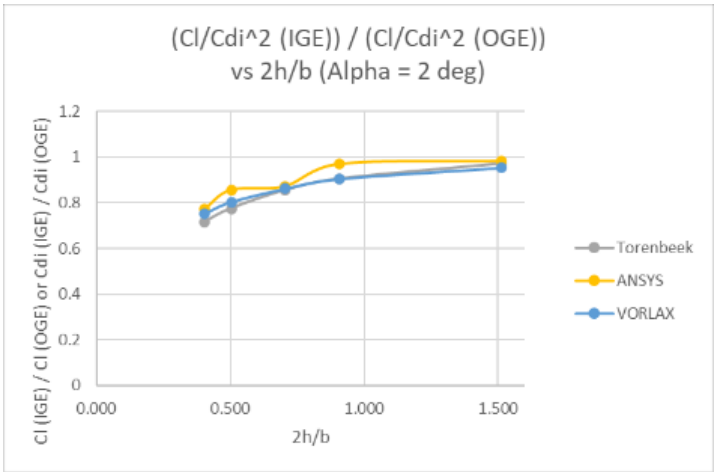

Figure 108. Ground Effect Influence, AR = 7.92, α=2°

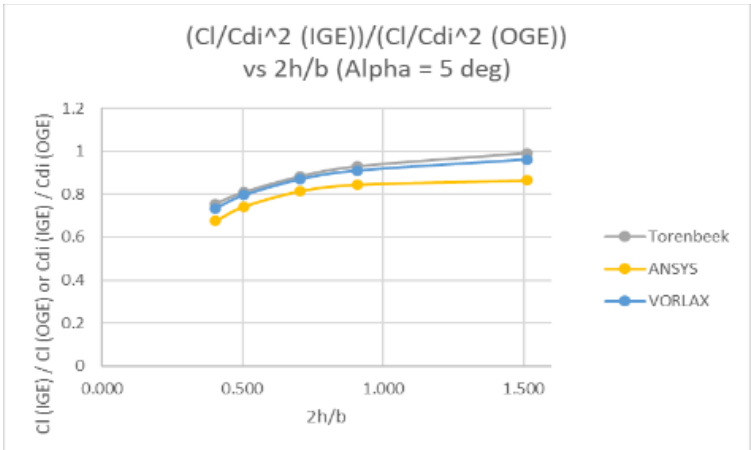

Figure 109. Ground Effect Influence, AR = 1.98, α=5°

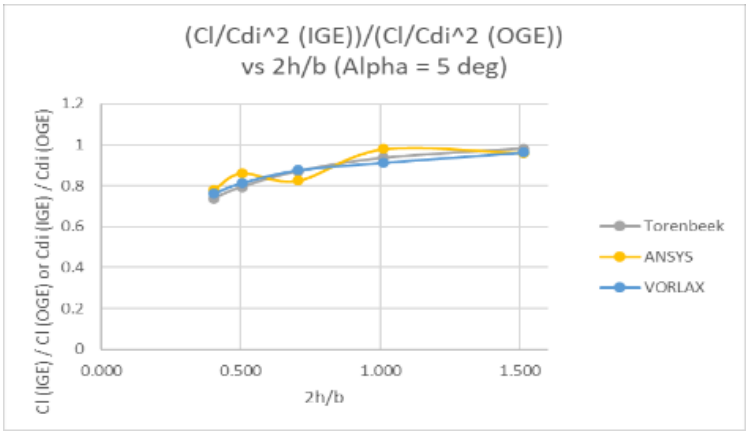

Figure 110. Ground Effect Influence, AR = 3.96, α=5°

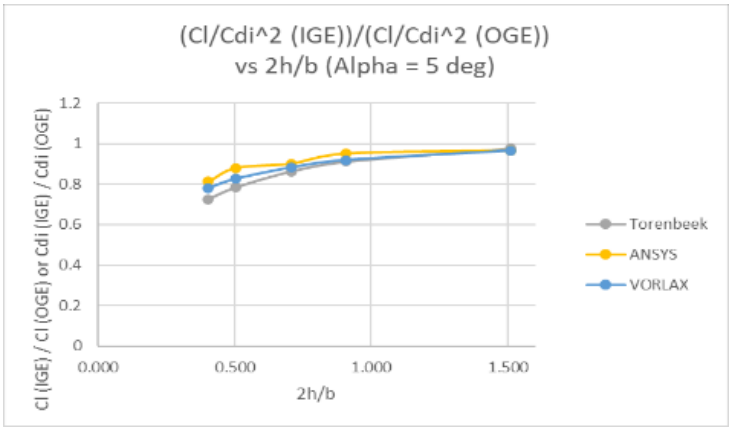

Figure 111. Ground Effect Influence, AR = 7.92, α=5°

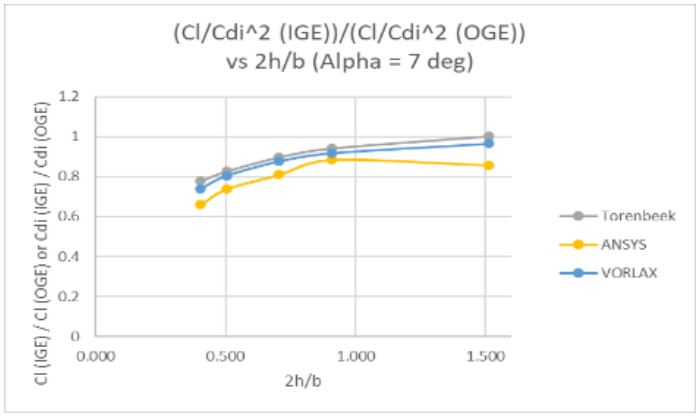

Figure 112. Ground Effect Influence, AR = 1.98, α=7°

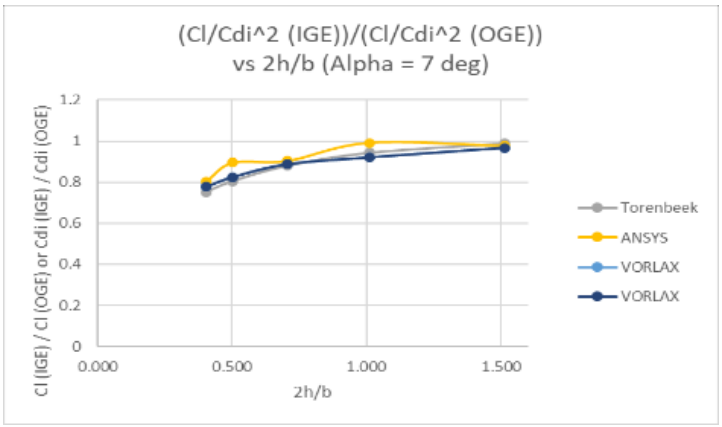

Figure 113. Ground Effect Influence, AR = 3.96, α=7°

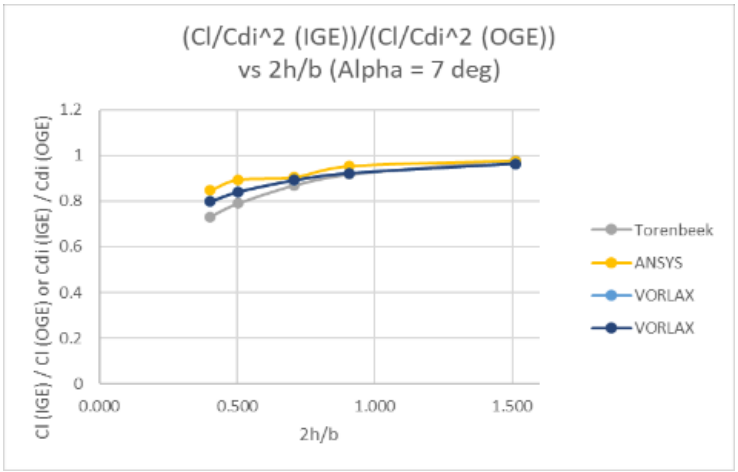

Figure 114. Ground Effect Influence, AR = 7.92, α=7

Figures 115 through Figure 117 show the results for the Oswald efficiency versus the height above the ground for different angles of attack. I can see a clear increase in efficiency as suspected when the wing is close to the ground since there is believed to be a reduction in induced drag and an increase in lift on wings operating in ground effect. Next, I can see that as the aspect ratio increases there is a clear reduction in efficiency due to the suspected reduction of these added benefits with increasing aspect ratio as previously discussed. Finally, it is interesting to see how this increase in efficiency is less significant for higher angles of attack. Note, that results for an incidence of 2-° may fall into the precision and rounding error since it involves a division of very small values.

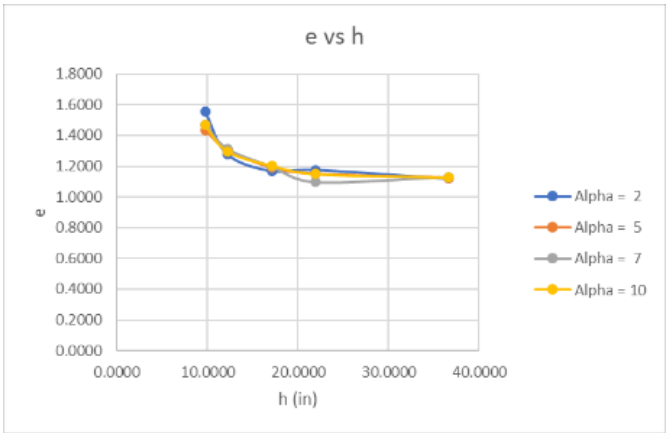

Figure 115. Oswald Efficiency vs. height above the ground, AR = 1.98

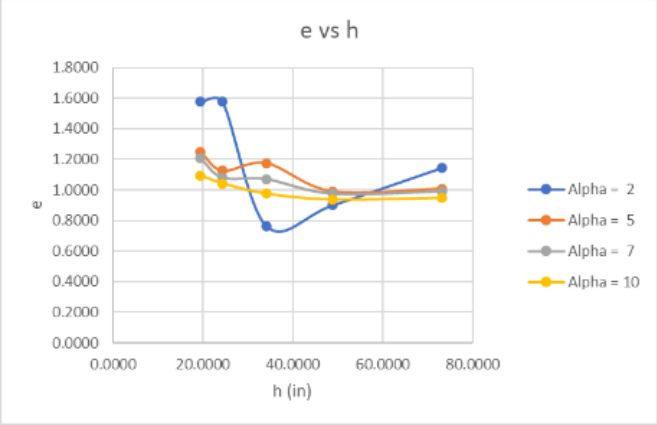

Figure 116. Oswald Efficiency vs. height above the ground, AR = 3.96

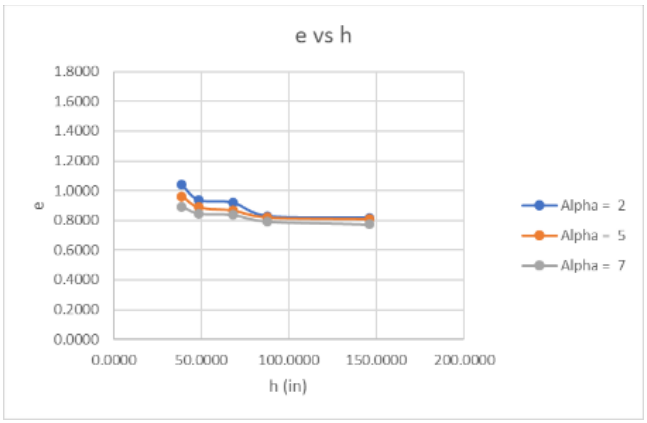

Figure 117. Oswald Efficiency vs. height above the ground, AR = 7.92

7.6 Isobars and Flow Separation Prediction with CFD ANSYS Fluent

Next, I show a sample of the results found from ANSYS Fluent for the NACA 0012 wing with an aspect ratio of 3.96. Figure 118 through Figure 135 shows a picture of the wing tunnel and wing showing the isobar patterns on both the airfoil and wing tunnel. Additionally, I can see the coefficient of drag and the coefficient of lift for each of the iterations. From these results I can clearly see as the coefficient of lift and the coefficient of drag converges in the simulation for angles of attack less than 10 degrees and how as angle of attack becomes greater than 10 degrees the flow starts to show signs of separation. Separation is suspected since the isobars shown on the airfoil start to show uneven patterns and a higher-pressure distribution shown in red in the following figures especially shown aft of the airfoil. In addition, this is apparent when I start to see a divergence in the coefficient of lift and the coefficient of drag plots. I can see how the flow starts to show signs of flow separation just passed 10 degrees. Thus, Figures 118 through Figure 135 show signs of flow becoming turbulent as the angle of attack increases and how can see a higher disturbance on the wall of the wing tunnel just as the suspected wing tip vortices are suspected to increase. All of this in conjunction helps to identify signs of flow separation using the CFD results with ANSYS Fluent.

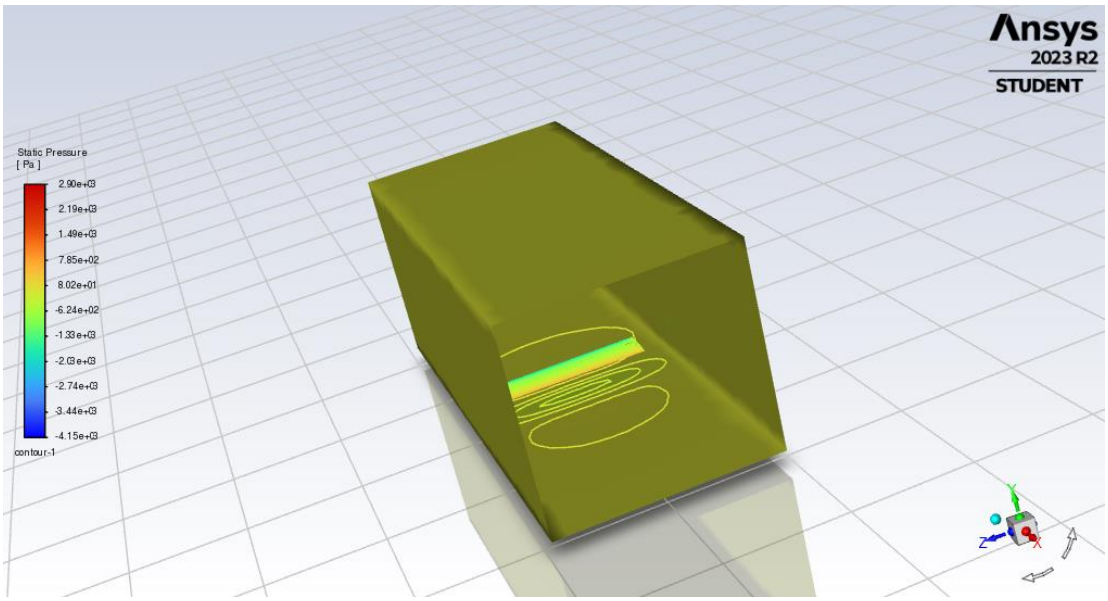

Figure 118. ANSYS Fluent Pressure Contours for NACA 0012, AR = 3.96, α=0°

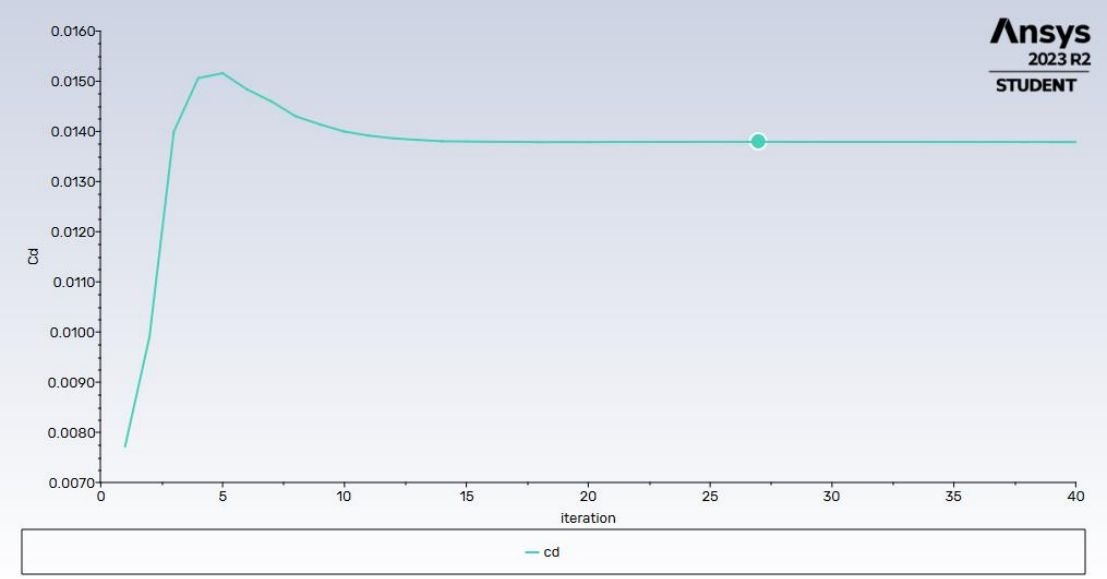

Figure 119. ANSYS Cd vs Iteration for NACA 0012, AR = 3.96, α=0°

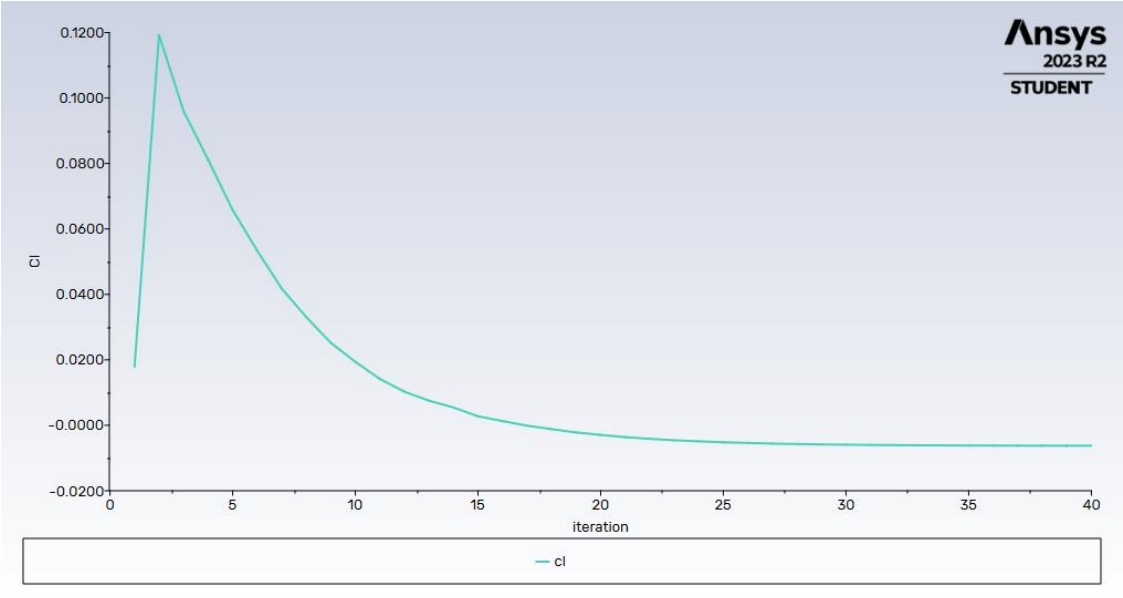

Figure 120. ANSYS Cl vs Iteration for NACA 0012, AR = 3.96, α=0°

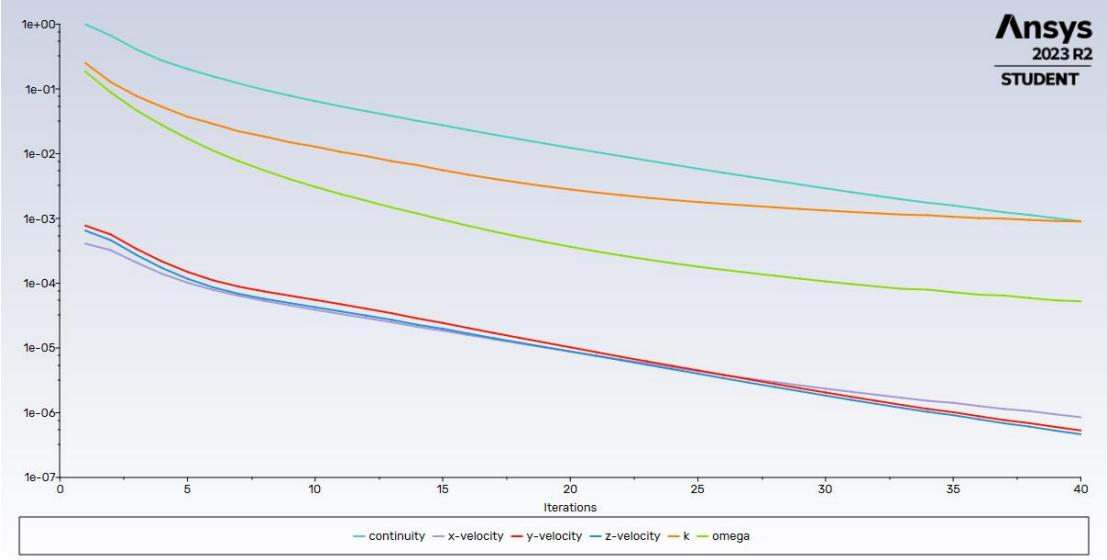

Figure 121. Scaled Residuals vs Iteration for NACA 0012, AR = 3.96, α=0°

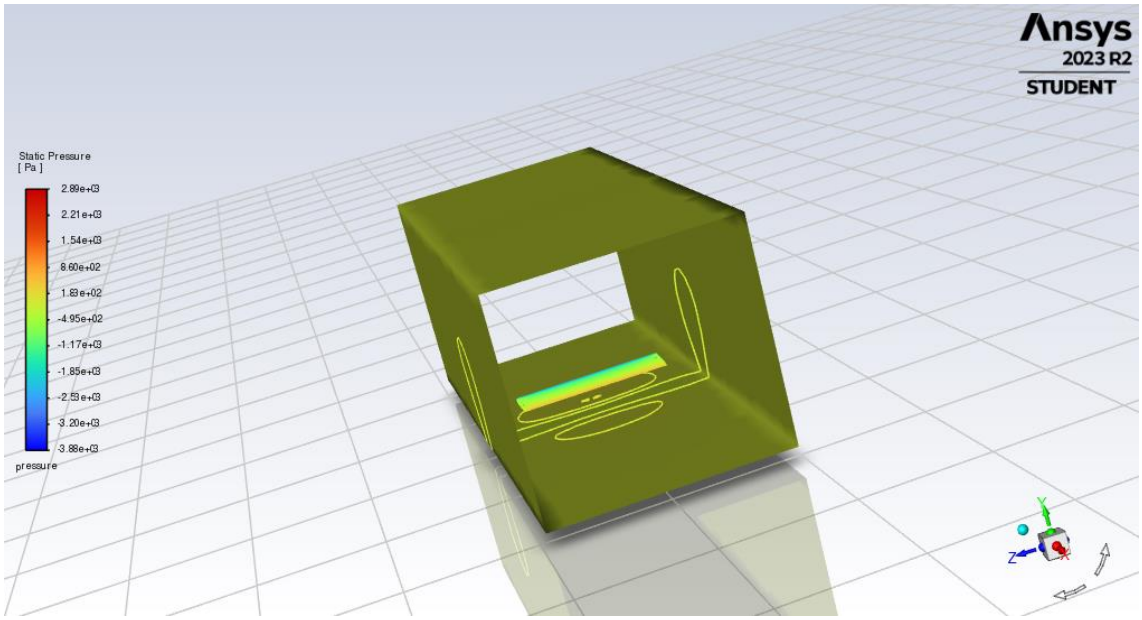

Figure 122. ANSYS Fluent Pressure Contours for NACA 0012, AR = 3.96, α=2°

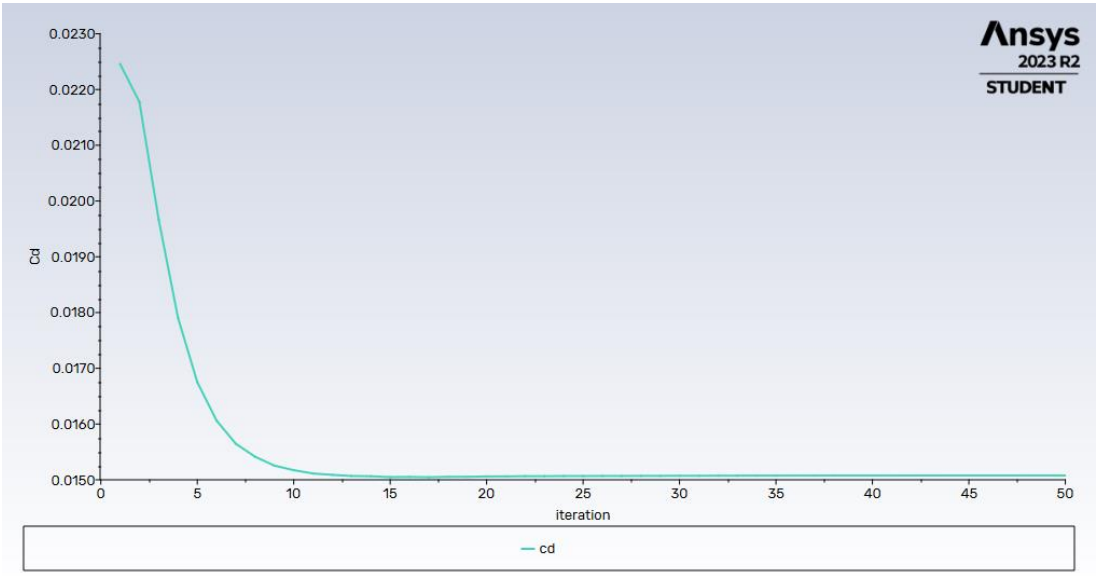

Figure 123. ANSYS Cd vs Iteration for NACA 0012, AR = 3.96, α=2°

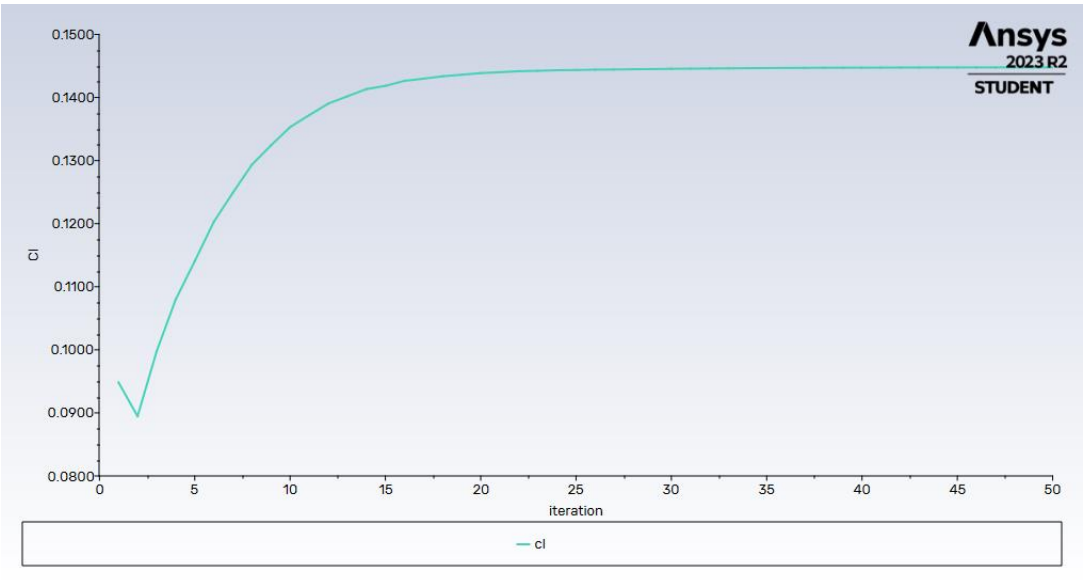

Figure 124. ANSYS Cl vs Iteration for NACA 0012, AR = 3.96, α=2°

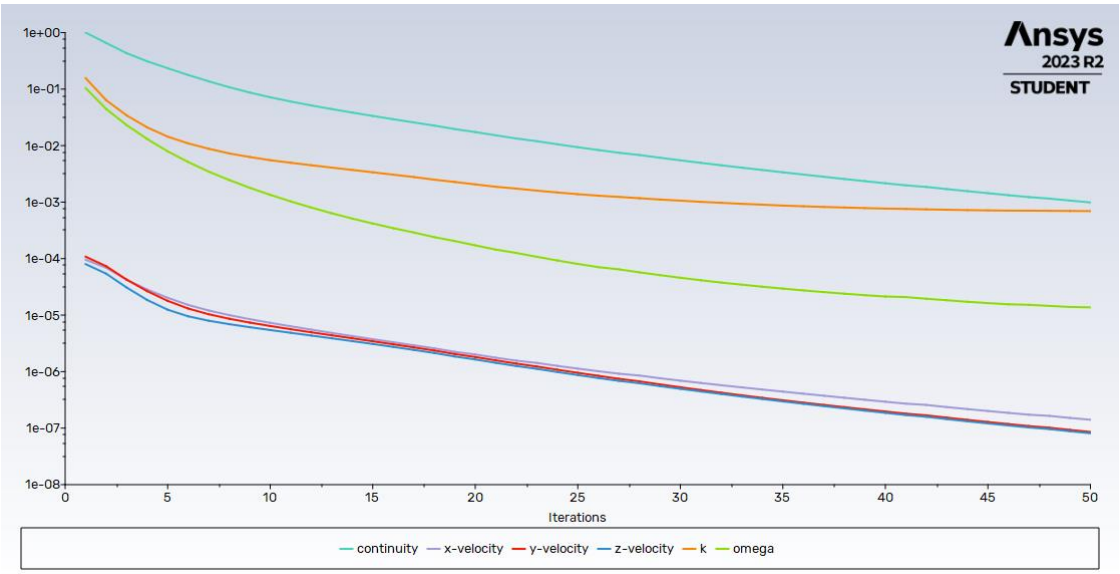

Figure 125. Scaled Residuals vs Iteration for NACA 0012, AR = 3.96, α=2°

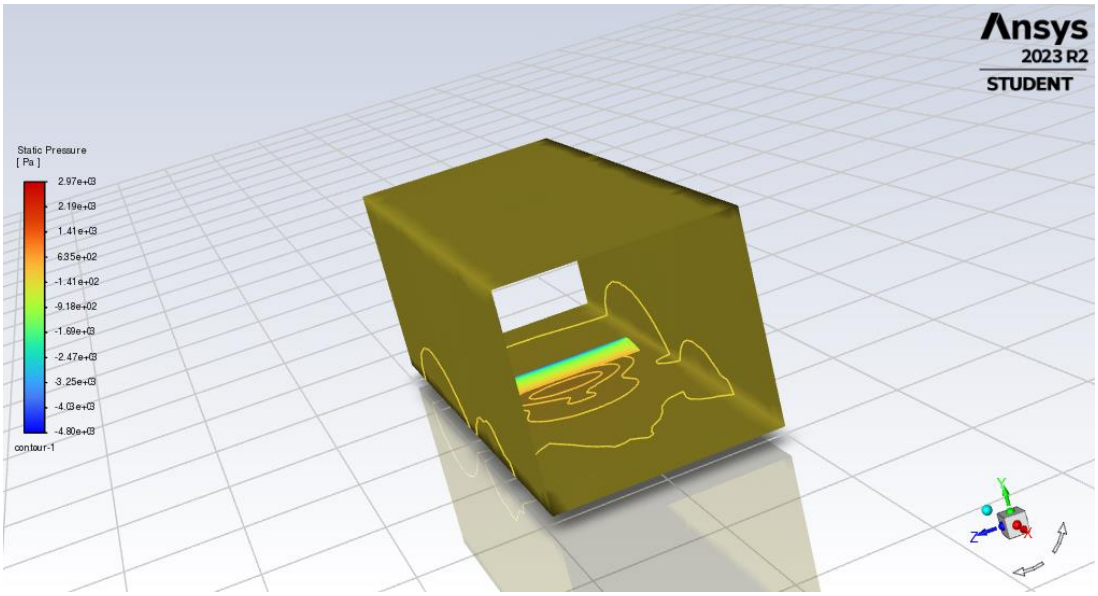

Figure126. ANSYS Fluent Pressure Contours for NACA 0012, AR = 3.96, α=5°

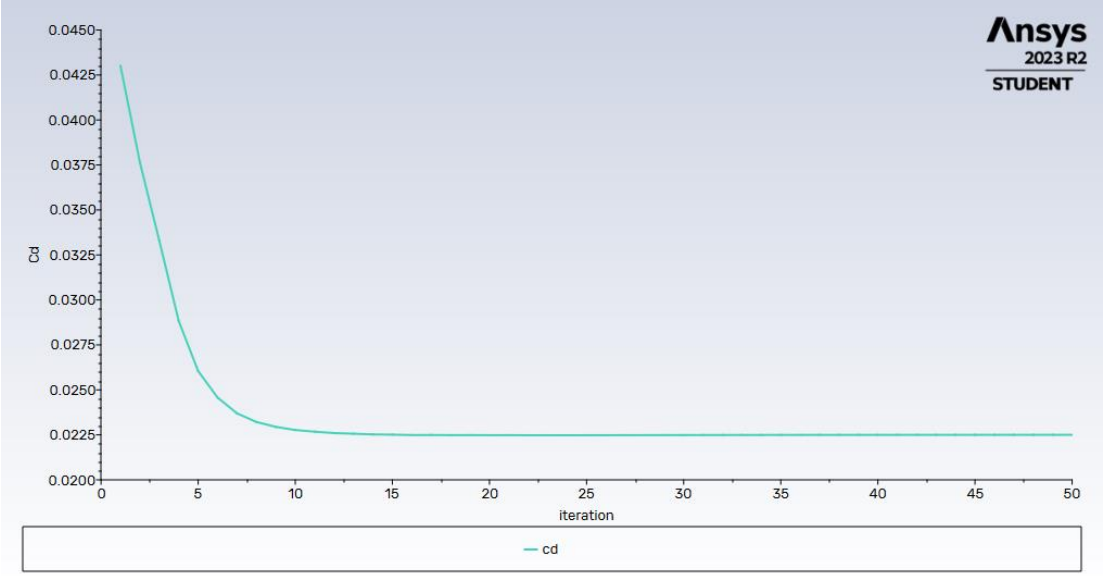

Figure 127. ANSYS Cd vs Iteration for NACA 0012, AR = 3.96, α=5°

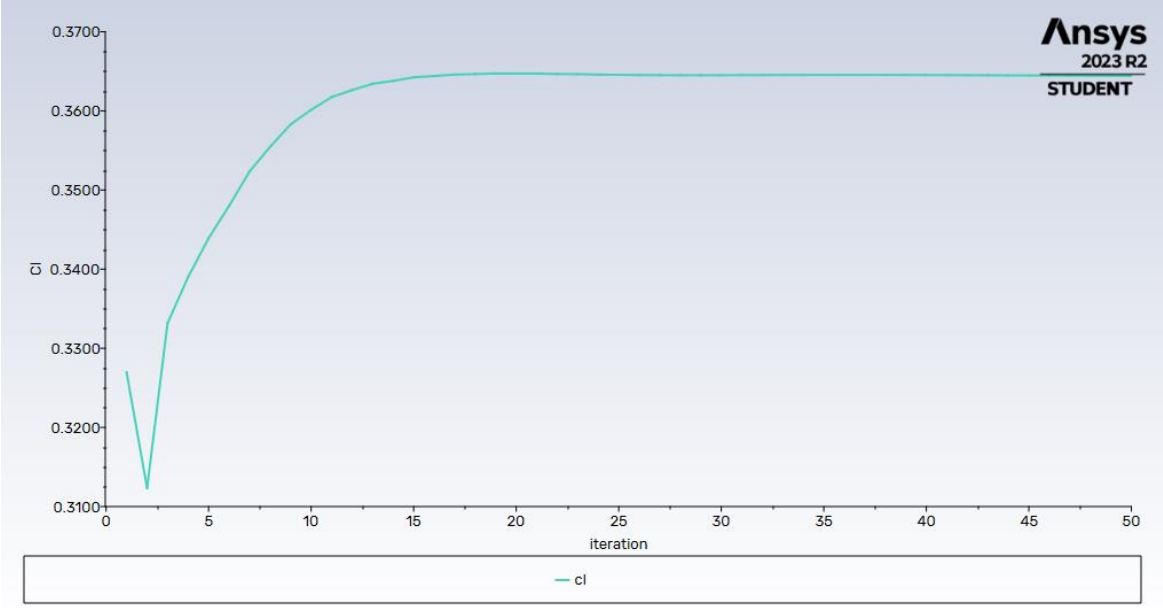

Figure 128. ANSYS Cl vs Iteration for NACA 0012, AR = 3.96, α=5°

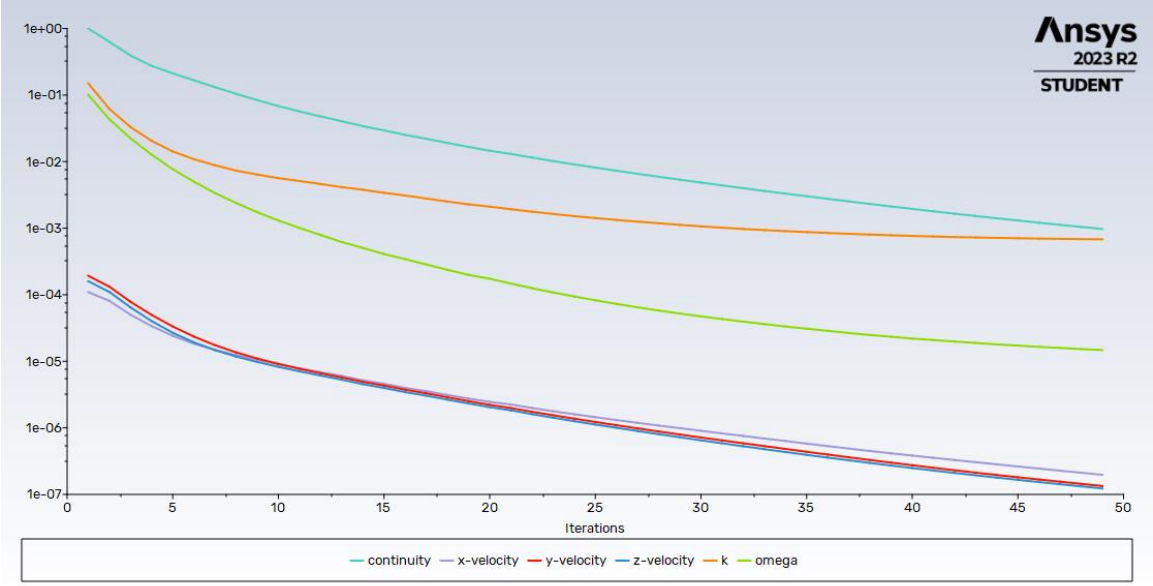

Figure 129. Scaled Residuals vs Iteration for NACA 0012, AR = 3.96, α=5°

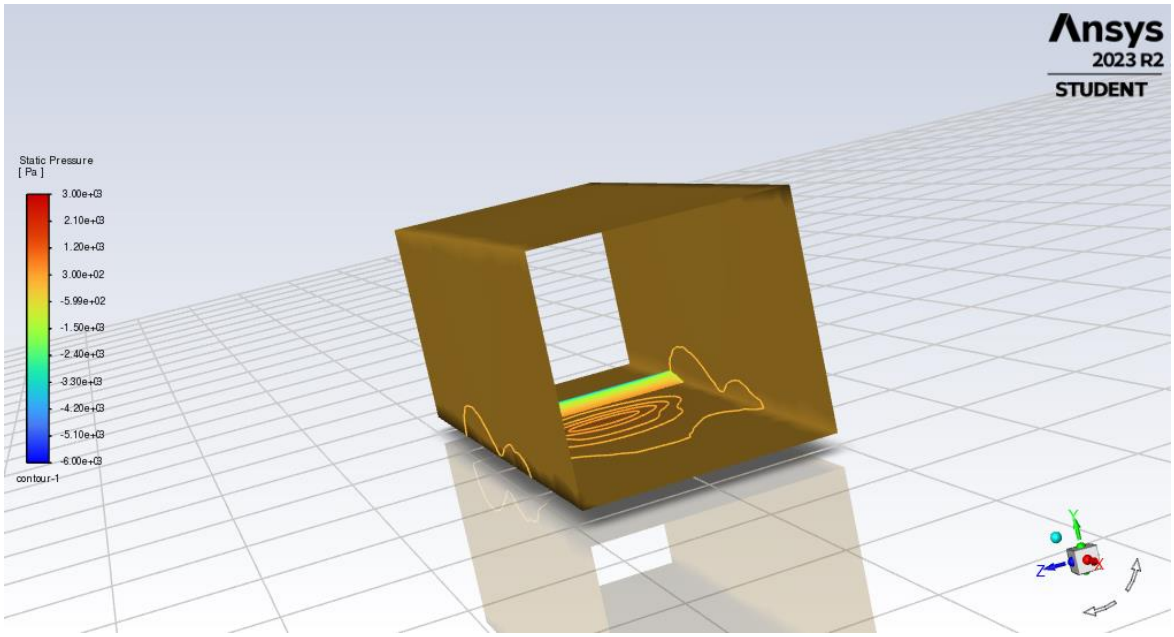

Figure130. ANSYS Fluent Pressure Contours for NACA 0012, AR = 3.96, α=7°

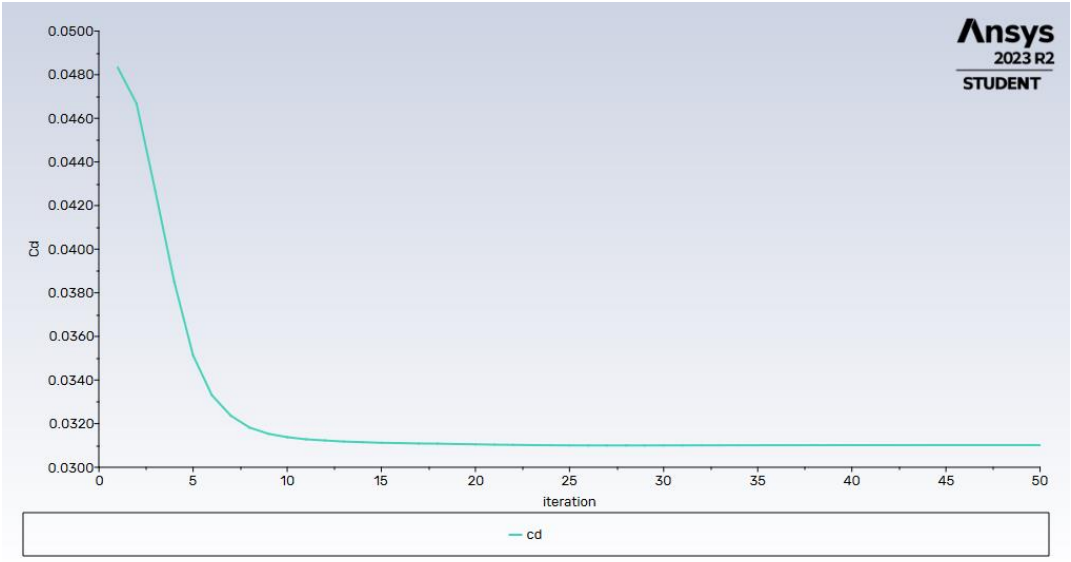

Figure131. ANSYS Cd vs Iteration for NACA 0012, AR = 3.96, α=7°

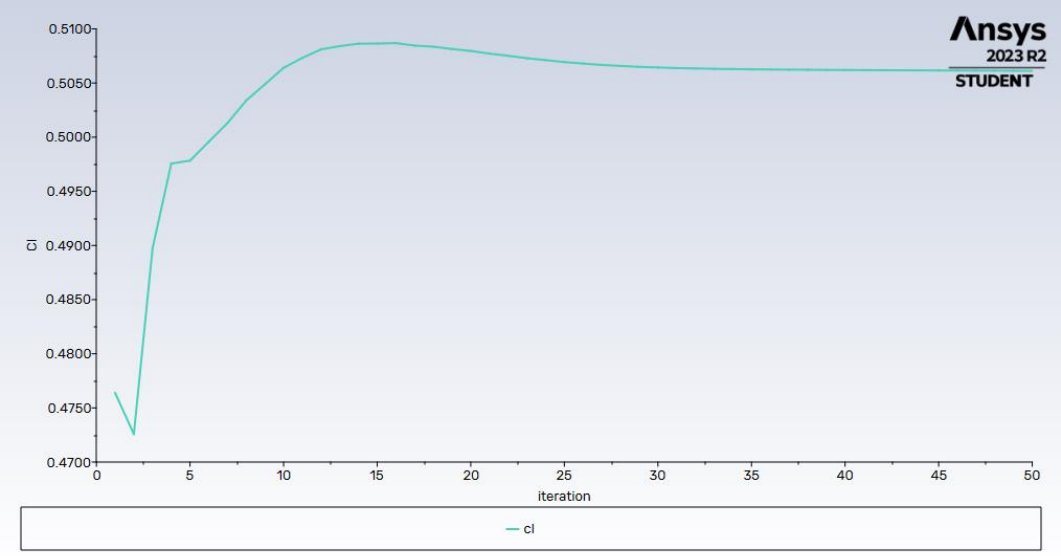

Figure 132. ANSYS Cl vs Iteration for NACA 0012, AR = 3.96, α=7°

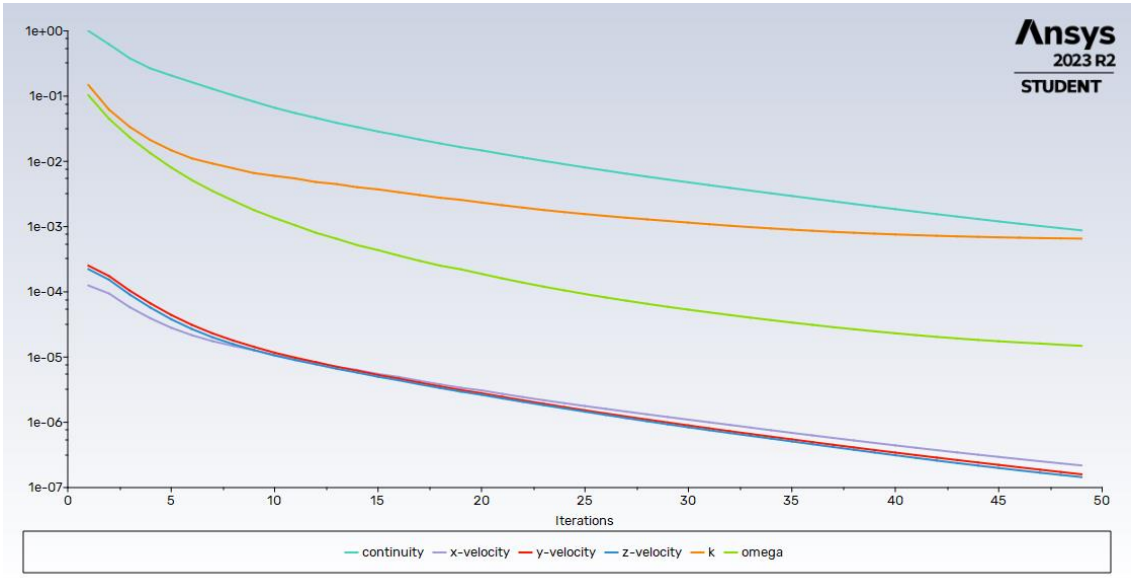

Figure 133. Scaled Residuals vs Iteration for NACA 0012, AR = 3.96, α=7°

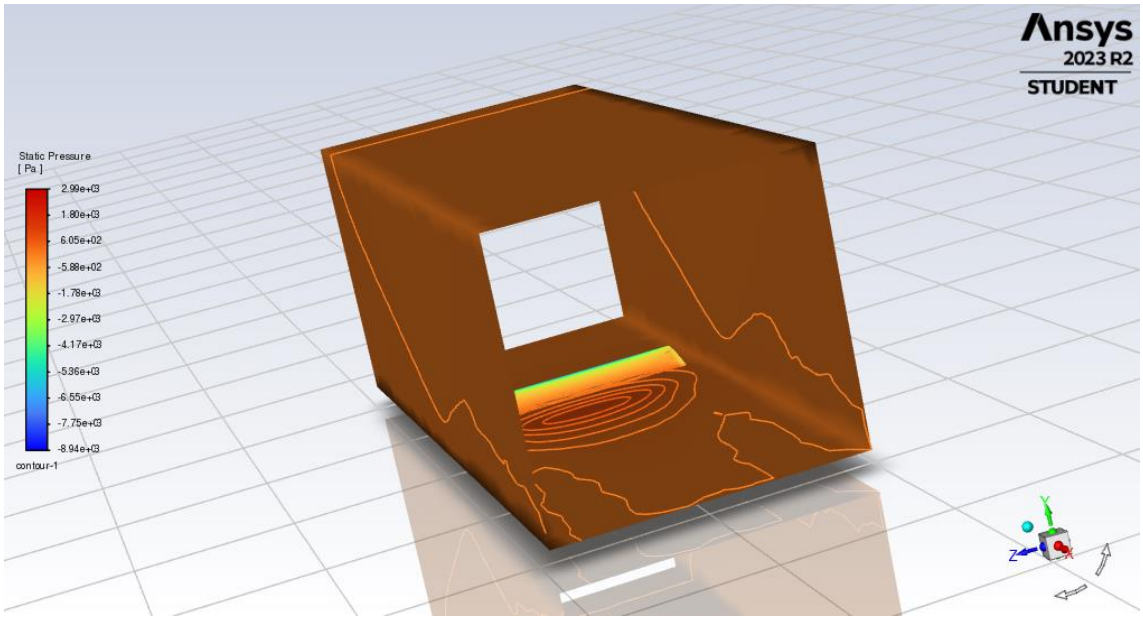

Figure 134. ANSYS Fluent Pressure Contours for NACA 0012, AR = 3.96, α=10°

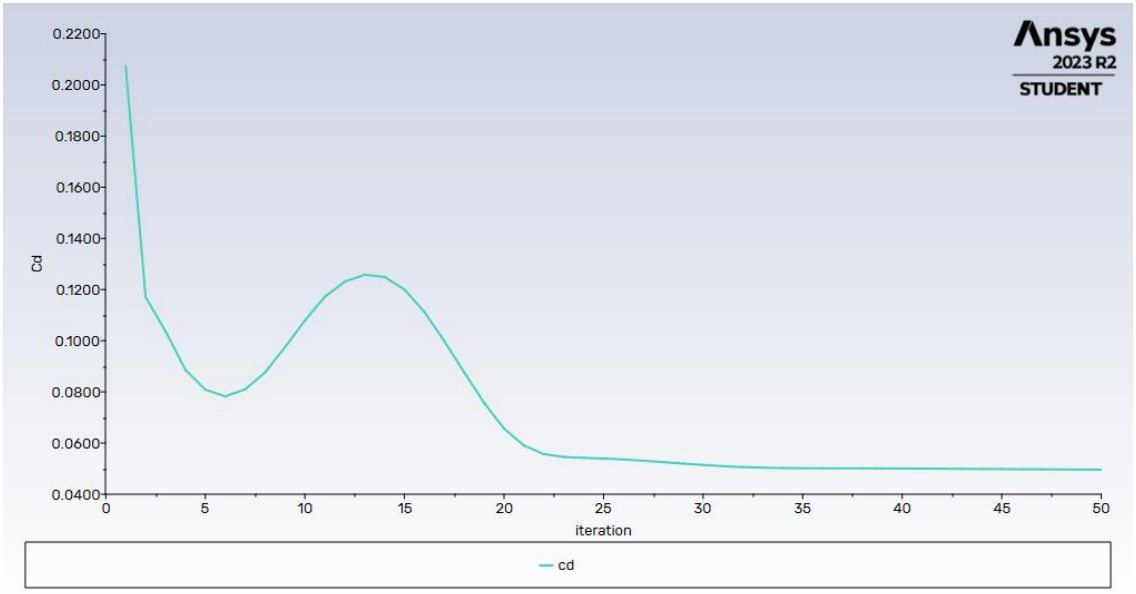

Figure 135. ANSYS Cd vs Iteration for NACA 0012, AR = 3.96, α=10°

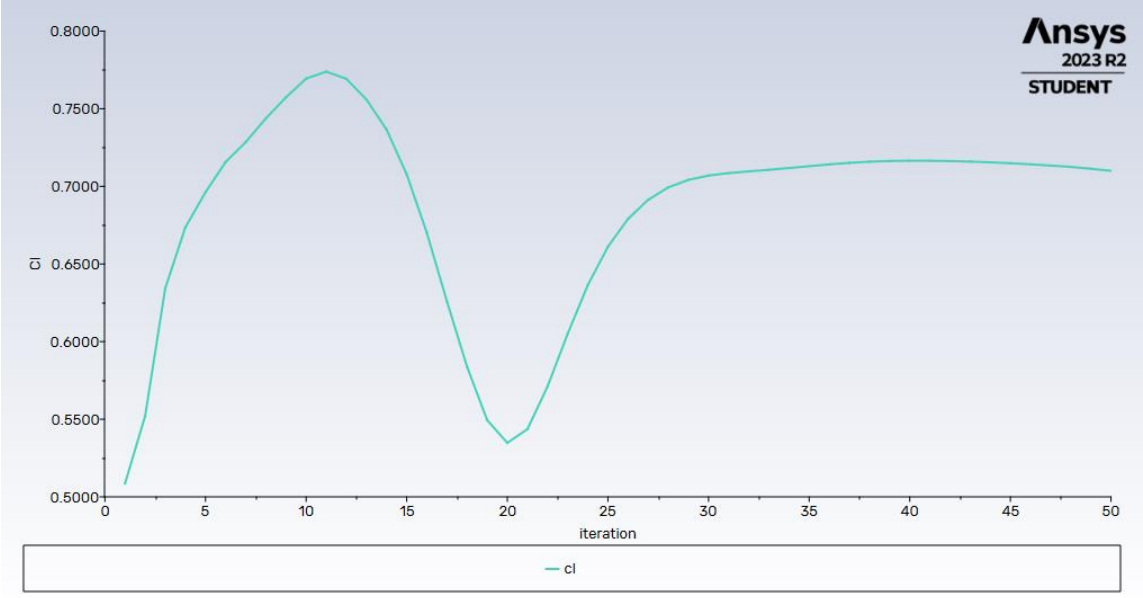

Figure 136. ANSYS Cl vs Iteration for NACA 0012, AR = 3.96, α=10°

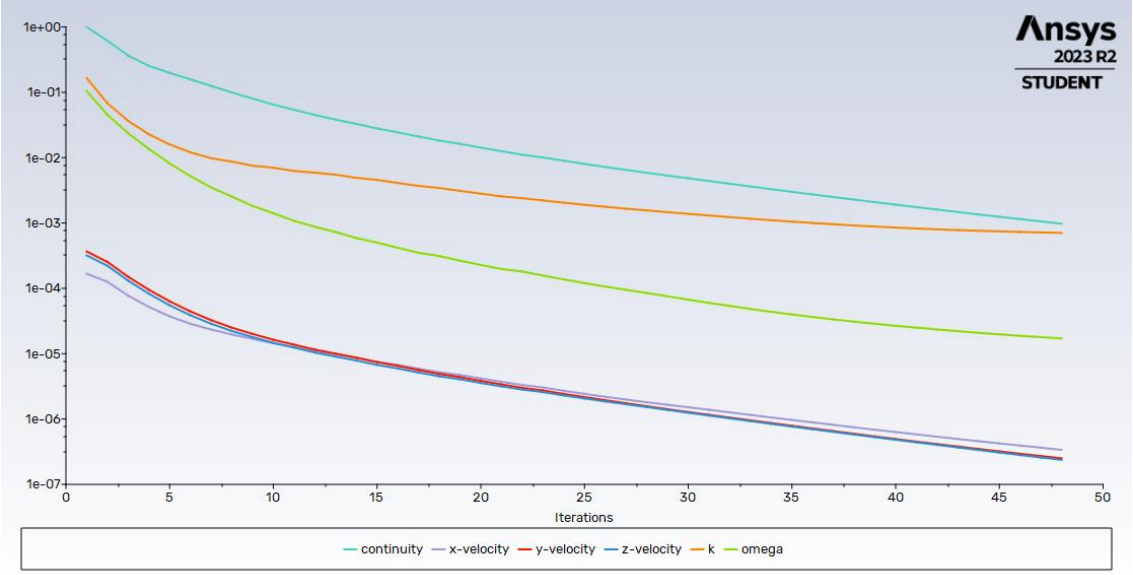

Figure 137. Scaled Residuals vs Iteration for NACA 0012, AR = 3.96, α=10°

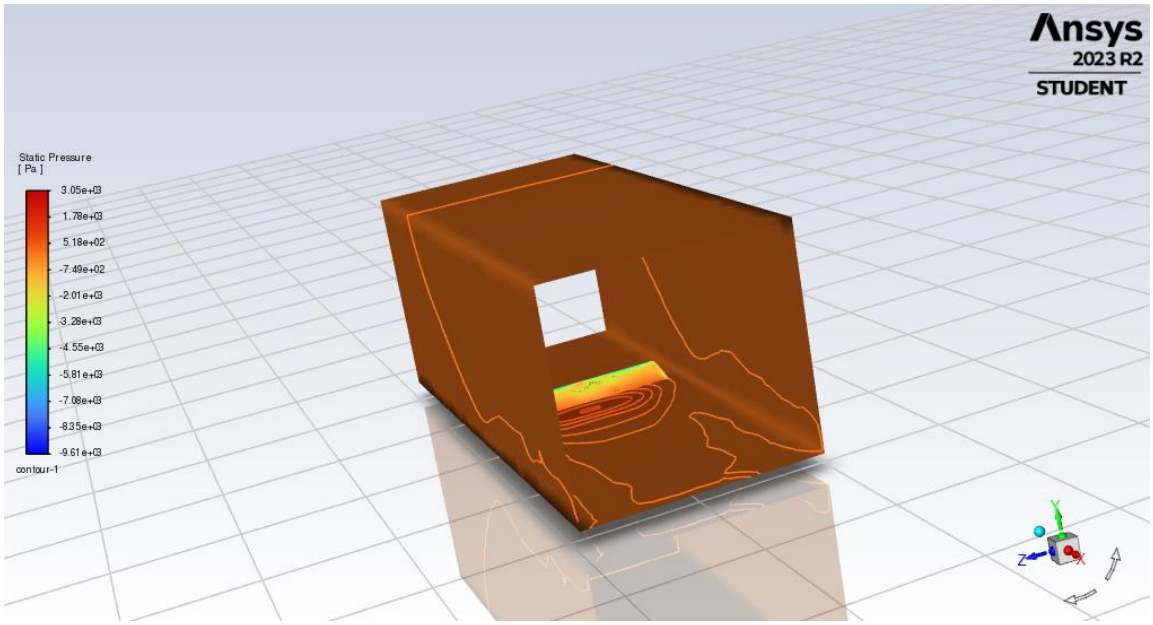

Figure 138. ANSYS Fluent Pressure Contours for NACA 0012, AR = 3.96, α=12°

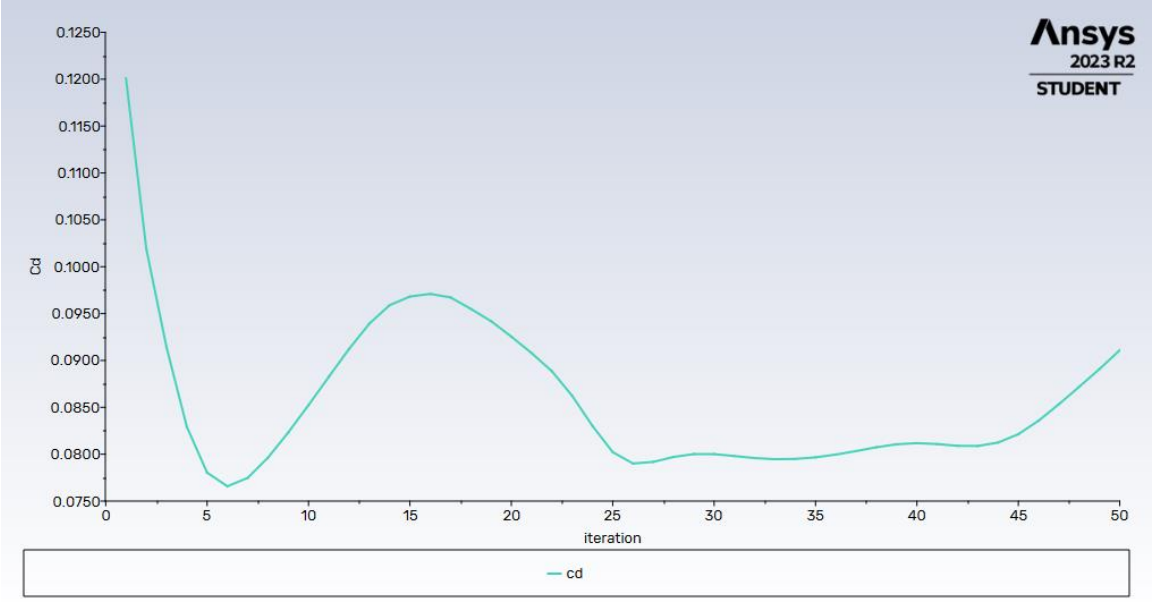

Figure 139. ANSYS Cd vs Iteration for NACA 0012, AR = 3.96, α=12°

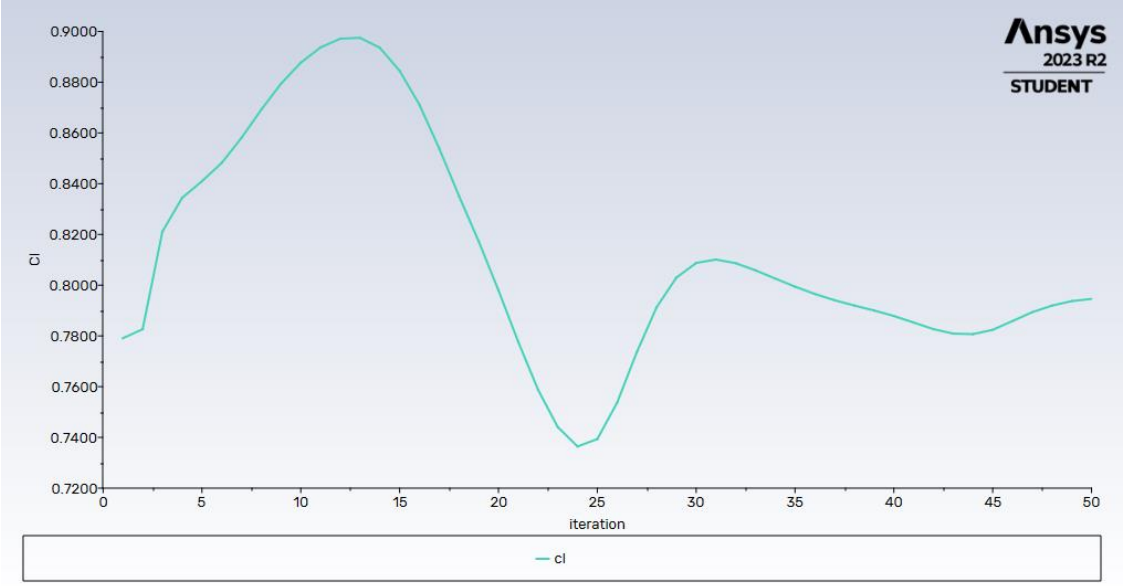

Figure 140. ANSYS Cl vs Iteration for NACA 0012, AR = 3.96, α=12°

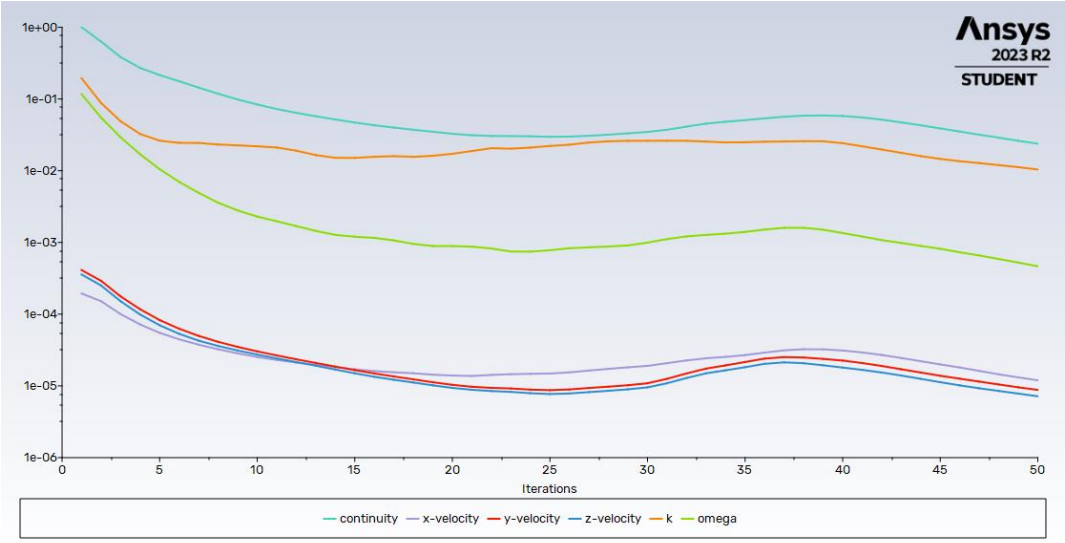

Figure 141. Scaled Residuals vs Iteration for NACA 0012, AR = 3.96, α=12°

Next, Figure 136 and Figure 137 shows a comparison of the pressure distribution of a wing with a 5-° incidence and $2h/b$ = 0.40. The top results were computed using ANSYS FLUENT, and the bottom results were obtained using VORLAX. I can clearly see a maximum pressure distribution near the trailing edge of the airfoil in both cases where flow starts to become detached from the airfoil. In addition, I can also see some similar changes in their spanwise pressure distribution. However, I can

see the similitudes in the flow patterns by looking at the isobars found using both methods individually. It is remarkable how close the results obtained using VORLAX are to those obtained with CFD using ANSYS Fluent.

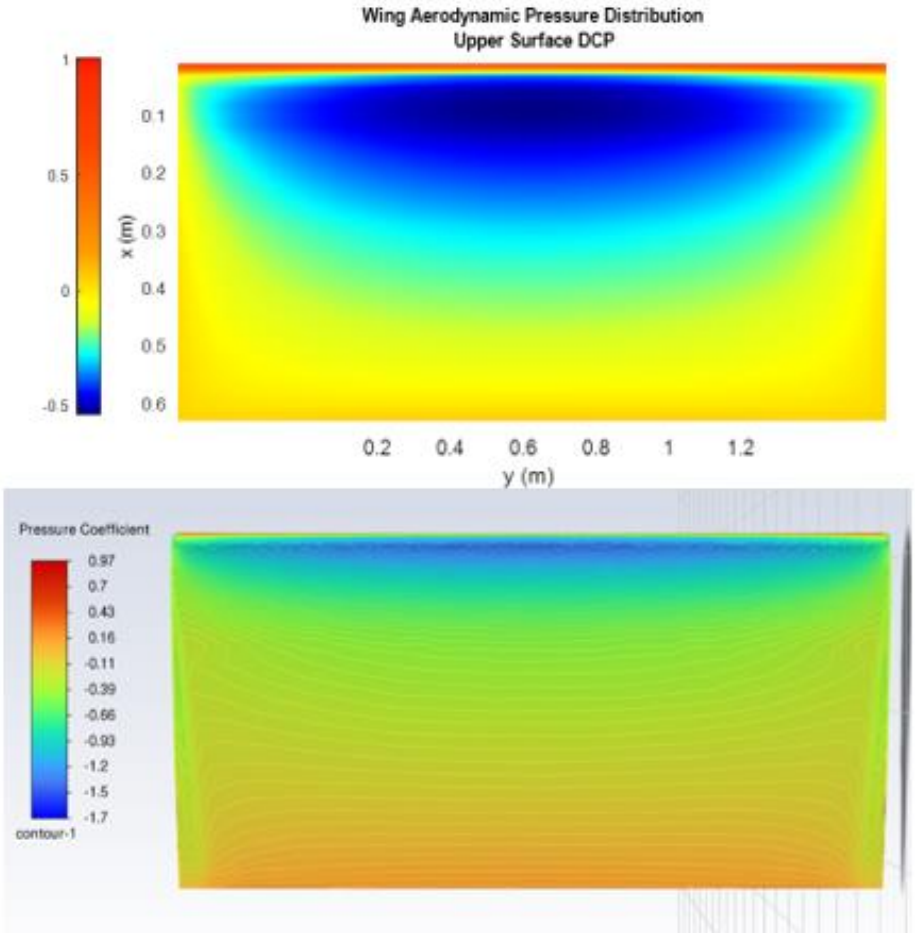

Figure 142. Top pressure distribution of AR = 1.98, α=5°, 2h/b = 0.40 airfoil. Top plot shows results from VORLAX. Bottom plot shows results from ANSYS FLUENT

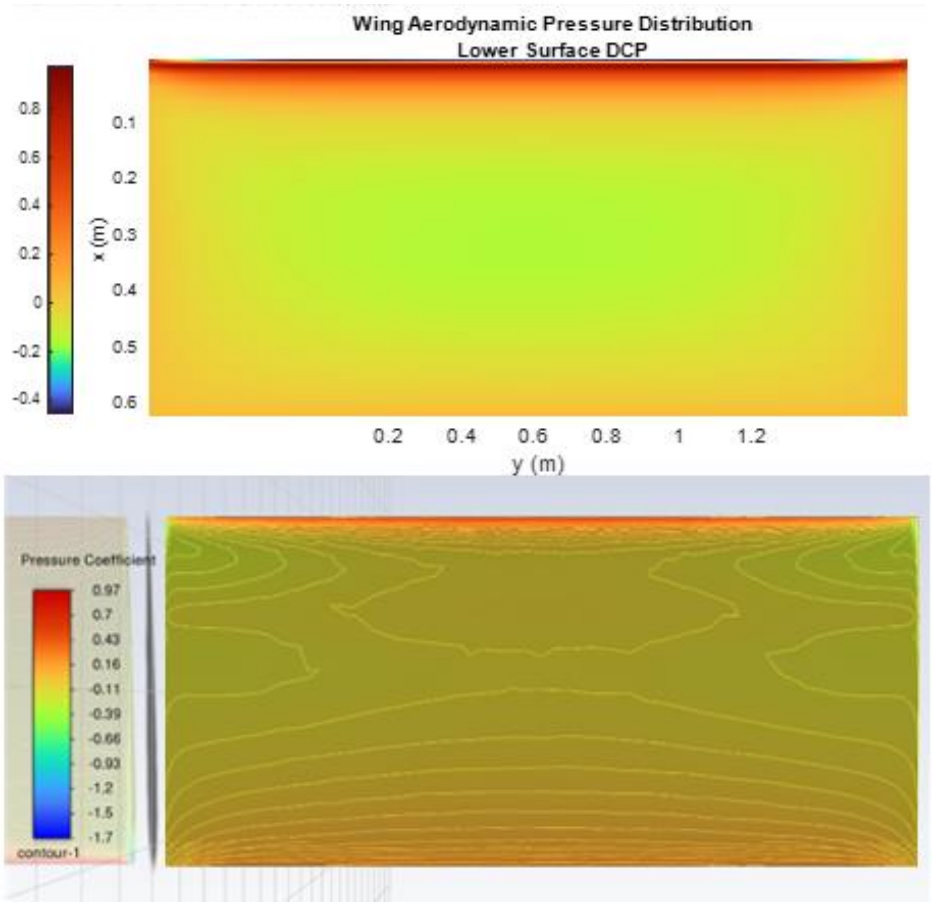

Figure 143. Bottom pressure distribution of AR = 1.98, α=5°, 2h/b = 0.40 airfoil. Top plot shows results from VORLAX. Bottom plot shows results from ANSYS FLUENT

Chapter 8: Conclusion

In this thesis, I documented how lifting properties of wings change significantly when in ground effect. I gained a deeper understanding of the changes in aerodynamic loading due to gap spacing.

I saw that properties of the flow conditions on wings in ground effect are very sensitive to changes in incidence and aspect ratio. Especially in small aspect ratio wings such as those found in racecars. While higher aspect ratio wings such as those found in aircraft may experience higher ground effect influences, they may not be as sensitive in these changes. Many race cars such as the one found in Formula 1 have multiple aerodynamic surfaces with flow close to the ground or enclosed. That is why it is important to have a deeper understanding of the nuances of the air flow in ground effects. Accurately predicting the values for the coefficient of lift or drag in aerodynamic surfaces in ground effect, or accurately predicting when the flow separates may be key to improve the performance of race cars.

When I compared widely cited equations with VORLAX results I observed that none of the methods agreed with one another; it is difficult to predict ground effect influence with a simple equation. Torenbeek's equation works well at small *AR* and low angles of attack, but failed to predict the results at higher angles of attack and/or *AR*. The opposite can be said about McCormick and Hoerner & Borst; they work better for relatively high *AR* wings.

I created a new equation that is not just a function of the height above the ground and span ratio but is also a function of the angle of attack and aspect ratio. "Valenzuela & Takahashi" equations seem to do a better job in predicting and fitting VORLAX results. However, this equation also fails at relative high angles of attack (a > 15 °) post stall as well as at very small height over span (*h/b*) ratios. Thus, the preferred choice of empirical equation depends on the application (aircraft or racecar).

I also studied the ground effect influences on the stall of a NACA 0012 airfoil in ground effect using a viscous CFD solution. These ANSYS FLUENT results found at best a weak relationship between the height above the ground and the stall angle of attack in the medium and large aspect ratio wings. The low *AR* wings are able to sustain higher angles-of-attack before stalling when

compared to the same proportion of *HAG*. I found that viscous CFD follows the same trends as observed with the updated Torenbeek's equation as well as with the inviscid VORLAX.

I found some deviation between the results of the lowest *AR* wings. I also observed a greater ground effect influence on small aspect ratio wings. Changes in induced drag, and Oswald efficiency were more pronounced in the lowest *AR* wings. I continue to be impressed with how closely the viscous CFD results height above the ground trends match those from VORLAX so long as I defined the gap based on the height above the ground from the aerodynamic center closely match those of VORLAX. However, for the chosen chord length there were not significant changes if the values were measured near the leading edge.

I looked at the use of Stratford's method to predict the onset of flow separation using the inviscid VORLAX model. These solutions did not exhibit significant changes in flow separation as the wings entered in ground effect. I did find that airfoils with higher aspect ratio would experience early signs of flow separation compared to smaller aspect ratio airfoils. Nevertheless, these differences may not be significant enough to change the stall angle in the airfoil. Thus, I believe that the stall angle of an airfoil may not be a function of the height above the ground in high aspect ratio wings but rather just a function of incidence and aspect ratio. These trends are confirmed with the parallel viscous CFD study.

I analyzed the transverse, spanwise load distribution of the airfoil. I found that to keep an ideal elliptical lift distribution in an airfoil in proximity to the ground it would be needed to twist the tips of the airfoils if needed to minimize ground effect influences. Since airfoils that were closer to the ground had a higher load distribution near the center of the center with a higher gradient towards the tips of the airfoil. However, a qualitative analysis of this area to find precise values of twist are beyond the scope of this thesis but are expected to be researched in later studies. In addition, I observed significant changes in the spanwise lift distribution with changing aspect ratio for airfoils found in ground effect. A smaller aspect ratio airfoil has a considerably different spanwise loading than that of an ideal elliptical airfoil agreeing with previous observations for flow separation using Stratford's method.

Some areas where this research could be improved, and some sources of error includes the following. There was some discrepancy between the results found using VORLAX and known equations and those found using CFD ANSYS FLUENT, especially in the low aspect ratio wing. Nevertheless, as previously stated a portion of this discrepancy could be the direct result of rounding, and precision error. Nevertheless, to increase the precision of the CDF results would require an increase in grid density in the Mesh, which in turn would significantly increase the computational time needed for each test trial. In addition, the results could be affected by the relatively small size of the wing tunnel. While I was interested in studying the effects of changing the lower surface, there is possibly some interference from the other surfaces as well such as the top surface. I tried to keep the top surface sufficiently far away to minimize this interference. However, increasing the size of the wing tunnel, in any direction also increases the size of the grid points needed for the calculation, therefore, in most cases the wake of the airfoil's could possibly still have had some interference with the top surface. Next, there could be some discrepancy in the definition used for "height above the ground." In some of the known equations this definition is clearly stated such as in the case for Torenbeek's equation defined it as the average between the height of the airfoil's aerodynamic center to and the height at the trailing edge, while in other instances this term was left ambiguous. Nevertheless, considering this difference becomes insignificant as the aspect ratio increases since the percentage of the chord to the span becomes smaller. Lastly, more accurate predictions could be made by increasing the sample size of this research. For instance, I could have determined a more accurate stall prediction by collecting finer incidence data rather than collecting the data at each whole degree. Nevertheless, I opted for this data size again in the interest of optimizing time and resources.

I hope this investigation can bring a deeper understanding of wings found in proximity to the ground. I qualitatively measured the ground effect influences by measuring changes in the coefficient of lift and induced drag, and I looked at how other quantities such as the Oswald efficiency varied, I believed that I collected sufficient evidence to see a significant difference in the ground effect influence and loading on wings with a considerable small aspect ratio compared to those of higher

aspect ratio. Small aspect ratio wings are often overlooked since most aerodynamic work may consist of aircraft wings. Nevertheless, I consider that understanding these nuances in small aspect ratio wings in ground effect can be crucial to accurately predict flow conditions on wings such as those found in racecars and other ground or low flying vehicles.

REFERENCES

[1] Wikipedia,"A-90 Orlyonok". Available at: https://en.wikipedia.org/wiki/A-90_Orlyonok

[2] TopGear. "2023 Red Bull RB16B Available at: https://www.topgear.com/car-news/formula-one/sergio-perez-has-signed-red-bull-until-end-2024

[3] "The NTSB's John O'Callaghan, a national resource specialist in aircraft performance, noted that all aircraft stall at approximately 2-4 deg. Loq1r AOA [angle of attack] with the wheels on the ground." (from NTSB Accident Report concerning loss of a swept wing business-class jet airplane in April 2011) *Thin Margins in Wintry Takeoffs* AWST, 24 December 2018

[4] Flight Safety Australia. "Comet." Available at: https://www.flightsafetyaustralia.com/2019/08/comet/

[5] Savannah Now. "NTSB: Warning signs unheeded before Gulfstream G650 crash." Available at: "https://www.savannahnow.com/story/news/2012/10/11/ntsb-warning-signs-unheeded-gulfstream-g650-crash/13452218007/

[6] Miranda, L.R., Baker, R.D., and Elliott, W.M., "A Generalized Vortex Lattice Method for Subsonic and Supersonic Flow," NASA CR 2875, 1977.

[7] Souders, T.J. and Takahashi, T.T., "VORLAX 2020: Making a Potential Flow Solver Great Again," AIAA-2021-2458, 2021.

[8] Smith, A.M.O., "High-lift aerodynamics," *Journal of Aircraft*, vol. 12, 1975, pp. 501–530.

[9] Stratford, B.S., "The Prediction of Separation of the Turbulent Boundary Layer," *Journal of Fluid Mechanics,* Vol. 5, 1959, pp. 1-16.

[10] Hoerner, S., Fluid Dynamic Drag. Self-Published by the author, 1958.

[11] Wieselsberger, C., "Über den Flügelwiderstand in der Nähe des Bodens." Z. Flugtechn. U. Motorluft-schiffahrt 12, 1921, (English translation: NACA TM-77, 1922).

[12] McCormick, B.W., Aerodynamics, Aerodynamics and Flight Mechanics, John Wiley & Sons, 2nd Edition, 1995.

[13] Torenbeek, E., Synthesis of Subsonic Airplane Design, Delft University Press Kluwer Academic Publishers, 1982.

[14] Fédération Internationale de l'Automobile, F2020 Formula One Technical Regulations, 2019

[15] Hoerner, S., and Borst, H., "Lift of Airplane Configurations," Fluid Dynamic Lift, self-published by the author, 1975.

[16] Philips, W.F., and Hunsaker, D.F., "Lifting-Line for Induced Drag and Lift in Ground Effect." *Journal of Aircraft*, vol. 50, pp.1226-1233, 2013.

[17] Martinez-Rodriguez, G., "A Study and Design of Multi-Element High Lift Systems for Commercial Transport Aircraft," M.S. Thesis, Arizona State University, 2021.

[18] Küchemann, Dietrich, The Aerodynamic Design of Aircraft, AIAA, 2012.

[19] Abbott, I.H, Von Doehnoff, A.E., and Stivers, L., Jr. "Summary of Airfoil Data," NACA TR-824, 1945.

[20] Anderson, J. D., Introduction to Flight, 7th ed., McGraw–Hill, New York, 2012.

[21] Anderson J. D., Modern Compressible Flow, 3rd Edition, LLC, McGraw-Hill, New York, 2003.

[22] Munk, Max, Principles of aerodynamics, Self-Published, Washington, D.C, 1933.

[23] Phys.Org, "wing tip vortices". Available at: https://phys.org/news/2018-05-wing-vortex.html

[24] ScarbsF1, "F1 wingtip vortices". https://scarbsf1.wordpress.com/2011/08/08/analysis-mclarens-rear-wing-vapour-trails/

[25] Researchgate, "Boundary Layer Separation". Available at: https://www.researchgate.net/figure/Boundary-layer-and-flow-separation_fig7_291821947

[26] Valenzuela, J.V. and Takahashi, T.T., "Wing Design Strategies for Vehicles Designed to Operate in Ground Effect," AIAA 2024-0003. AIAA SCITECH 2024 Forum. January 2024.

[27] Dahm, W.J.A., & Hamlington, P.E. (2022). Introduction to Turbulent and Turbulent Flows: Physical Concepts, Statistical Theory and Modeling. Arizona State University Course Materials.

[28] Gad-el-Hak, M., Moses, R.W., & Ross, M.D. (1993). Methods for predicting separation in laminar and turbulent boundary layers. Progress in Aerospace Sciences, 29 (5), 289-350.

[29] Cebeci, T., Mosinskis, J., & Smith, A.M.O. (1970). Calculation of Viscous Drag and Turbulent Boundary-Layer Separation on Two-Dimensional and Axisymmetric Bodies in Incompressible Flows. Report No. MDC J0973-OI, November. Prepared Under Contract N000I4-70-C-0099. Naval Ship Systems Command, General Hydromechanics Research Program, Subproject SR 009 01 01, Administered by the Naval Ship Research and Development Center. Approved for public release, distribution unlimited.

APPENDIX A

CASE STUDIES AND AIRFOIL PROFILE USED

Next, Table 1 and Table 2 show the different cases used for this study, where multiples of the aspect ratio for the NACA 0012 were used by varying the span, and the height above the ground.

		AR	**2*AR**	**4*AR**	**6*AR**	**8*AR**	**16*AR**
	AR	1.98	3.96	7.92	11.88	15.84	31.68
WING	**Span**	1230	2455	4910	7380	9820	19640
DIMENSIONS:	**Chord**	620	620	620	620	620	620
	2h/b	**HAG**	**HAG**	**HAG**	HAG	**HAG**	**HAG**
	0.40	*0.25*	*0.50*	*0.99*	1.49	1.98	3.96
	0.50	*0.31*	*0.62*	*1.24*	1.86	2.47	4.95
	0.60	0.37	0.74	1.48	2.23	2.97	5.94
	0.71	*0.43*	*0.87*	*1.73*	2.60	3.47	6.93
	0.81	0.50	0.99	1.98	2.98	3.96	7.92
	0.91	*0.56*	*1.11*	*2.23*	3.35	4.45	8.91
	1.01	0.62	1.24	2.47	3.72	4.95	9.90
	1.51	*0.93*	*1.86*	*3.71*	5.58	7.42	14.85

Table 1. Different case studies using a Flat Plate, where HAG is the height above the ground. Values shown in italic indicate the computed values with ANSYS FLUENT

α (°) /	b = 4910 mm				b = 2455 mm				b = 1230 mm			
2h/b	**0.4**	**0.71**	**1.51**	**0**	**0.4**	**0.71**	**1.51**	**0**	**0.4**	**0.71**	**1.51**	**0**
0	3.8	3.8	3.8	3.8	1.4	1.4	1.4	1.4	1.4	1.4	1.4	1.4
2	3.8	3.8	3.8	3.8	3.8	3.8	3.8	3.8	1.4	1.4	1.4	1.4
5	7.4	7.4	7.4	7.4	3.8	7.4	7.4	7.4	1.4	1.4	1.4	3.8
7	12.0	12.0	12.0	12.0	7.4	7.4	7.4	7.4	3.8	3.8	3.8	3.8
8	12.0	12.0	12.0	12.0	7.4	7.4	7.4	7.4	3.8	3.8	3.8	3.8
9	12.0	12.0	12.0	12.0	7.4	7.4	12.0	12.0	3.8	3.8	3.8	3.8
10	12.0	12.0	12.0	12.0	12.0	12.0	12.0	12.0	3.8	3.8	3.8	7.4
11	12.0	12.0	17.5	17.5	12.0	12.0	12.0	12.0	3.8	3.8	7.4	7.4
12	17.5	17.5	17.5	17.5	12.0	12.0	12.0	12.0	7.4	7.4	7.4	7.4
13	17.5	17.5	17.5	17.5	12.0	12.0	12.0	17.5	7.4	7.4	7.4	12.0

Table 2. Values found for percentage of detached flow from the trailing edge for varying (2h/b) and span (b).

Finally, Figure 138 shows a top view of the airfoil used in the flat panel method and Figure 139 shows the side profile of the NACA 0012 airfoil used in the Sandwich method also using the vortex lattice method.

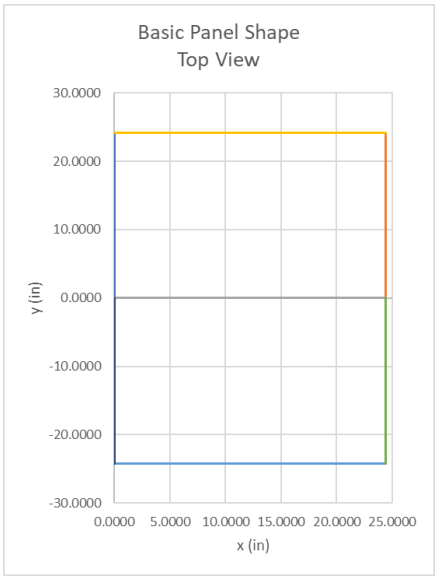

Figure 144. Top view of wing used for flat plate analysis of a NACA 0012 airfoil

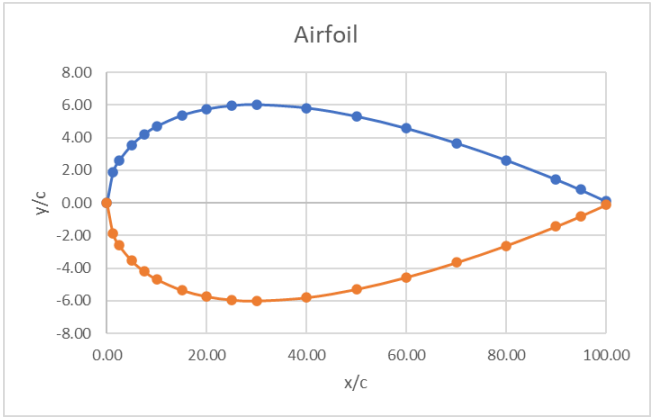

Figure 145. Airfoil view of NACA 0012 used for sandwich model